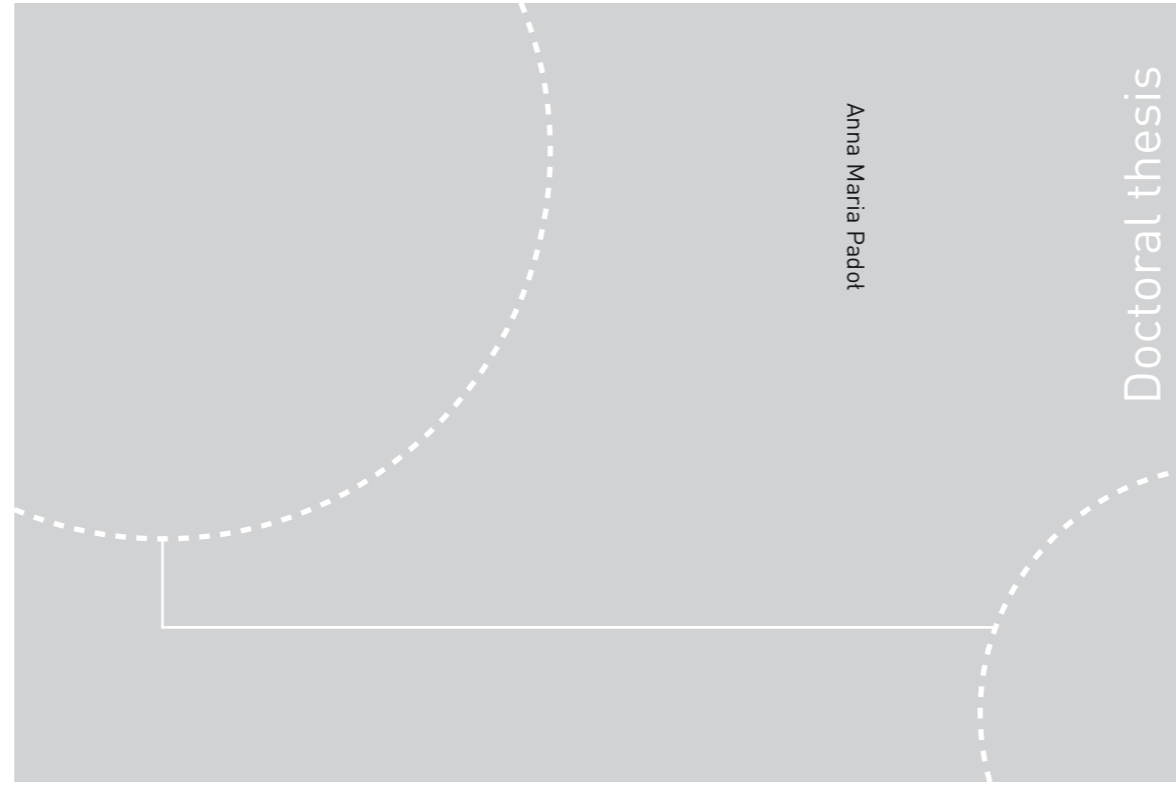


ISBN 978-82-326-1456-1 (printed ver.)
ISBN 978-82-326-1457-8 (electronic ver.)
ISSN 1503-8181



Doctoral theses at NTNU, 2016:59

Anna Maria Padot

Influence of oligoguluronates on alginate gelation and on alginate gel properties

NTNU
Norwegian University of
Science and Technology
Thesis for the Degree of
Philosophiae Doctor
Faculty of Natural Sciences and Technology
Department of Physics

Doctoral theses at NTNU, 2016:59

 NTNU

 **NTNU**
Norwegian University of
Science and Technology

 **NTNU**
Norwegian University of
Science and Technology

Anna Maria Padot

Influence of oligoguluronates on alginate gelation and on alginate gel properties

Thesis for the Degree of Philosophiae Doctor

Trondheim, March 2016

Norwegian University of Science and Technology
Faculty of Natural Sciences and Technology
Department of Physics



Norwegian University of
Science and Technology

NTNU
Norwegian University of Science and Technology

Thesis for the Degree of Philosophiae Doctor

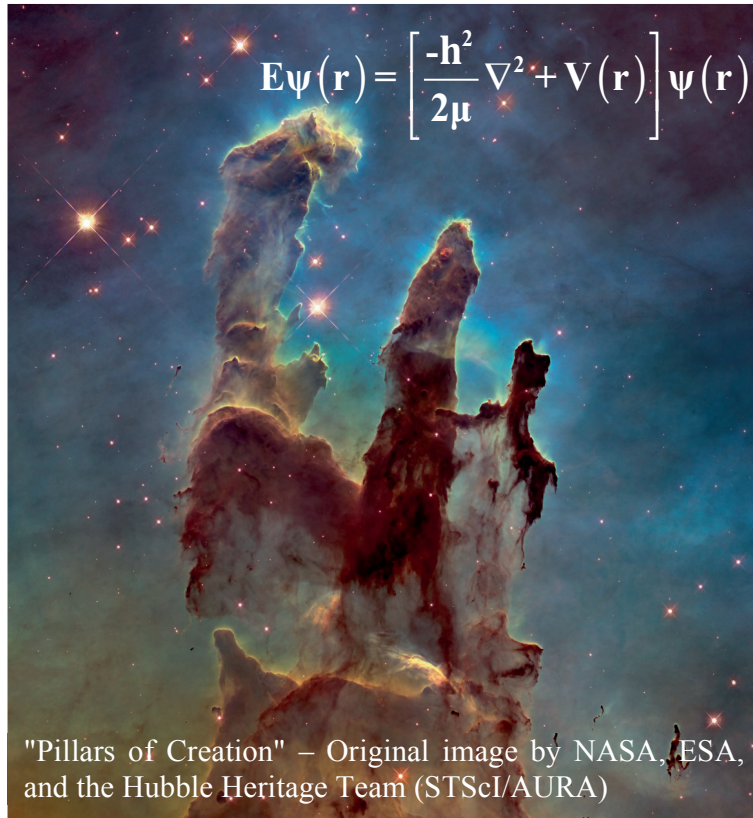
Faculty of Natural Sciences and Technology
Department of Physics

© Anna Maria Padot

ISBN 978-82-326-1456-1 (printed ver.)
ISBN 978-82-326-1457-8 (electronic ver.)
ISSN 1503-8181

Doctoral theses at NTNU, 2016:59

Printed by NTNU Grafisk senter



Excerpt of life of my high school class:

Physics teacher walking in the class, with some kind of inspiration of his own thoughts. He looks like mix-up of Albert Einstein and polish composer Fryderyk Chopin:

J.M: Hydrogen is very important, (pause)

J.M: In the beginning there was hydrogen

V: In the beginning there was the Word

Quietness in the class, J.M is looking at the end of the room searching who said it. Not finding but still answering after a moment.

J.M: You have old data man

J.M: mgr. Jerzy Mazur (physics teacher)

V: voice of one of boy classmates literally from last desk in the class

Preface

This thesis is submitted by Anna Maria Padol to the Norwegian University of Science and Technology (NTNU) for partial fulfillment of the requirements for the Philosophiae Doctor degree (PhD). The work was carried out at the Department of Physics, NTNU, Trondheim. The work was financed by the Norwegian Research Council (contract number 1826595/I40), which is highly acknowledged.

Acknowledgements

I would like to thank my first supervisor Bjørn Torger Stokke for introducing me to the field of alginates. I would also like to thank my second supervisor Arne Mikkelsen for all the help I got – thank you that your office door was always open for me. I am also grateful to my opponents – Anna-Lena Kjøniksen and Stephen Ernst Harding – thank you for going through my thesis and defence.

I would like to acknowledge help of my co-authors Yoshiaki Yuguchi, Ami Hasegawa and Kurt Ingar Draget for work we did together. Special thanks to my co-author and co-worker

Gjertrud Maurstad for teaching me how to write scientific papers, how to work in a lab and for all the support you gave me all those years.

I also want to share my gratitude to Kristin Høydalsvik for introducing me to SAXS technique and for all the support.

I would like to thank Erik Wahlström, Magni Rise Stølen, Julie Hansen, Mikael Lindgren, Catharina de Lange Davies and Justin Wells, I could not have end it without your help.

I would like to thank my co-workers Kristin Elisabeth, Gunvor, Lize, Rajesh, Tatyana, Astrid, Kristin, Nori, Sravani, Igor and Mercy for the time we had, eating lunches together and sharing both good and bad moments. Special thanks also to Kamila Gawel for sharing your scientific experience with me.

Furthermore, I would like to thank all my friends which I have met in Trondheim but which are not my co-workers: Anna Stroisz, Kasia and Dawid Szewczyk, Andreas Klarstrom, Gyrid Gunnes, Hege Sandnes, Maia Økland and Marita Syversen thank you for being there for me. Special thanks to Lars Erik Walle, Neelam Panjwani and Panjwani team, thank you for letting me to be a part of your worlds.

The last but not the least is the group of people who had not been here physically but have been around me all the time although living thousands of kilometres away:

Life without best friends would be empty. I am lucky to have you: Efcia, Marta, Kama and Pawel. Thank you for all the skype calls when needed, for all the support, for being in my life even when I wasn't in Kraków. You never let me feel alone or that I am away. And thank you for much more than that, words cannot describe all the goodness you brought to my life.

The most important element of human life is family, and I am lucky to have the greatest one. I would like to thank my Parents – Urszula and Roman Padołowie – for creating me the person who I am. My Father for showing me how diverse world is and teaching me to think. You created in me the ideal state of Plato. I thank my Mother for giving me more technical approach to everything, teaching me how the forms work and thus creating Plato's state of form in me. But that wouldn't be all me if not my Brother Piotr and your unwavering trust in me which made me capable to move mountains. That's You who make me always want to be scientist like Maria Skłodowska-Curie. To my Nephew Michał. Thank you for always being there and for being my small one.

And I would like to “finnish” my acknowledgements by thanking my Finnish family. To Love of my life Mikko-Heikki for standing by my side during this journey. For all the support, love, and dreams you gave me. Thank you, Hilikka and Markku for being such warm spirits and supporting people as you are.

Table of content

	Preface	iii
	Acknowledgements	iii
	Table of content	v
	List of papers	vii
	Contributions to papers	ix
	Important abbreviations	xi
	Motivation for the thesis	xiii
1.	Introduction	1
1.1	Alginate	1
1.1.1	Origin and applications	1
1.1.2	Chemical structure	2
1.2	Oligoguluronates	2
1.3	Gelation of Alginate	4
1.3.1	Ion binding	4
1.3.2	Alginic acid gels	4
1.3.3	Iontropic gelation	5
1.3.4	Zipper mechanism	5
1.3.5	Gelation techniques	6
	Diffusion technique	6
	In-situ technique	6
1.4	Parameters governing gelation	6
1.4.1	Molecular weight of alginate	7
	Number averaged molecular weight M_n	7
	Weight averaged molecular weight M_w	7
1.4.2	Degree of polymerization (DP_n)	7
1.4.3	Guluronic content (F_G) and mannuronic content (F_M)	8
1.4.4	Average length of G-blocks larger than one unit ($N_{G>1}$)	8
1.4.5	Intrinsic viscosity	8
1.4.6	Fractional saturation	9
2	Measurements techniques	11
2.1	Dynamic light scattering (DLS)	12
2.1.1	Instrumental setup	12
2.1.2	Analysis of the correlation data	14
2.1.3	Gelation threshold features	15
2.2	Nanoindentation	18
2.2.1	Instrumental setup	18
2.2.2	Force-distance curves	19
2.2.3	Young's modulus (E)	20
2.2.4	Hertz model for spherical indenter	21

2.3	Small angle X-ray scattering (SAXS)	23
2.3.1	Principle of scattering in a solution	24
2.3.2	Description of the SAXS instruments	25
	Beamline BL-10C, Photon Factory, Tsukuba, Japan	25
	Beamline BL45XU, RIKEN Harima Institute SPring-8 Center	28
2.3.3	Measurement geometry	28
2.3.4	How to analyze the results	29
	The cross-sectional Guinier plots and cross-sectional radius of gyration	29
	Kratky plots	30
	Kratky plots for a broken rod-like model	30
2.4	Rheology	32
2.4.1	Instrumental setup	32
2.4.2	Shear and loss modulus	33
2.4.3	Analysing G' and G'' during gelling	34
3.	Sample preparation	35
3.1	Samples	35
3.1.1	Alginate	35
3.1.2	Oligoguluronates	37
3.1.3	Preparing of stock solutions	37
	CaEGTA stock solution	37
	Decrease of pH by slowly hydrolyzing lactone	38
3.2	Preparing samples for DLS measurements	38
3.2.1	Alginate and oligoguluronate stock solution	38
3.2.2	CaEGTA stock solution for DLS	39
3.2.3	Preparing sample for DLS measurements	39
3.2.4	Saturations and reduced concentration for samples used during DLS measurements	39
3.3	Preparing samples for nanoindentation	39
3.3.1	Alginate and oligoguluronate stock solution	39
3.3.2	CaEGTA stock solution for nanoindentation	39
3.3.3	Preparing sample for nanoindentation measurements	39
3.3.5	Issues with sample preparation	40
3.3.6	Alginate hydrogel samples – final preparation	40
3.3.7	Saturations and reduced concentration for samples used during nanoindentation measurements	41
3.4	Preparing samples for SAXS	42
3.4.1	Alginate and oligoguluronate stock solutions	42
3.4.2	CaEGTA stock solution	42
3.4.3	Preparing sample for SAXS measurements	42
3.4.4	Saturations and reduced concentration for samples used during SAXS measurements	42
3.5	Preparing samples for rheology	43

3.5.1	Alginate gels prepared at 19.3 mM CaEGTA with final pH 3.44	43
3.5.1.1	Stock solutions	43
3.5.1.2	Preparing sample for rheology measurements	43
3.5.2	Alginate gels prepared at 20 mM CaEGTA with final pH 4.0	44
3.5.2.1	Stock solutions	44
3.5.2.2	Preparing sample for rheology measurements	44
3.5.3	Alginate gels prepared at 40 mM CaEGTA with final pH 4.0	44
3.5.3.1	Stock solutions	44
3.5.3.2	Preparing sample for rheology measurements	44
3.5.4	Issues with sample preparation	44
3.5.5	Saturations and reduced concentration for samples used during rheology measurements	46
4.	Rheology results	47
4.1	Alginate gels prepared at 19.3 mM CaEGTA with final pH 3.44	47
4.2	Alginate gels prepared at 20 mM CaEGTA with final pH 4.0	48
4.3	Alginate gels prepared at 40 mM CaEGTA with final pH 4.0	50
5.	Summary of results	51
5.1	Paper I: Delaying cluster growth of ionotropic induced alginate gelation by oligoguluronate.	52
5.2	Paper II: Effects of added oligoguluronate on mechanical properties of Ca-alginate-oligoguluronate hydrogels depend on chain length of the alginate.	55
5.3	Paper III: Local structure of Ca induced hydrogels of alginate – oligoguluronate blends.	57
	Static measurements	58
	Dynamic measurements (time-resolved SAXS)	59
5.4	Rheology	60
	Discrepancy with nanoindentation	60
	References	61

List of papers

I.	Delaying cluster growth of ionotropic induced alginate gelation by oligoguluronate. A.M.Padoł, G.Maurstad, K.I.Draget, B.T.Stokke, Carbohydrate Polymers Vol.133, 2015, 126–134
II.	Effects of added oligoguluronate on mechanical properties of Ca-alginate-oligoguluronate hydrogels depend on chain length of the alginate. A.M.Padoł, K.I.Draget, B.T.Stokke - submitted to Carbohydrate Polymers
III.	Local structure of Ca induced hydrogels of alginate – oligoguluronate blends, Y.Yuguchi, A.Hasegawa, A.M.Padoł, K.I.Draget, B.T.Stokke

Contributions to papers

I.	<p style="text-align: center;">Delaying cluster growth of ionotropic induced alginate gelation by oligoguluronate.</p> <p>Anna Maria Padol: Has prepared all samples and carried all measurements and all data analysis. Drafted a first version of the paper, responsible for about ½ of the final draft of paper.</p> <p>Gjertrud Maurstad: Introduction to the first measurements and assisted with initial data analysis.</p> <p>Kurt Ingar Draget: Extraction of oligoguluronates and its characterization.</p> <p>Bjørn Torger Stokke: Writing of the program in IDL to analyse data. Follow up of all data analysis. Responsible for about ½ of the final draft of the paper.</p> <p>All authors contributed to the revisions and approved the final version of the paper</p>
II.	<p style="text-align: center;">Effects of added oligoguluronate on mechanical properties of Ca - alginate - oligoguluronate hydrogels depend on chain length of the alginate.</p> <p>Anna Maria Padol: All sample preparations, all measurements, all data analysis. Drafted an initial version of the paper.</p> <p>Kurt Ingar Draget: Extraction of oligoguluronates, and its characterization.</p> <p>Bjørn Torger Stokke: Final conclusion of data. Provided interpretation of data in terms of network parameters. Final draft of paper. Follow up of all versions of paper.</p> <p>All authors contributed to the revisions approved the final version of the paper</p>
III.	<p style="text-align: center;">Local structure of Ca induced hydrogels of alginate – oligoguluronate blends.</p> <p>Yoshiaki Yuguchi: All sample preparations, all measurements, all data analysis. Contributed to writing the manuscript.</p> <p>Ami Hasegawa: All sample preparations, all measurements, all data analysis.</p> <p>Anna Maria Padol: Establishing experimental preparation protocol. Drafted the materials section in paper.</p> <p>Kurt Ingar Draget: Extraction of oligoguluronates, and its characterization. Introduction section in paper.</p> <p>Bjørn Torger Stokke: Abstract and conclusions section in paper. Final draft of paper.</p> <p>All authors contributed to the revisions and approved the final version of the manuscript</p>

Important abbreviations

AFM	atomic force microscopy
$\text{Alg}_X^Y\text{-}[c]$	alginate samples, where the numerical values of X depict the M_w (in kg/mol), Y depicts F_G of the actual sample and c is concentration of sample in (mg/ml) when denoted.
CaEDTA	Ca - ethylenediaminetetraacetic acid
CaEGTA	Ca - ethylene glycol tetraacetic acid
$c[\eta]$	reduced concentration
DLS	dynamic light scattering
DPn	number-average degree of polymerization
EGTA	ethylene glycol tetraacetic acid
F_G	guluronic acid content
F_M	mannuronic acid content
F_{sat}	fractional saturation
GDL	d-gluconic acid δ -lactone
ICF	intensity–time correlation function
K_d	dissociation constants
M_w	weight averaged molecular weight
$N_{G>1}$	average length of G-blocks larger than one unit
NIBS	non-invasive backscatter detection mode
NMR	nuclear magnetic resonance
$\text{oligoG}_X^Y\text{-}[c]$	oligogulonate samples, where the numerical values of X depicts F_G , Y depicts the M_w (in kg/mol) and c is concentration of actual sample in (mg/ml) when denoted.
pK_a	acid dissociation constants
SAXES	small-angle X-ray equipment for solutions
SAXS	small Angle X-ray scattering
SEC-MALLS	size exclusion chromatography with multiple laser light scattering

Motivation for the thesis

Alginates are very abundant material in nature, and nowadays there are also possibilities of producing tailormade alginate in laboratory. Further, ionotropic alginate hydrogels have found applications in many fields. Preparation of such material is in this case a key technology. There is however still a need to understand how to better control its valuable properties. If we understand how to control its gelation kinetics and how to yield mechanical properties of alginate hydrogels, we could fully exploit the properties of alginate.

Oligoguluronates, which chemically are alginates, opens possibility of such control. Moreover there is no need for additional additives, since the chemical structure of the compounds are the same. From previous studies it is known that oligoguluronates open the possibility of controlling the gelling kinetics, gel strength, viscosity, equilibrium properties, and syneresis. Thus mixing oligoguluronates with a high M_w alginate at different mixing ratios opens such possibility [Jorgensen et al. *Biomacromolecules* 8 (2007) p. 2388; Draget et al. *Applied Microbiology and Biotechnology* 31 (1989) p. 79.]

1. Introduction

1.1 Alginate

1.1.1 Origin and application

Alginate was first described and patented by the British chemist E.C.C. Stanford in 1881 [1]. Between 1929-1932 three different groups (Nelson and Cretcher [2-4]; Bird and Haas [5]; and Miwa [6]) found that alginate is built up from d-mannuronic acid and till 1955 it was believed that alginate was a homopolymer. In 1955 Fischer and Dörfel introduced l-guluronic acid as a part of alginate [7-10]. Finding that alginate is a copolymer of mannuronic and guluronic acid introduced the need for techniques to examine chemical composition of alginate. These tasks were mainly done by Haug and his coworkers [8].

Alginate is very abundant in nature [9]. It naturally occurs as cell wall component of brown algae up to 40% of its dry matter [8, 9]. Alginate in seaweed is playing role in mechanical stability and flexibility of the algae plant [8, 9]. It is located in intercellular matrix as gel containing certain ions. Alginate can also be produced by soil bacteria like *Azotobacter*

vinelandii and several of *Pseudomonas* species [9, 11, 12]. In addition to the selection of alginate with sequences obtainable from natural sources, tailormade alginate sequences can be manufactured by ex vivo enzymatic modification applying mannuronan C5 epimerases converting mannuronate to guluronate residues [12-14]. Up till date all commercially available alginates are of algae origin [9, 15].

Alginate is mostly known for its gelling ability, and this has paved a way to different industries. Within the food area, alginates are used as thickeners, stabilizers, film formers and gelling agents [9, 16]. Exploiting the mild ionotropic gelation of alginates, combined with alginate's biocompatibility and nontoxicity, have paved the way to biomedical and pharmaceutical applications, such as functionality for cell entrapment, immunological isolation barriers between implant and host, and for controlled drug delivery [17-19].

1.1.2 Chemical structure

Alginate is a family of linear copolymers of (1→4) glycosidically linked β-D-mannuronic acid and α-L-guluronic acid designed later as M and G [9, 20]. Originally alginate is biosynthesized as homopolymers of β-D-mannuronic acid and in post polymerization step by C5 epimerase it is converted to α-L-guluronic acid. The composition and sequential arrangements of monosaccharide fractions differ with alginate source (species, plant, part from which it is extracted (stem, leaf) or even harvesting season) [7, 9]. Mannuronic and guluronic acids residues are usually arranged in alginate in a block structure. There are three different ways to arrange this block structure. When mannuronic acid residues are neighbouring with itself it is called a M-block, and when guluronic acid residues are neighbouring with its own residues it is called a G-block. The third possible composition is a structure of strictly alternating guluronic and mannuronic acids residues called MG-block (Fig 1.1.1) [7, 9]. The M-residues in M-blocks are linked by diequatorial linkages creating flat-ribbon like structure [9, 16, 21]. G-blocks in G-residues are connected by diaxial linkages, creating buckled, shorter and a more rigid-like structure [9, 16, 21]. Whereas in MG-block, coexisting equatorial-axial and axial-equatorial linkages give its high flexibility [16]. Stiffness of alginate blocks increase in the order MG<MM<GG [22].

1.2 Oligoguluronates

Oligoguluronates are almost pure α-L-guluronic acid which can be obtained with its G-content above 90% and number-average degree of polymerization DP_n around 20 [23]. They are isolated by acid hydrolysis and selective precipitation from high molecular weight alginate [7, 20]. As they are almost entirely build from G-blocks they compete for cations with G-blocks belonging to alginate chain. However due to lack of elastically active segments they are not able to create gel-like structures [9, 23, 24]. In this text to distinguish α-L-guluronic acid residues blocks, by oligoguluronates we will call the one which do not

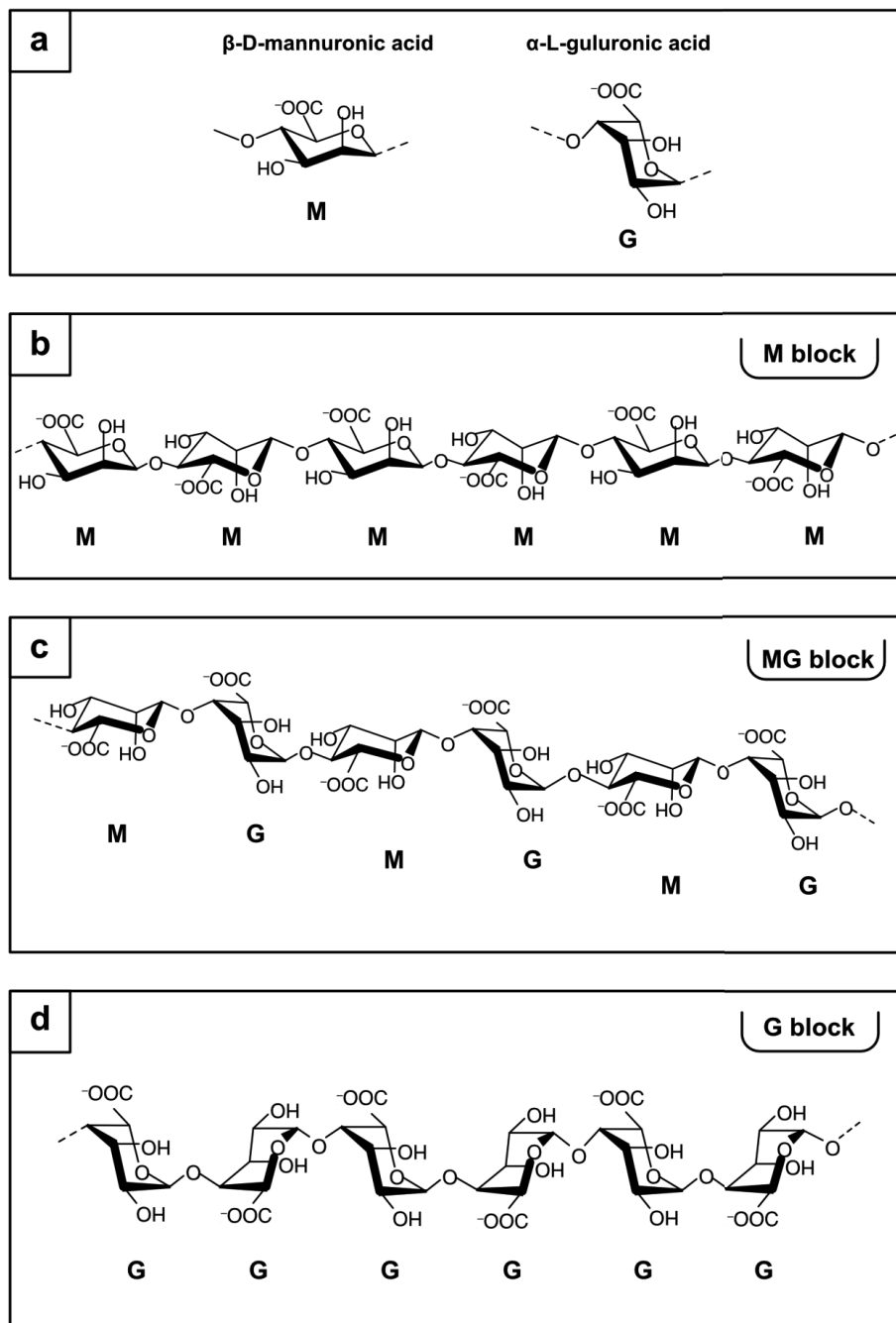


Fig. 1.1.1 Chemical structure of alginate. (a) conformation of β -D-mannuronic acid and α -L-guluronic acid (b) M-block composition (c) MG-block composition (d) G-block composition

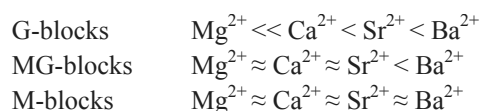
belong to longer alginate chain, whereas by G-blocks will be mean one which are part of longer alginate chain

1.3 Gelation of alginate

With the presence of e.g. Ca^{2+} ions in the solution, G-blocks of alginate may form egg-box-like structures and further hydrogels. Ca^{2+} is most often used (also in this thesis), but other divalent or multivalent cations may be used. This ion-binding of cations to alginate molecules in solution will first be discussed.

1.3.1 Ion binding

Alginate salts of magnesium, ammonium and alkali-metals are soluble in water [24], and after addition of multivalent cations like Al^{3+} and Fe^{3+} or divalent cations like Ca^{2+} , Ba^{2+} , Sr^{2+} , Mn^{2+} , Cu^{2+} , Pb^{2+} [16, 21, 24] they form gels. The binding of ions depends on alginate composition and affinity towards the multivalent cations. It has been shown by Smidsrød [25] that binding strength of cations towards uronic residues is as follows:



The differences in selectivity between similar cations suggest that interactions between alginate and cations are not purely electrostatic and that a complexation of cations related to G-block residue is taking place.

1.3.2 Alginic acid gels

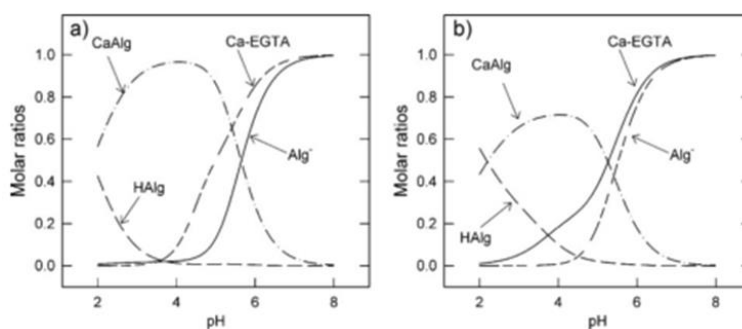


Fig. 1.3.1 Figure presents various molar ratios of CaAlg, protonated alginate (HAAlg), CaEGTA and Alg^- vs calculated pH for a) 15mM Alg, 30mM CaEGTA b) 40mM Alg, 30mM CaEGTA. Reproduced with permission from John Wiley and Sons: Macromolecular Symposia 2010, p. 345-353 (Fig. 2) [23].

The pK_a values of uronic acid residues of alginate were found to be 3.38 and 3.65 for mannuronic and guluronic acid residues, respectively [26]. By slowly lowering pH under these pK_a values, controlled release of protons may lead to formation of alginic acid gels [8, 9, 27, 28]. Alginic acid gels are equilibrium gels stabilized by hydrogen bonding [8, 27, 29]. According to calculations of Sletmoen et al. 2010 [23], reducing the pH below 4 causes increase of the protonated form of alginate (HAlg), and subsequently decrease of the Ca-alginate form fraction (CaAlg), see Figure 1.3.1. At such conditions there exists a blend of acid-gelation mechanism and ionotropic induced gelation mechanism.

1.3.3 Ionotropic gelation

According to Sletmoen et al. 2010 [23] at pH=4 most alginate exists in the Ca-form with protonated alginate not being a significant fraction. When solution of alginate is mixed with divalent cations e.g. Ca^{2+} , Ca^{2+} cations preferentially bind to G-blocks. The reason for this is that the diaxial glycosidic linkages of the G-blocks create cavity-like structures, which can be occupied by cation (Fig. 1.3.2). Due to the resemblance it is called an egg-box-model [30, 31]. In the egg-box model each cation is interacting with four guluronic acid residues, two of them being a part of one alginate chain and other two belonging to another alginate chain.

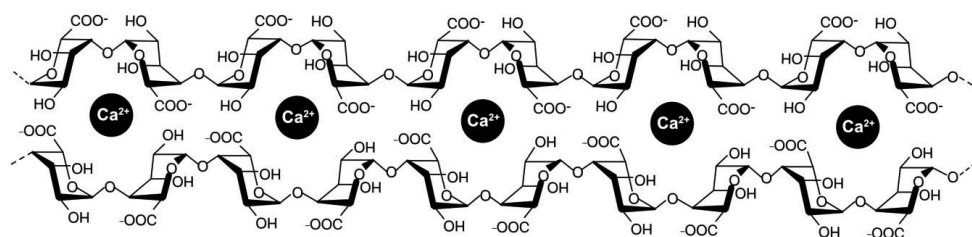


Fig. 1.3.2 Structure of egg-box model

1.3.4 Zipper mechanism

Creation of junction zones between G-blocks and Ca^{2+} can be explained by near-neighbour autocoperative process, where the binding of the first divalent cation is entropically unfavourable in comparison to binding of the following cations [8, 9].

1.3.5 Gelation techniques

Introduction of cations into the alginate solution may be done by two different techniques:

Diffusion technique

In the diffusion technique the cations are introduced by diffusion from an outer reservoir into the alginate solution. The method is rapid and characterized by inhomogeneous distribution of alginate [9, 32].

In-situ technique

Cation Ca^{2+} can be introduced to the solution of alginate by means of inactive form in CaEDTA (Ca-ethylenediaminetetraacetic acid), CaEGTA (Ca-ethylene glycol tetraacetic acid) or CaCO_3 . In this research we used CaEGTA, and there is no reaction between alginate and Ca ions as long as pH of solution is kept over $\text{pH} = 5$. Decrease of pH is achieved and controlled by use of slowly hydrolysing lactone d-gluconic acid δ -lactone (GDL). GDL is freshly dissolved and mixed with CaEGTA-alginate solution as described by Stokke et al. 2000 [31]. By varying the ratio of Ca^{2+} to GDL, this technique gives the opportunity to control the speed of gelation and the final pH of the gels. Assuring slow release of Ca^{2+} leads to homogenous distribution of alginate in gel [8, 9, 31].

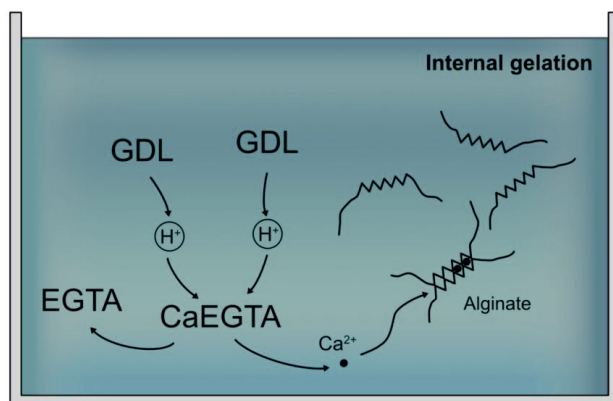


Fig. 1.3.3 Schematic picture of internal gelation technique using EGTA

1.4 Parameters governing gelation

Many different parameters affect the gelation properties of alginate, both parameters describing the alginate itself and properties and contents of the solution. Here we present the parameters varied in the experiments of this thesis.

1.4.1 Molecular weight of alginate

Alginate samples are polydisperse in length chain, which will make them polydisperse in molecular weight. Due to this the molecular weight is given as the average molecular weight over whole distribution of molecular weights. The most commonly used are the number average molecular weight and the weight average molecular weight [9].

Number averaged molecular weight M_n

$$M_n = \frac{\sum_i N_i M_i}{\sum_i N_i} \quad (1.4.1)$$

Weight averaged molecular weight M_w

$$M_w = \frac{\sum_i w_i M_i}{\sum_i w_i} = \frac{\sum_i N_i M_i^2}{\sum_i N_i M_i} \quad (1.4.2)$$

Where: N_i is the number of molecules with molecular weight M_i , w_i is weight of molecules with molecular weight M_i and $w_i = N_i M_i$

The ratio of M_w / M_n is referred to as the polydispersity index (PI). In our case M_n and M_w were determined by size exclusion chromatography with multiple laser light scattering (SEC-MALLS) by Department of Biotechnology NTNU.

For a monodisperse molecule population $PI = 1$, whereas for a polydisperse one $PI > 1$. Typical values of polydispersity indices for commercial alginates are from 1.5 to 3.0 [33].

Alginates with low molecular weight have a high content of short G-blocks. As these do not take part in the gel-network formation, low molecular weight alginate do not contribute to the gel strength [9].

1.4.2 Degree of polymerization (DP_n)

The degree of polymerization is the number of monomeric units in a macromolecule. Number-average degree of polymerization is given by $DP_n = M_n / M_0$, where M_0 is the molecular weight of the monomer unit.

1.4.3 Guluronic acid content (F_G) and mannuronic acid content (F_M)

Generally alginates with high guluronic content yield strong and brittle gels [9]. Due to that it is important to know the guluronic and the mannuronic content of the sample. The content of each residue is given as a number from 0 to 1. So for example $F_G=0.66$ means that the sample is 66% made from G residues. Analogically $F_M=1-F_G$. It is also possible to characterise the content of diads (F_{GG} , F_{GM} , F_{MM}) and triads (F_{GGG} , F_{GGM} , F_{GMM} , F_{MGM} , F_{MMG} , F_{MGG} , F_{GMG} , F_{MMM}) in the sample. Knowing the detailed structure of the alginate becomes possible by the use of high-resolution proton and carbon nuclear magnetic resonance (NMR) spectroscopy as described by Grasdalen et al. [34, 35].

The content of guluronic residues differs in a range of 0.2-0.85 for algal alginate and 0.1-0.95 for alginate from *Azotobacter*, whereas alginate from *Pseudomonas* is purely mannuronic [9, 21].

1.4.4 Average length of G-blocks larger than one unit ($N_{G>1}$)

Having e.g. $F_G=0.5$ means that half of the alginate chain is made from G-residues and half from M-residues. This creates the question how the residues are arranged along the chain. The two most extreme cases are:

- Two blocks, one of M and the other of G residues: MMMMMMMGGGGGG
- Strictly alternating structure: MGMGMGMGMGMGM

All the other possibilities are interjacent of those two. As MG-blocks are much more flexible than G-blocks, knowing only the content of M or G is not enough. $N_{G>1}$ is the average length of G-blocks, and can be calculated by:

$$N_{G>1} = \frac{F_G - F_{MGM}}{F_{GGM}} \quad (1.4.3)$$

The minimum consecutive number of guluronic acid residues needed to support Ca^{2+} mediated junctions is reported to be 8 ± 2 [36]. For Sr^{2+} mediated junction it is 3 [36].

1.4.5 Intrinsic viscosity

The polymer intrinsic viscosity $[\eta]$ describes the substances ability to induce viscosity in solution. It is defined as:

$$[\eta] = \lim_{c \rightarrow 0} \frac{1}{c} \left(\frac{\eta_s - \eta_0}{\eta_0} \right) \quad (1.4.4)$$

where: η_s is solution viscosity, η_0 is solvent viscosity and c is polymer concentration. It is dependent on the polymer conformation. The intrinsic viscosity may be described by the Mark-Houwink-Sakurada equation:

$$[\eta] = K \cdot \overline{M}_v^a \quad (1.4.5)$$

where: K is a constant, \overline{M}_v is the viscosity average molecular weight, and a is an empirical exponent describing the conformation of the polymer (which increase with increasing chain extension: $a = 0$ for globular proteins and $a = 1.8$ for rods) [9, 21].

For alginate the intrinsic viscosity depends on molecular weight, composition (both content and sequence) and ionic strength of solution. A typical value of for an alginate is $a \approx 1$ (at ionic strength of 0.1 mM) [21].

1.4.6 Fractional saturation

Mannuronic acid residues bind Ca^{2+} with dissociation constants $K_d = 2 \times 10^{-4}$ M, whereas for guluronic acid residues $K_d = 1 \times 10^{-3}$ M as used by Jorgensen et al. [24]. As the dissociation constant of Ca-guluronic acid complexes is much larger than Ca-mannuronic acid complexes, binding of Ca^{2+} to mannuronic acid may be ignored. The fractional saturation of guluronic residues by calcium can be calculated from the equation:

$$F_{SAT} = \frac{[\text{Ca}^{2+}] Z_{Ca}}{[G] Z_G} \quad (1.4.6)$$

where: $[\text{Ca}^{2+}]$ is the concentration of calcium, $[G]$ is the concentration of guluronic acid residues, Z_{Ca} is the valence of Ca^{2+} and Z_G is the valence of guluronic acid residues ($Z_{Ca}=2$ and $Z_G=1$).

There are reported three ranges of saturations in this case [37-39]:

For $F_{SAT} < 0.5$ gelation does not occur, however creation of monocomplexes (Fig. 1.4.1.b) can take place. When $F_{SAT} = 0.5$, there is exactly one calcium cation for four guluronic acid residues in the solution. As can be seen in Fig.1.4.1.c that is exactly what would be needed to create egg-box dimers in the whole solution. In range $0.5 < F_{SAT} < 1.2$ dimers will prevail. If the saturation of sample will increase over $F_{SAT} > 1.2$ lateral association of egg-box dimers into multimers will take place Fig.1.4.1.d.

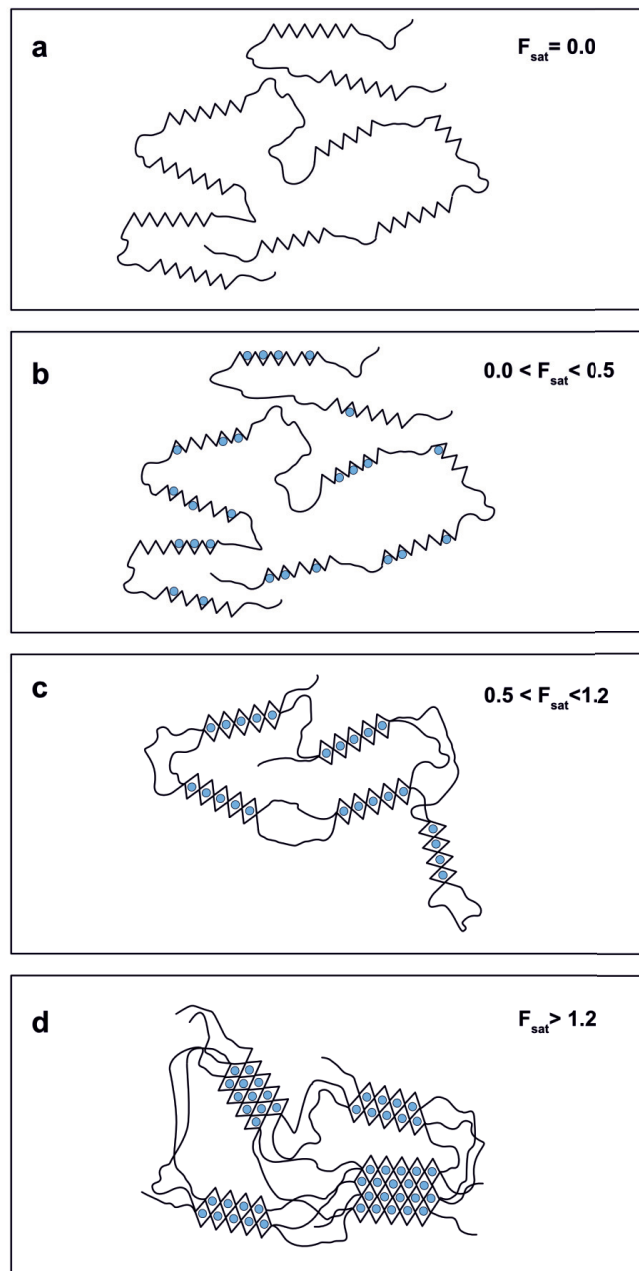


Fig. 1.4.1 Schematic illustration of the effect of various values of the fractional saturation of guluronic residues by calcium. The $\wedge\wedge$ represents G-blocks belonging to alginate chain, — M-blocks, \bullet Ca^{2+} (a) solution of pure alginate (b) formation of monocomplexes upon addition of Ca^{2+} , (c) formation of egg-box dimers, (d) lateral association of egg-box dimers into multimers.

2. Measurements techniques

The three experimental techniques that were used with success during my PhD-work are dynamic light scattering, nanoindentation and small angle X-ray scattering. An introduction to these methods with focus on applications used in the papers included in my thesis is given in the following. I also spent long time on rheology measurements on gelling alginate samples (without oligoguluronates). Results from this method are not included in any paper for the thesis, but a short introduction to this method is included in this chapter and the results are presented in a chapter 4. I also have spent months doing measurements by atomic force microscopy (AFM). I have also tested a various number of different sample preparation for AFM that is not presented here. Unfortunately AFM provides only few and invaluable results and are thus not presented. Further, measurements done by microindentation were unreproducible and unfortunately did not yield any useful information and are not documented. Samples measured by microindentation were prepared in the same way as for nanoindentation.

2.1 Dynamic light scattering (DLS)

In dynamic light scattering (DLS) the intensity of the scattered laser light from macromolecules in a solution is measured as function of time. The intensity variation has shorter characteristic times the smaller the molecules are. This fluctuation is due to the fact that the molecules in solutions are undergoing Brownian motion and the distance between the molecules is constantly changing with time. The scattered light from different molecules then interferes either constructive or destructive. This means that the scattered intensity contains information about the time scale of movement of the molecules and thus the size of the molecules. The characteristic time of the Brownian motion will be inverse proportional to the translational diffusion coefficient, D_T , of the biopolymers.

The intensity of the scattered light at a certain angle is measured as function of time, $I(t)$. The correlation function $G(\tau)$ is the time average of the product of intensity I at time t and the intensity at a certain time $t + \tau$:

$$G(q, \tau) = \langle I(t) I(t + \tau) \rangle \quad (2.1.1)$$

Here q is the wave vector defined by

$$q = \frac{4\pi n_0}{\lambda} \sin\left(\frac{\theta}{2}\right) \quad (2.1.2)$$

where θ is the scattering angle, n_0 is the refractive index of the solvent and λ is the wavelength of the light.

Commercially available autocorrelators measure $I(t)$ and yield the correlation function $G(q, \tau)$.

The aim of using this technique in our study was to check if it is possible to follow up the progress of cluster growth during the gelation process of alginate.

2.1.1 Instrumental setup

The DLS instrument used during the measurements is a Zetasizer Nano instrument (Zetasizer Nano, Malvern instrument, UK).

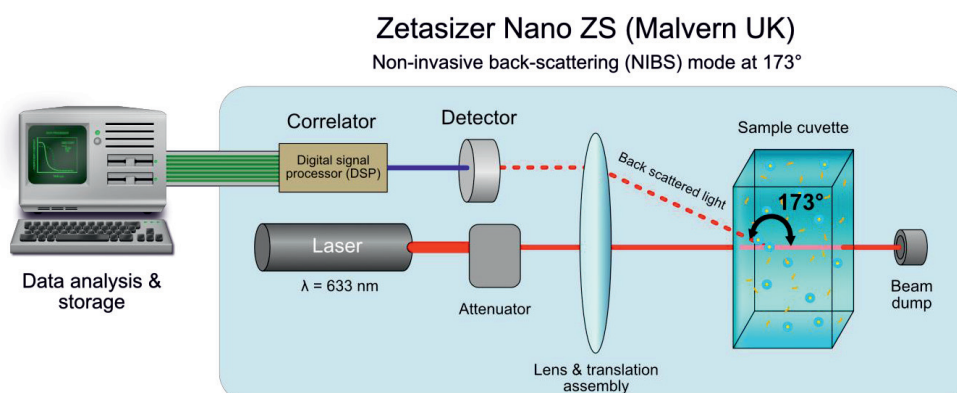


Fig. 2.1.1 Schematic illustration of DLS setup

A monochromatic light beam produced by a helium–neon laser with wavelength 633 nm, passes through an attenuator before reaching the sample. Molecules in the solution scatter light in all directions. The scattered light is measured by a detector. In our studies we use the so-called Non-Invasive Backscatter detection mode (NIBS), in which the detector is set to 173° angle. The advantage of this mode as compared to the forward scattering mode, is that the effect of multiple scattering is reduced. Multiple scattering occurs when light scattered from one particle again is scattered by another particle and so on. As the scattered light passes only through a short length of the sample, the amount of multiple scattering is significantly reduced. This also allows measurement of higher sample concentrations, which is important when measuring a gelling sample. The effect of scattering from dust particles is also reduced due to the fact that such particles mostly scatter light forward.

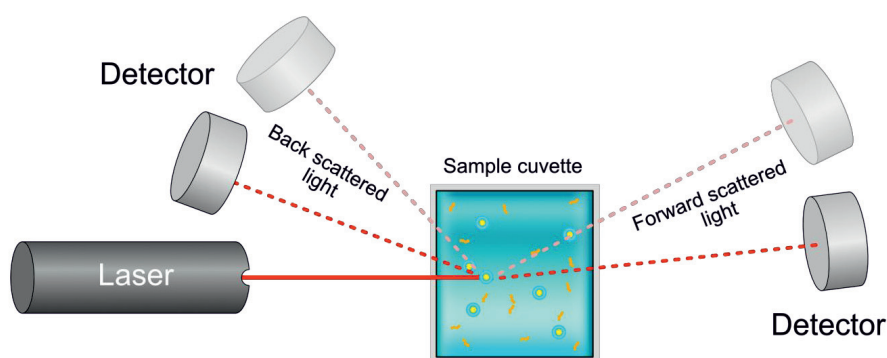


Fig. 2.1.2 Schematic illustration of light scattering on sample

To assure that the detector is not over-saturated or that the signal is not too weak, the attenuator might decrease or increase the intensity of the laser light according to a feedback from the detector. From the detector the signal is sent to the correlator and to the computer (Fig. 2.1.1).

2.1.2 Analysis of the correlation data

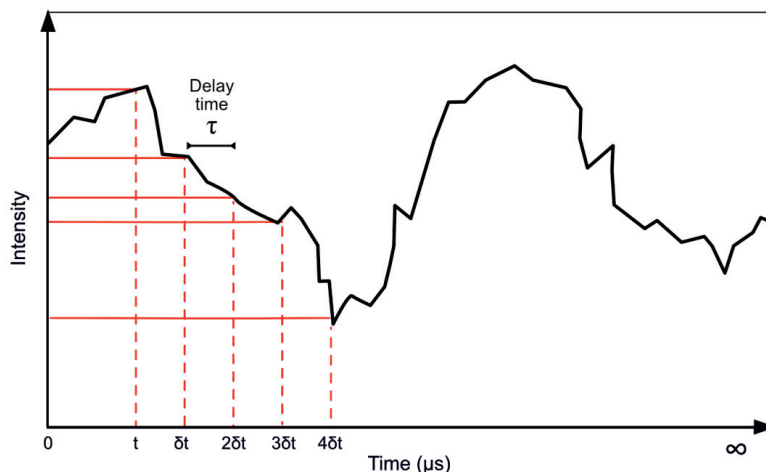


Fig. 2.1.3 Schematic fluctuations of scattered light intensity versus time

The essential part of the DLS-instrument is the autocorrelator, which compares the intensity signal at time t to the intensity at time $t + \tau$. The dimensionless second order autocorrelation function $g^{(2)}(\tau)$ equals

$$g^{(2)}(q, \tau) = \frac{\langle I(t) I(t + \tau) \rangle}{\langle I(t) \rangle^2} \quad (2.1.3)$$

And the first order autocorrelation function $g^{(1)}(\tau)$ is defined by the equation:

$$g^{(2)}(q, \tau) = 1 + g^{(1)}(q, \tau)^2 \quad (2.1.4)$$

A plot of $g^{(1)}(\tau)$ as a function of time τ yields typical curves as shown in Fig. 2.1.4. The green curve shows the correlation for small molecules and the blue for larger molecules. For polydisperse samples the correlation curves will be a sum of decay curves for different molecule sizes, and thus decay more slowly, i.e. the curve will be less steep. The time at which the decay starts is an indication of the mean size of the molecules in the sample.

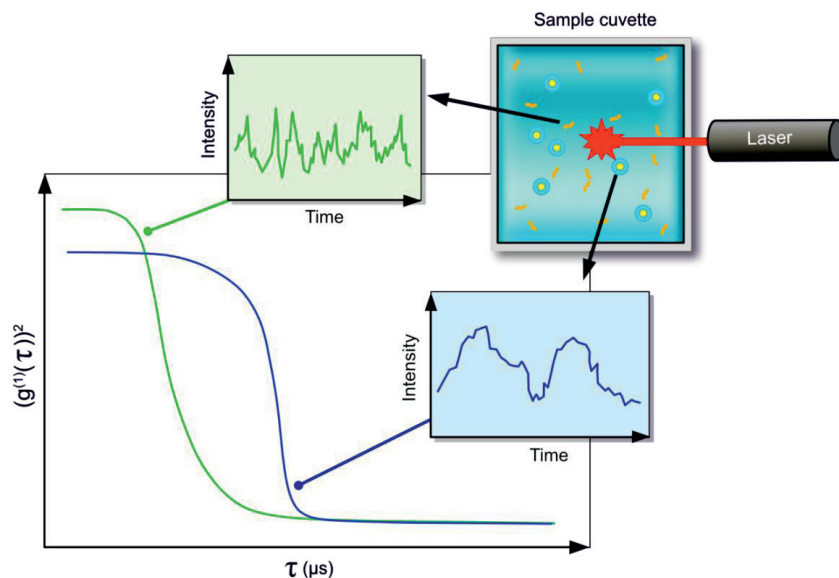


Fig. 2.1.4 Typical correlograms for small (green) and large (blue) particle with small insets of fluctuation in intensity of scattered light as a function of time (accordingly color coded)

If the signal does not change with time, the correlation coefficient $g^{(1)}(\tau)^2$ is equal to 1 and if the signal is not correlated at all, it would give value 0. The signals obtained at short intervals are more correlated than the signals obtained at large intervals.

2.1.3 Gelation threshold features

DLS is a powerful tool to measure the properties of particles in solutions or suspensions. It is especially suitable to observe the transition process from liquid state to gelled state in an alginate solution. Our target was to observe cluster growth of alginate during gelation process. During cluster growth, water is entrapped inside the gel. By weight, most of the hydrogel consists of water entrapped in the three dimensional cross-linked network.

However, as the sol to gel transition is also an ergodicity to nonergodicity transition [40-45], additional disfavours appear and those can be used to distinguish the gelled sample from one which is still gelling. Shibayama et al. proposed [41-45] that the gelation threshold can be characterized by four features:

- (1) the steep increase in the scattering intensity $\langle I \rangle_T$
- (2) a power-law in the intensity-time correlation function (ICF),
- (3) a specific broadening of the distribution function,
- (4) a noticeable lowering of the initial amplitude of ICF.

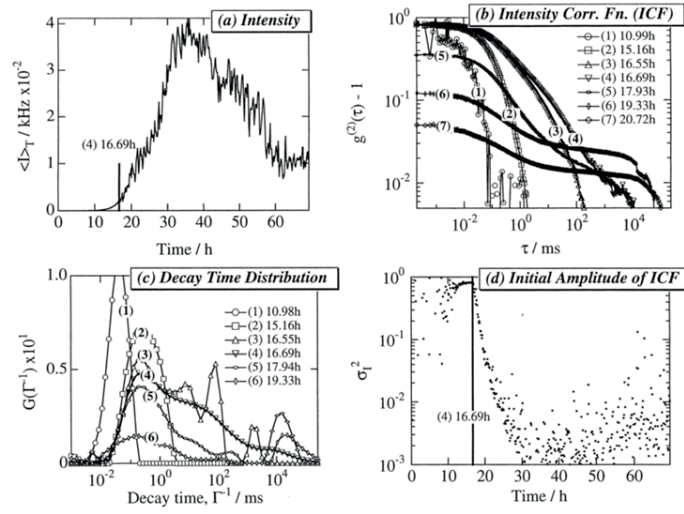


Fig. 2.1.5 Illustration of the four features characterizing the gelation threshold. a) intensity change b) a power-law behavior in ICF c) a characteristic broadening of distribution function, and d) suppression of the initial amplitude of ICF. Reproduced with permission from the Chemical Society of Japan from Bulletin of Chemical Society of Japan (2002) Vol 75, p.641-659 (Fig. 12) [41].

According to feature (2) the gelation threshold can be characterized by a power law behaviour in $g^{(1)}(q,t)$ [41-45]. The ICF can be described by two relaxation processes: a stretched exponential decay process and a power law decay process. In the fitting program to our measurements we used the equation from Maleki et al. [46], which is also similar to the analysis used by others [41, 42, 44, 45, 47] :

$$g^{(1)}(t) = A_f \exp \left[- \left(\frac{t}{\tau_{fe}} \right)^{\beta_f} \right] + \frac{A_s}{\left(1 + \frac{t}{V} \right)^d} \quad (2.1.5)$$

The first term describes the stretched exponential decay process of the fast relaxation mode, associated with disengagement relaxation of individual chains or cluster relaxation. Parameter A_f is the amplitude of fast relaxation mode, τ_{fe} the effective relaxation time and β_f the measure of the width of the distribution of relaxation times where $0 < \beta_f < 1$. The second term in the equation is the slow relaxation mode, for the gelled sample is described by power law behaviour according to earlier mentioned features by Shibayama et al. [41, 43-45]. Parameter A_s is the amplitude of slow relaxation mode and $A_f + A_s = 1$, the variable V indicates at which time the power law tail begins, and d is the power law coefficient.

We use a custom designed program implemented by the Interactive Data Language, ITT Solutions to fit all the parameters using a least square fitting routine. Each file contains data from one day of gelation contain 72 ICF curves. Each ICF curve from the DLS measurement was fitted by me using this program, and an example is shown in Fig. 2.1.6.

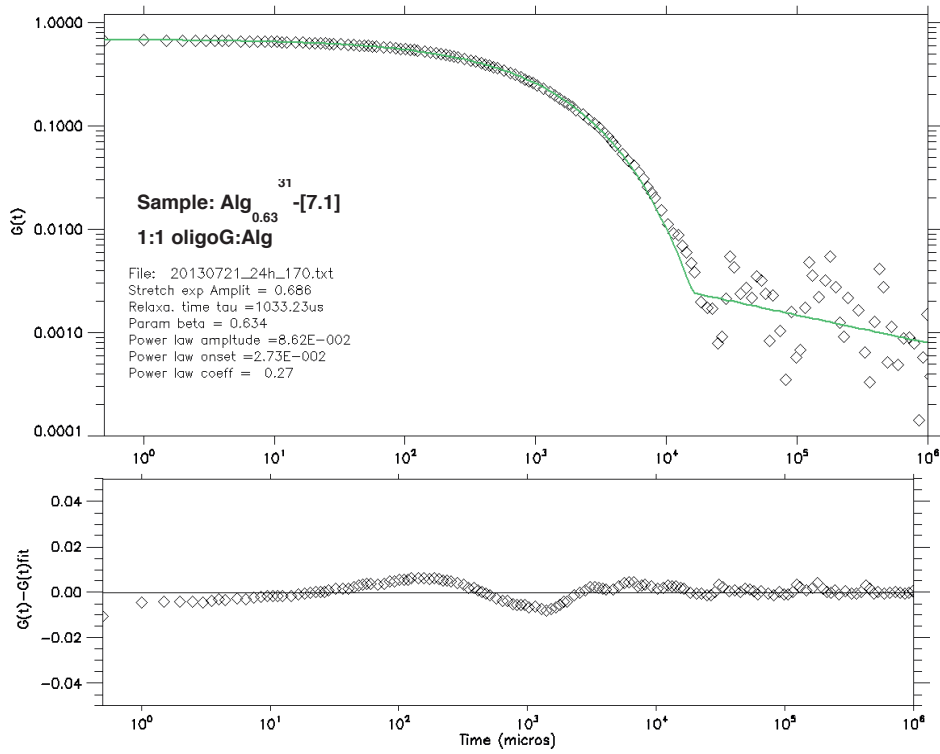


Fig. 2.1.6 Fitting the experimentally determined $g^{(1)}(t)$ ($G(t)$ in the figure) by a least square fitting routine.

All six parameters A_f , τ_{fe} , β_f , A_s , V and d were determined by the fitting procedure.

Using:

$$\tau_f = \int_0^{\infty} \exp \left[- \left(\frac{t}{\tau_{fe}} \right)^{\beta_f} \right] dt = \frac{\tau_{fe}}{\beta_f} \Gamma \left(\frac{1}{\beta_f} \right) \quad (2.1.6)$$

the mean relaxation time τ_f of the fast mode averaged over the distribution of species was calculated. Here Γ is the gamma function. Results are presented in chapter 5.1 and in Paper I included in this thesis.

2.2 Nanoindentation

The aim of nanoindentation measurements on alginate is to study how the gel stiffness changes when mixing high molecular weight alginate with oligogulonates. Along we checked how the stiffness of the sample changes with different molecular parameters of alginate, with its concentration and with changes of oligogulonate concentration of the sample.

Nanoindentation measurements were done by Nanoindenter (AFM ForceRobot® 300, JPK Instruments AG, Germany) with JPK precision mapping stage.

2.2.1 Instrumental setup

Nanoindentation consists of pressing a very stiff spherical tip (Young's modulus $E \approx 3.5$ GPa [48, 49] and $\varnothing = 4.5$ μm) into the sample. The tip is attached to a cantilever (see Fig. 2.2.1). The spring constant and deflection sensitivity were determined prior to measurements each time the cantilever was mounted. The sample, positioned on a moveable stage, is moved towards the tip by a piezo-scanner, causing bending of the cantilever. Laser light is directed on the cantilever, and being reflected from the cantilever it hits a photodiode.

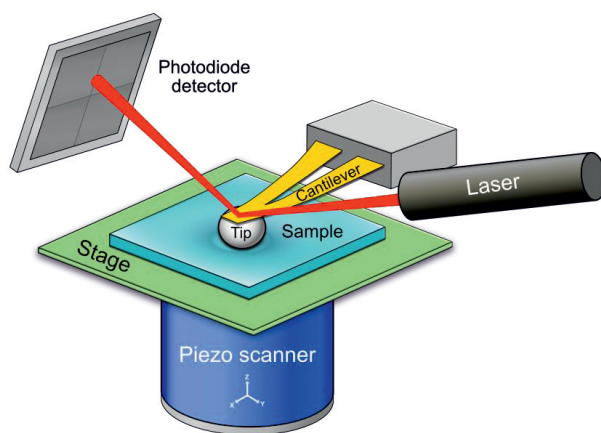


Fig. 2.2.1 Schematic illustration of the nanoindentation using the AFM setup

The reflected beam hits a position sensitive photodiode detector consisting of four segments illustrated in Fig. 2.2.2. When the tip is not in contact with the sample, the reflected beam hits the middle of the photodiode. While the tip is in contact with the sample, the cantilever is bending. This bending causes changes in the position where the reflected beam of light hits

the photodiode. The light intensity on each of the segments allows us to find the exact positioning of laser beam on the photodiode.

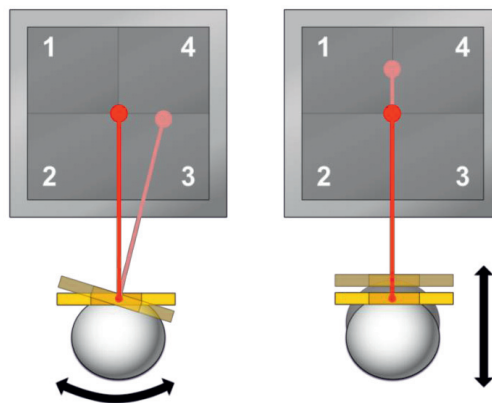


Fig. 2.2.2 Schematic illustration of reflected beam from the cantilever movement hitting the photodiode detector

2.2.2 Force-distance curves

The signal from the position sensitive detector is interpreted and drawn as force-distance curves shown in Fig. 2.2.3. The highlighted regions are described in Table 2.2.1 [50].

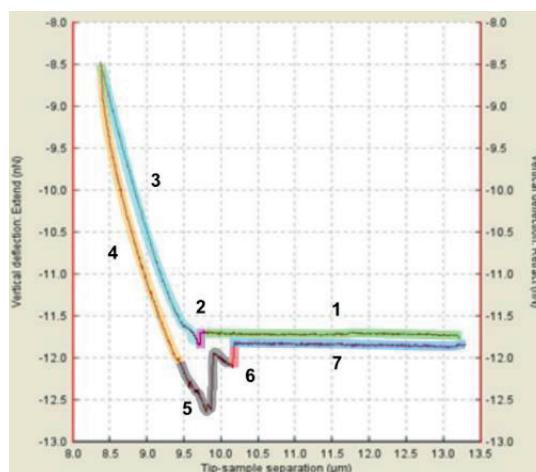
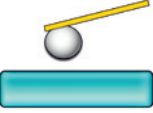
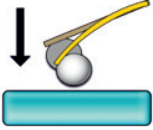
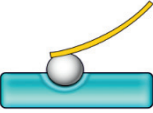
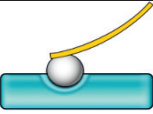
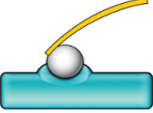
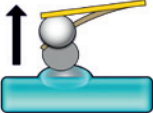
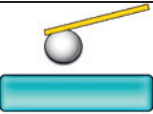


Fig. 2.2.3 Typical force-distance curve with highlighted regions of importance, described in Table 2.2.1.

Table 2.2.1 Detailed description of regions of typical force-distance curve

Point on Fig. 2.2.3	Tip position	Cantilever shape	force-distance curve shape
Extend curve			
1	not in contact	equilibrium position	 flat
2	approaching surface	Downward deflection (deflection increases with snap to contact)	 straight down
passes through its equilibrium position			
3	pushed against the surface	deflected upwards	 increase measured force
Retract curve			
4	starts to retract	The deflection starts to decrease	 decrease measured force
passes through its equilibrium position			
5	moving away from the surface the tip	deflected downwards	 adhesion
6	tip-sample interactions are terminated due to increased distance (tip snaps out)	returns to its equilibrium position	 straight up
7	not in contact	equilibrium position	 flat

2.2.3 Young's modulus (E)

A solid body deforms under an applied force. If the force is removed and the body returns to its previous shape, the material is elastic. To deform a stiff material a larger force is needed than to deform a soft material. The ratio of the tensile stress, σ , to the tensile strain, ϵ :

$$E = \frac{\sigma}{\varepsilon} \quad (2.2.1)$$

is the Young's modulus and is a measure of the stiffness of the object. The stress $\sigma = F/A$, where F is the force exerted on an object under tension and A is the original cross-sectional area through which the force is applied. The strain $\varepsilon = \Delta l/l$, where Δl is the amount by which the length of the object changes, l is the original length of the object. See Fig. 2.2.4.

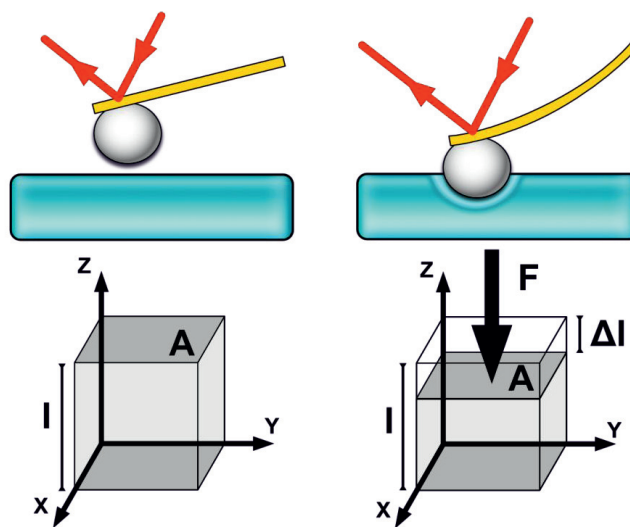


Fig. 2.2.4 Schematic illustration of Young's modulus deformation

2.2.4 Hertz model for spherical indenter

Young's modulus, E , was measured using Hertz model for spherical indenter [51-54]

$$E = \frac{3}{4} \frac{F(1-\nu^2)}{\delta^{3/2} \sqrt{R_s}} \quad (2.2.2)$$

here F is force, ν is the Poisson's ratio, R_s is the radius of the spherical bead and δ is the indentation $\delta = a^2 / R_s$ where a is the radius of the contact circle defined in Fig. 2.2.5.

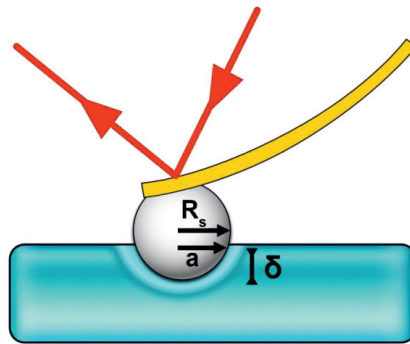


Fig. 2.2.5 Illustration of parameters needed in equations of Hertz model for spherical indenter

We have chosen the value of Poisson's ratio equal to 0.5, as this gives the best fit with data received by us from rheology measurement - data shown in chapter 4 - and as expected for high water content alginate gels [55-57]. The parameters from Eq. 2.2.2 were fitted by Levenberg–Marquardt algorithm implemented into analysis program provided by JPK Instruments AG, Germany. Fitting of the contact point is done using the extend curve, as this curve does have less adhesion artefacts than the retract curve. In Fig. 2.2.6 can be seen an example of such fitting.

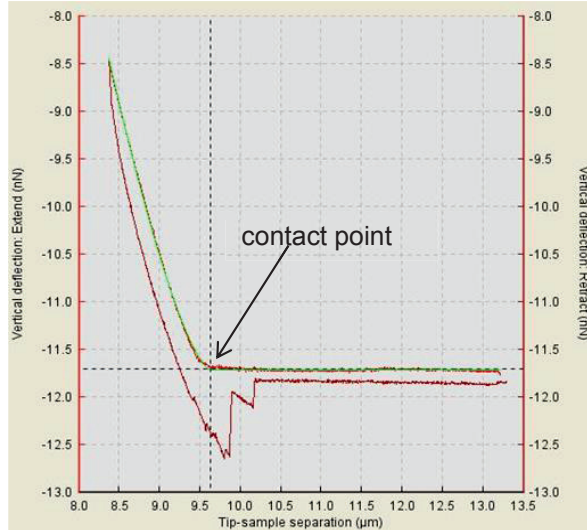


Fig. 2.2.6 Illustration of contact point fitting done by JPK software – graph come from our own measurements. The light red curve is the extend curve, the dark red curve is the retract curve, while green curve represent fitting of extend curve. The cross point of dashed vertical and horizontal line represent fitted contact point.

2.3 Small angle X-ray scattering (SAXS)

After the discovery of synchrotron radiation in 1946, synchrotron radiation facilities around the world have opened up a range of new possibilities in many research fields and have become a common tool for various types of material studies, replacing more traditional radiation sources, such as X-ray tubes [58]. In case of X-ray radiation, the intensity of synchrotron radiation is 10^6 - 10^7 times higher than the radiation produced in a classical X-ray tube [58]. The main advantages of synchrotron radiation are the following [58]:

1. Broad spectrum of electromagnetic radiation (from microwaves to hard X-rays)
2. The wavelength required for the experiment can be selected with high accuracy. Resolving power $\lambda/\Delta\lambda=10^4$ - 10^6 .
3. High brilliance (high intensity photon beam).
4. Highly collimated radiation.
5. Polarized radiation (linear, circular).

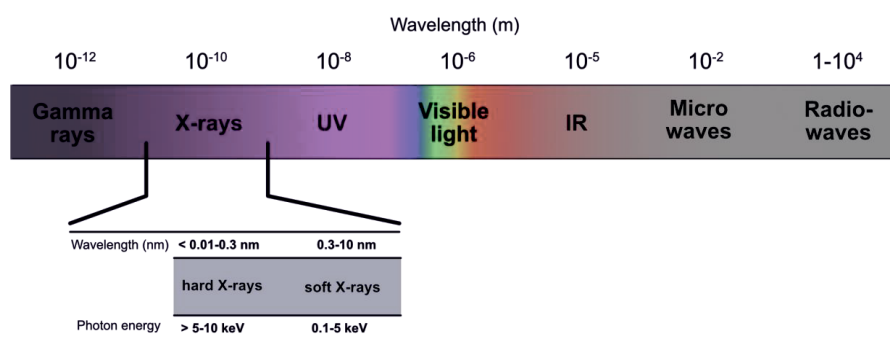


Fig. 2.3.1 Spectrum of electromagnetic radiation with detailed X-rays range.

The electromagnetic radiation is classified by its wavelength and, as shown in Fig. 2.3.1, electromagnetic radiation varies from radio waves through visible light ultimately up to gamma-rays. Radiation with wavelength λ in range of 0.01 nm - 10 nm (photon energy 100 eV – 100 keV), is called X-rays, and due to its short wavelength it is well suited to characterize atomic and macromolecular scale structures.

Small angle X-ray scattering (SAXS) is used to study various types of samples and provides information about the particle size, molecular weight and inter-atomic effects. While other X-ray scattering techniques, such as X-ray diffraction and wide-angle X-ray scattering, typically give structural information at atomic-level scale, SAXS can be used to probe ordered structures up to 150 nm and particles of 1 - 500 nm [59]. In addition to ordered structures,

SAXS enables also investigation of randomly oriented particles, such as alginate, situated in solutions.

2.3.1 Principle of scattering in a solution

In SAXS, a collimated beam of X-ray is guided through the sample and upon interaction of the radiation with the electrons of the sample's atoms, part of the incidence radiation is scattered away in a small angle typically $2\theta=2^\circ$ [60]. Scattering is schematically presented in Fig. 2.3.2.

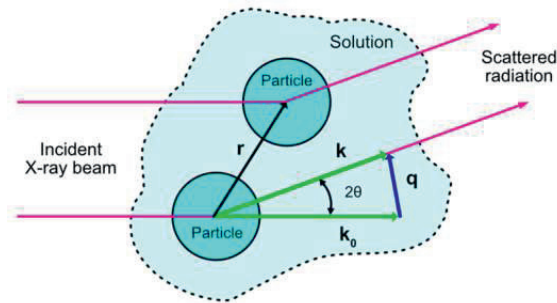


Fig. 2.3.2 Scattering on two particles

The scattering vector \mathbf{q} is defined as:

$$\mathbf{q} = \mathbf{k} - \mathbf{k}_0 \quad (2.3.1)$$

where \mathbf{k}_0 and \mathbf{k} are the wave vectors of incident and scattered waves, respectively.

In SAXS we assume the phase and wavelength of the scattered radiation to remain invariant and therefore the amplitudes of wave and scattering vectors are:

$$k = |\mathbf{k}| = \frac{2\pi}{\lambda} \quad (2.3.2)$$

$$q = |\mathbf{q}| = \frac{4\pi \sin(\theta)}{\lambda} \quad (2.3.3)$$

The scattered waves interfere with each other and, depending on the scattering vector, the waves can be out of phase – causing a destructive interference – or in phase – causing a constructive interference. In SAXS measurements, this is seen as an interference pattern at the detector, which holds information about intensity and scattering angle (2θ) of the scattered radiation.

The scattering amplitude of a single particle with random orientation – situated in a solution – is given by the equation:

$$A_p(\mathbf{q}) = V_p \Delta\rho_e F(\mathbf{q}, \mathbf{r}) \quad (2.3.4)$$

Here $\Delta\rho_e = \rho_e - \rho_{es}$ is the difference of the electron density between sample particles and surrounding matrix (solution). V_p is the volume of the particle and $F(\mathbf{q}, \mathbf{r})$ is the so-called form factor of the particle.

Respectively, the intensity of the scattering radiation is [61]:

$$I_p(\mathbf{q}, \mathbf{r}) = |A_p(\mathbf{q})|^2 = V_p^2 \Delta\rho_e^2 F^2(\mathbf{q}, \mathbf{r}) \quad (2.3.5)$$

and the intensity of scattering from N_p number of particles is [61]:

$$I(\mathbf{q}, \mathbf{r}) = N_p I_p(\mathbf{q}, \mathbf{r}) = N_p V_p^2 \Delta\rho_e^2 F^2(\mathbf{q}, \mathbf{r}) \quad (2.3.6)$$

2.3.2 Description of the SAXS instruments

The SAXS measurements of this work were performed at The High Energy Accelerator Research Organization (KEK), Photon Factory, Tsukuba, Japan, at the hard X-ray beamline BL-10C. Whereas the time resolved SAXS measurements were performed at the beamline BL45XU at RIKEN Harima Institute SPring-8 Center. Details of the instruments will be shown subsequently.

Beamline BL-10C, Photon Factory, Tsukuba, Japan

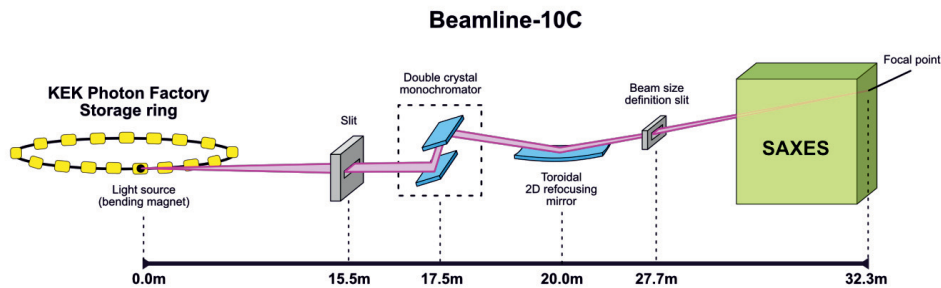


Fig. 2.3.4 Schematic view of the beamline BL-10C at Photon Factory, Tsukuba, Japan. The horizontal axis depicts the physical distances along the beamline from the outlet of the storage ring. The figure is based on [62, 63].

In the beamline BL-10C, the synchrotron radiation is produced by a bending magnet of the 2.5 GeV storage ring and X-ray beam is at first directed through an aperture slit (W 2 mm x H 10 mm) and then is monochromatized in a Si (111) double grating monochromator. In the experiments the wavelength of the X-ray beam was $\lambda = 0.149$ nm. The monochromatized beam is focused to the beamline end-station, in two dimensions by a toroidal refocusing rhodium coated silicon mirror. Before entering the end-station, the beam goes through a beam size definition slit.

The beamline end-station is a so-called small-angle X-ray equipment for solutions (SAXES), presented in Fig. 2.3.5, and it is designed for scattering experiments carried out on materials without crystal structure, like for example polymer solutions such as our alginate samples. SAXES consists of four elements which the focused light beam passes through:

1. Slit assembly (tapered 3 mm thick Ta plate)
2. Specimen holder (a flat cell of 0.2 cm path-length with thin mica windows).
3. Vacuum chamber
4. One dimensional position sensitive detector (PSPC) (1 meter from the sample holder)

All optics is set up on double optical rails. The solutions were injected into a flat cell immediately after preparation, and left there for one day. The SAXS intensities were collected for 300 s in order to ensure enough statistical accuracy and at the same time to not degrade the samples.

All the setup parameters are taken from The High Energy Accelerator Research Organization (KEK), Photon Factory, Tsukuba, Japan [5,6].

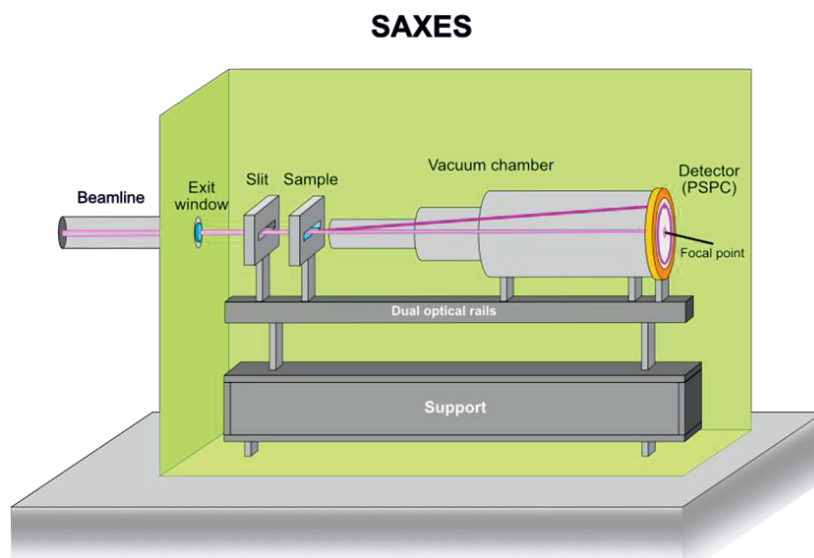


Fig. 2.3.5 Schematic presentation of the SAXES end-station of the BL-10C beamline [63].

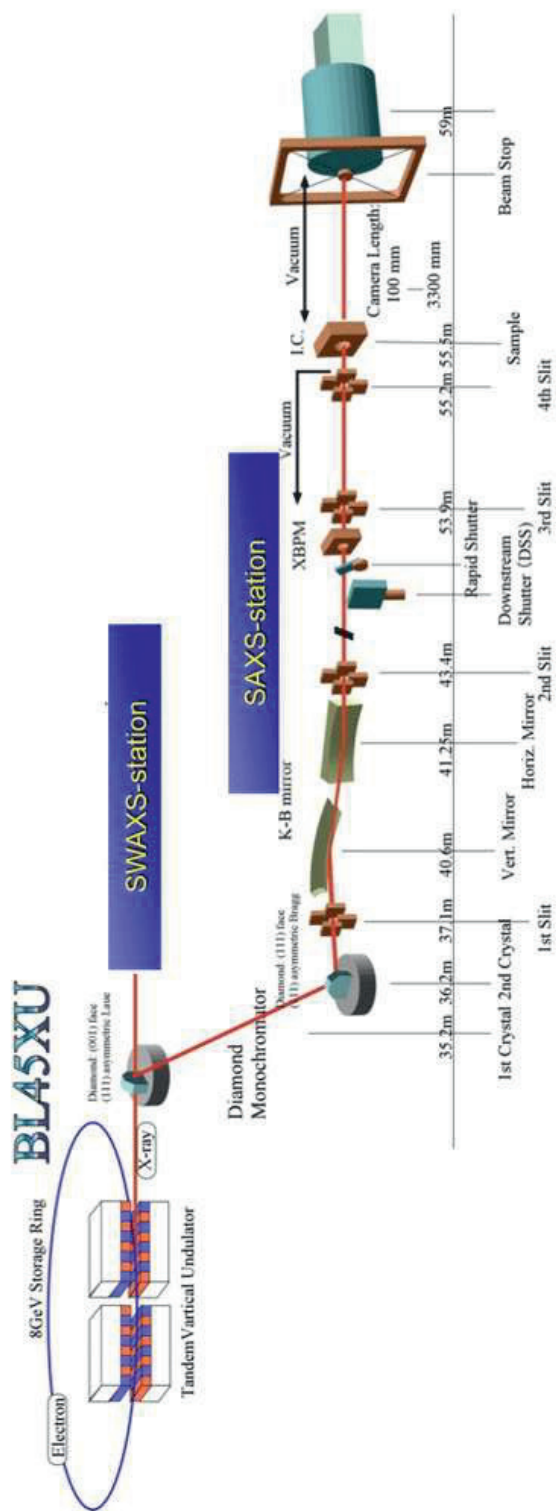


Fig. 2.3.6. Illustration of the beamline BL45XU at RIKEN Harima Institute Spring-8 Center, Japan. The figure is based on graphics in [64]. Reproduced with permission from the RIKEN Harima Institute Spring-8 Center, Japan

Beamline BL45XU, RIKEN Harima Institute SPring-8 Center

Unlike the beamline BL-10C, where a bending magnet is used to produce synchrotron radiation, in BL45XU synchrotron radiation is produced by a tandem undulator at a 8 GeV storage ring (photon flux $\sim 1 \times 10^{12}$ photons/sec). The beam size at the experiment is 0.4×0.2 mm (H \times W) and was monochromatized to $\lambda = 0.052$ nm. The optics of that beamline contain, in order of passing light:

- Two sets of a double-crystal monochromator (beam can be monochromatized from 6.7 keV to 14 keV (usually 12.4 keV)).
- 1st slit used to reduce parasitic scattering (together with later slits).
- Rhodium coated K-B mirrors (82% of reflectivity is expected at 12 keV and focusing ratio is 2.48 to 1).
- 2nd slit.
- Downstream shutter and rapid shutter.
- X-ray beam position detector.
- 3rd and 4th slit with vacuum chamber in between
- Sample holder (in flat cell of 0.2 cm path-length made of thin mica windows)
- Vacuum chamber
- Beam stop (stopping the direct beam)
- PILATUS detector (3 meters from the sample holder)

The solutions were injected into a flat cell immediately after preparation. The sample was measured at appropriate time intervals with 120 s accumulation time.

All the setup parameters and picture of setup are taken from RIKEN Harima Institute SPring-8 Center [64].

2.3.3 Measurement geometry

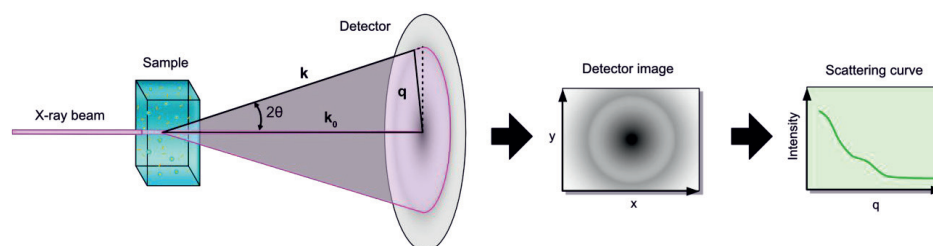


Fig. 2.3.7 Geometry behind plotting the scattering curve

The X-ray beam is directed through the sample and scattered. The scattered light at small angles is measured by a two-dimensional detector. Results from the detector are translated into a one-dimensional scattering curve $I(q)$ vs q as shown in Fig. 2.3.7.

2.3.4 How to analyze the results

The results were analyzed by:

- the cross-sectional Guinier plots $\ln(qI(q))$ vs q^2
- the Kratky plots $q^2 I(q)$ vs q

as described in the following.

The cross-sectional Guinier plots and cross-sectional radius of gyration

The scattering plot for small scattering vectors \mathbf{q} , can be described by the so-called Guinier approximation. For elongated objects $I(\mathbf{q})$ may be described by [65]:

$$I(\mathbf{q}) = \frac{I_0}{q} \exp\left(\frac{-\mathbf{q}^2 R_{Gc}^2}{2}\right) \quad (2.3.7)$$

Analysis is done by plotting $\ln(qI(q))$ vs q^2 (see Fig. 2.3.8) and then fitting the curve for low q^2 by a straight line. The slope of this line is equal to $-\frac{R_{Gc}^2}{2}$, where R_{Gc} is the cross-sectional radius of gyration of the scattering objects [66].

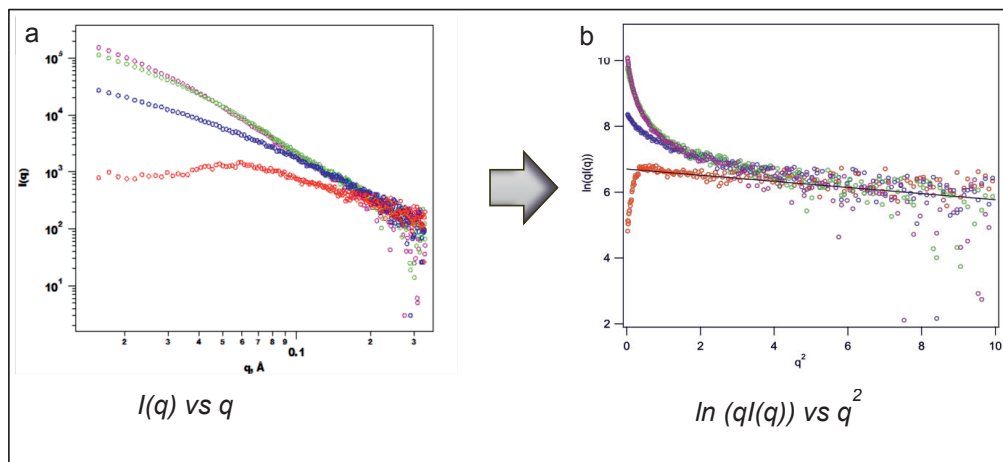


Fig. 2.3.8 (a) Typical scattering curves. (b) Cross-sectional Guinier plots

Kratky plots

The scattering plot for larger q can be analyzed by plotting $q^2 I(q)$ vs q , called Kratky plot. For a Gaussian chain $q^2 I(q)$ vs q will tend to a horizontal asymptotic behavior, while a deviation from this indicates a non-Gaussian nature. At high- q region the form factor for Gaussian chains may be described by [66]:

$$I(x) = \frac{I_0}{1+x^2} \quad (2.3.8)$$

where $x = qa$ and a is a characteristic length. The typical Kratky plot in Fig. 2.3.9 shows an approximately horizontal asymptotic behaviour, indicating a Gaussian nature.

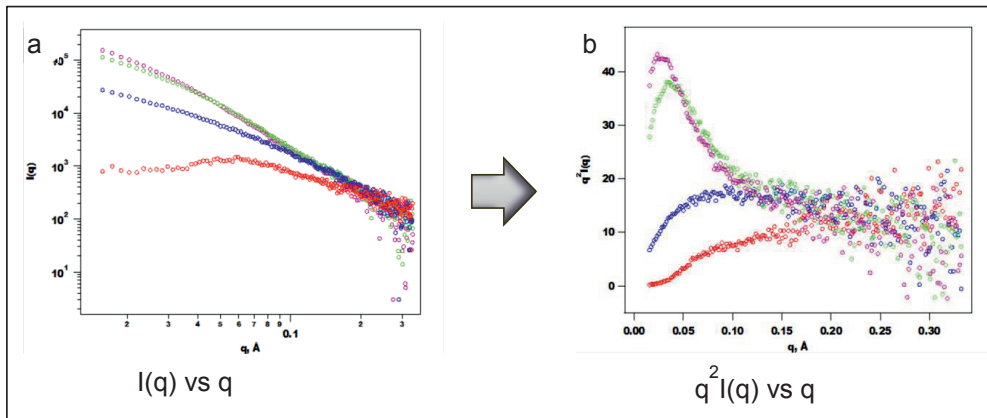


Fig. 2.3.9 (a) Typical scattering curves. (b) Kratky plots

Kratky plots for a broken rod-like model

The R_{Gc} values for alginate and oligogulonate in solution can be estimated from a rod-like model using a Guinier plot as described in upper. However it becomes more problematic in case of gelled and gelling samples.

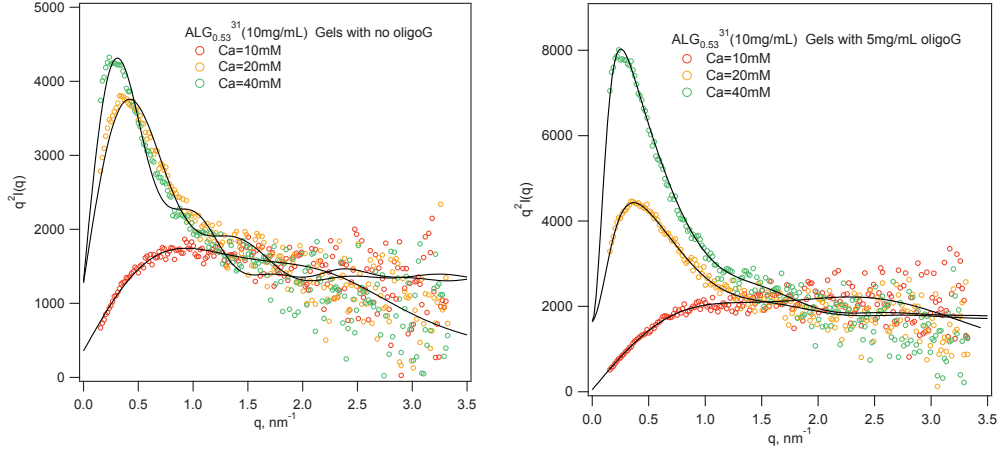


Fig. 2.3.10 Kratky plots for static SAXS measurements from $\text{Alg}_{0.53}^{31}$ -[10] (notation explained in section 3.1.2) at $\text{Ca}=10, 20$ and 40 mM (a) without oligoG and (b) 1:2 oligoG to alginate ratio. Data (symbols) and the corresponding model fits (curves) are depicted

In case of fitting alginate hydrogels (without oligoguluronates and with oligoguluronates at $c_{\text{CaEGTA}} = 10$ mM) the rod-like model was not adequate, and the broken rod-like model (fitting Kratky plot) had to be used [31, 67]. This model includes scattering from a one- or two-component rod with circular cross-section. The model accounts for heterogeneity in the cross-section, and can be written as:

$$q^2 I(q) \sim \sum_{i=1}^{\text{1or2}} q k_i \left[\frac{J_1(q R_{\text{Gci}})}{q R_{\text{Gci}}} \right]^2 + \text{const} \quad (2.3.9)$$

where q is the scattering vector, I is the intensity, k_i is the adjustable constant, J_1 is the first order Bessel function, R_{Gci} is the cross-sectional radius of i th component rod and const is a constant parameter.

In case of blended samples of alginate and oligoguluronate (for $c_{\text{CaEGTA}} = 20$ or 40 mM) we had to use Debye-Bueche type scattering function implemented into the two-component broken rod-like model:

$$q^2 I(q) \sim \frac{k_d q^2}{(1 + a^2 q^2)^2} + \sum_{i=1}^{\text{1or2}} q k_i \left[\frac{J_1(q R_{\text{Gci}})}{q R_{\text{Gci}}} \right]^2 + \text{const} \quad (2.3.10)$$

where k_d is an adjustable parameter and a is a measure of the extension of the inhomogeneities. From a plot of $q^2 I(q)$ vs. q (a Kratky plot), values for the parameters R_{Gci} and a are estimated.

2.4 Rheology

Rheology is the method of measuring material properties like shear storage modulus (G') and shear loss modulus (G''), using an oscillating shear strain load. This gives us information about material stiffness and viscosity.

Measurements in this thesis were performed by Paar Physica Rheometer MCR 300 with a LAUDA ecoline low temperature thermostat RE 104.

2.4.1 Instrumental setup

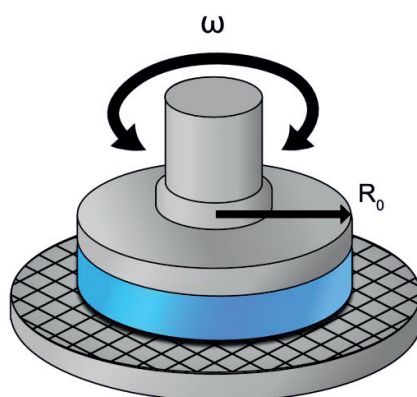


Fig. 2.4.1 Schematic illustration of rheology setup.

The instrumental setup consists of two parallel circular plates PP50 with serrated surface and diameter 50 mm. The gap load between the plates was 1 mm height. The frequency f used during the gel curing was always 1 Hz and the temperature was kept constant at 20 °C. The measurement was done in oscillation mode. Every rheology measurement was done continuously for 25 hours.

2.4.2 Shear and loss modulus

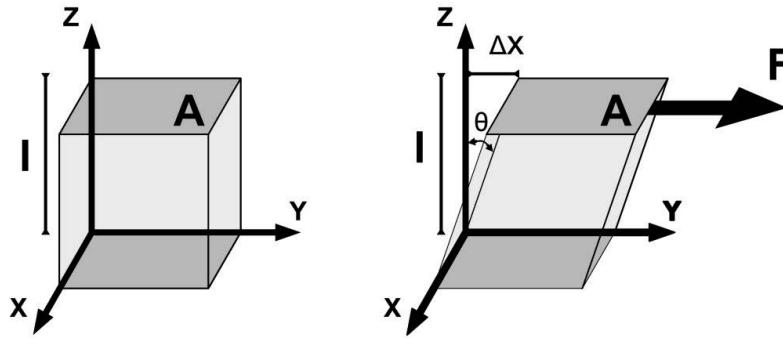


Fig. 2.4.2 Schematic illustration of shear deformation.

Similar to the Young's modulus described in chapter 2.2.3, the shear modulus is also a way of measuring stiffness of the materials. Shear modulus G is defined as the ratio of shear stress τ to the shear strain γ :

$$G(t) = \frac{\tau(t)}{\gamma(t)} \quad (2.4.1)$$

The shear stress $\tau = F/A$, where F is the force exerted on an object by shear and A is the original cross-sectional area through which the force is applied. The strain $\gamma = \Delta x/l$, where Δx is the transverse displacement and l is the original length of the object. See Fig. 2.4.2.

Using oscillating shear strain with a certain frequency ω , the analysis can be carried out using complex analysis. Using complex stress τ^* and complex strain γ^* , the complex shear modulus is defined $G^* = \tau^* / \gamma^*$ and can be expressed

$$G^* = \frac{\tau^*}{\gamma^*} = G' + iG'' \quad (2.4.2)$$

G' is the shear storage modulus and describes the shear elastic properties of the material and G'' is the shear loss modulus and describes the viscous properties of material.

2.4.3 Analysing G' and G'' during gelling

The shear storage modulus and loss modulus of viscoelastic materials can be expressed by [68]:

$$G' = \omega \int_0^{\infty} G(t) \sin(\omega t) dt \quad (2.4.3)$$

$$G'' = \omega \int_0^{\infty} G(t) \cos(\omega t) dt \quad (2.4.4)$$

where ω is angular frequency, $G(t)$ is the relaxation modulus and t is time.

To study the time response of the gelling of alginate samples, the values of G' and G'' for a sample were measured as function of time.

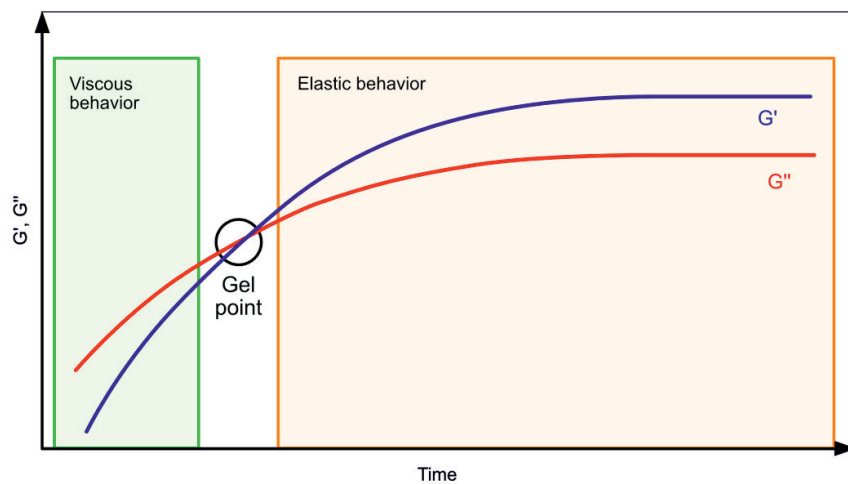


Fig.2.4.3 Typical curves of G' and G'' demonstrating the gelation process.

In the initial part of experiment, when substance is still liquid, the viscous behaviour will prevail and $G'' > G'$. Whereas for the gelled substance $G' > G''$, as the elastic behaviour will be dominating. The crossover point between G' and G'' is considered to be the gel point. The network stiffness continues to increase beyond a gel point with increasing density of cross-links. The stiffening process continues till the system reach completion of the chemical reaction [68].

3. Sample preparation

3.1 Samples

3.1.1 Alginate

In the measurements presented in the papers attached to this thesis three (in DLS and nanoindentation) and two (SAXS measurements) different sodium alginate samples were used. All alginate samples come from different sources of *Laminaria Hyperborea* algae kindly provided by Department of Biotechnology NTNU, Trondheim. Prior to our measurements samples were characterized by NMR and light scattering techniques (also by Department of Biotechnology NTNU, Trondheim). The results of those measurements, which characterize chemical composition of samples, can be seen in Table (3.1.1). What is worth noticing is that two of the samples have the same molecular weight M_w but different guluronic content F_G , whereas two have almost the same guluronic content but different molecular weight. That enables us to compare the influence of guluronic content F_G or molecular weight M_w on the final gels properties. Alginate samples are denoted as $\text{Alg}_x^Y\text{-}[c]$, where the numerical values of X depict the F_G , Y depicts M_w (in kg/mol) and c is concentration of actual sample in (mg/ml) when denoted.

Table 3.1.1 Chemical composition of employed alginates and oligoguluronates. The weight average molecular weight (M_w), intrinsic viscosities $[\eta]$, number average degree of polymerization DPn, average length of G-blocks larger than one unit ($N_{G>1}$), and the fractions of the α -L-GulA, F_G , β -D-ManA (M), $F_M = 1 - F_G$, as well as fraction of diad and triad combinations in samples are depicted. M_w was determined by SEC-MALLS as stated in the text. All fractions F were determined by NMR as stated in the text.

Alginate source:	Sample notation	M_w kg/mol	$[\eta]$ ml/g	DPn	$N_{G>1}$	F_G	F_M	F_{GG}	F_{MG}/F_{GM}	F_{MM}	F_{MGG}/F_{GGM}	F_{MGM}	F_{GGG}
<i>L.Hyperborea</i> – leaf	Alg _{0.53} ³¹	31	132	-	8	0.53	0.47	0.35	0.19	0.28	0.05	0.14	0.30
<i>L.Hyperborea</i> – stem	Alg _{0.63} ³¹	31	149	-	11	0.63	0.37	0.50	0.13	0.24	0.05	0.10	0.46
<i>L.Hyperborea</i> – stem	Alg _{0.66} ¹¹⁴	114	610	-	13	0.66	0.34	0.55	0.12	0.22	0.05	0.09	0.50
<i>L.Hyperborea</i> – stem	oligoG _{0.94} ¹⁹	-	-	19	-	0.94	0.06	0.83	0.11	0.05	0.03	0.08	0.80
<i>L.Hyperborea</i> – stem	oligoG _{0.90} ²⁰	-	-	20	-	0.90	0.10	-	-	-	-	-	-

3.1.2 Oligoguluronates

The chemical composition of oligoguluronate used in our measurements is stated in Tab. 3.1.1. They were kindly provided by Professor Kurt Ingar Draget from Department of Biotechnology NTNU, Trondheim. The oligoguluronates were mixed with alginate stock solution in different ratios (exact ratios will be stated at each of technique). Oligoguluronate samples are denoted as oligoG_X^Y, where the numerical values of X depict the F_G and Y depicts DP_n of the actual sample respectively.

Samples Alg_{0.53}³¹, Alg_{0.63}³¹, Alg_{0.66}¹¹⁴ and OligoG_{0.94}¹⁹ were used in DLS and nanoindentation measurements. Whereas in SAXS measurements were used Alg_{0.53}³¹, Alg_{0.66}¹¹⁴ and OligoG_{0.90}²⁰ samples.

3.1.3 Preparing of stock solutions

Throughout the sample preparation all samples were dissolved in double deionized water with resistivity 18.2 MΩ cm. Further it will be stated as just ddH₂O.

CaEGTA stock solution

The CaEGTA solution was prepared according the recipe described by Stokke et al. [31]. For our needs we needed higher concentration of stock solution and here we present the recipe for 300 mM CaEGTA:

100 mL of 300 mM CaEGTA was prepared by mixing 11.4 g of EGTA and 4.41 g of CaCl₂•2H₂O into ddH₂O. Then pH was adjusted to 7.0 with NaOH and HCl and the volume was adjusted to 100 ml. Finally pH was once again checked and adjusted if not equal to 7.0.

Decrease of pH induced by slowly hydrolysing lactone

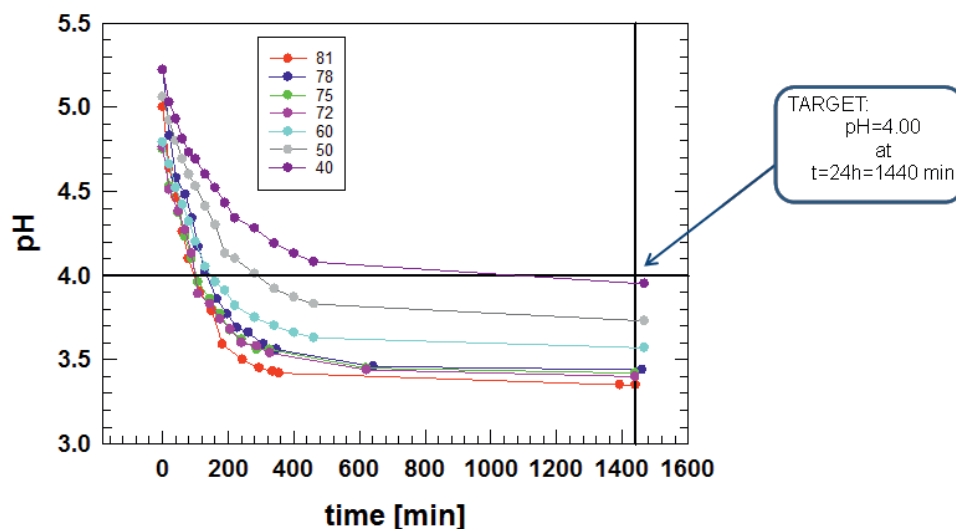


Fig. 3.1.1 Results of pH measurements for CaEGTA with different GDL concentrations, concentrations of GDL (in mg per 4.406 mL of sample) are given in legend. The concentration of CaEGTA was constant and equal to 19.3.

As described in chapter 1.3.5 GDL causes decrease of pH and release of Ca^{2+} from CaEGTA. Concentration of GDL was calibrated according to the concentration of CaEGTA and adjusted to reach pH 4.00 after 24 h from the mixing (see chapter 1.3.3). The pH decrease during this process was followed with the use of a conventional pH electrode.

Fig. 3.1.1 shows some examples of pH measurements done as preparation for rheology and nanoindentation measurements. For each measurement technique different concentrations of alginate and CaEGTA were used, pH measurements were done to check and correct concentration of GDL needed to receive pH=4.0 after 24h.

3.2 Preparing samples for DLS measurements

3.2.1 Alginate and oligoguluronate stock solution

Alginate stock solutions were prepared by dissolving alginate powder in 50 mM NaCl over night to achieve final concentrations of 5 and 10 mg/ml. The oligoguluronates were mixed with alginate stock solution in ratios 0:1; 1:2; 1:1 oligoguluronate to alginate. All alginate/oligoguluronate stock solutions were filtered with *Acrodisc® Syringe Filters with Supor® Membrane from PALL*. For alginates with $M_w = 31$ kg/mol a 0.2 μm syringe filter was used and for alginate with $M_w = 114$ kg/mol the syringe filter was 0.45 μm .

3.2.2 CaEGTA stock solution for DLS

CaEGTA solution was prepared dissolving 300 mM CaEGTA stock solution to new less concentrated stock solutions with concentrations of 25.91 and 51.82 mM, and adjusting pH to 7.0. CaEGTA was filtered using a 0.2 μm syringe filter.

3.2.3 Preparing sample for DLS measurements

The alginate/oligoguluronate stock solution and CaEGTA were mixed to achieve final concentrations of alginate 3.6 or 7.1 mg/mL and CaEGTA 4.6 or 9.2 mM accordingly. So the ratio between alginate and Ca^{2+} concentration was constant. To this mixture was added GDL freshly dissolved in 50 mM NaCl (saline was filtered with 0.2 μm syringe filter before mixing with GDL). Each sample was right away poured into the DLS cuvette and each measurement was started right away.

3.2.4 Saturations and reduced concentration for samples used during DLS measurements

Table 2 in Paper I shows the fractional saturation F_{sat} calculated according to Eq. (1.4.4) and the reduced concentration calculated as $c[\eta]$, where $c = c_p$ is the concentration of alginate and $[\eta]$ is the intrinsic viscosity of alginate taken from Table 3.1.1. c_{CaEGTA} is the concentration of CaEGTA.

3.3 Preparing samples for nanoindentation

3.3.1 Alginate and oligoguluronate stock solution

Alginate stock solutions were prepared by dissolving alginate powder in ddH₂O over night to achieve final concentrations of 21.8 and 32.7 mg/ml. The oligoguluronates were mixed with alginate stock solution in ratios 0:1; 1:6; 1:3, 1:2 oligoguluronate to alginate.

3.3.2 CaEGTA stock solution for nanoindentation

CaEGTA solution was prepared dissolving 300 mM CaEGTA stock solution to stock solutions with concentration of 112.9 mM and adjusting pH to 7.0.

3.3.3 Preparing sample for nanoindentation measurements

The alginate/oligoguluronate stock solution and CaEGTA were mixed to achieve final concentration of alginate 15.5 and 23.2 mg/mL and CaEGTA 20 mM for both concentrations. Then to this mixture was added freshly dissolved GDL. Sample was poured into a mould and left there for 24h.

3.3.5 Issues with sample preparation

Comparing results received previously by our group, and by rheology measurement done by me on the same pure alginate samples, a decrease in Young's modulus was expected when the concentration of alginate was increased [23, 24]. Generally that trend was fulfilled in the present study. However, samples Alg_{0.63}³¹ and Alg_{0.66}¹¹⁴ without additional oligoGs do have opposite trend. This unexpected result initiated a series of investigations of the preparation techniques, trying to explain and possibly solve this issue:

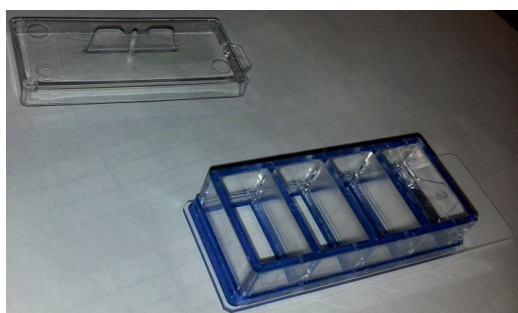


Fig. 3.3.1 Chamber Slide™ with cover - 4 Well Glass Slide from Lab-Tek ®II

In the beginning gel samples were prepared and left for gelling in small wells, shown in Fig. 3.3.1. The wells were closed from top, however sample surface still had contact with air inside mould. Drying of the substance starts from its surface and that was suspected to be a main problem. Trying to exclude this possibility, we tried leaving those gels for gelation in humid environment. But the trend still occurs. Then we tried preparing gels in petri dishes and seal their surface with water saturated isobutanol, but that created even more issues.

Despite of all our efforts, the unexpected results were reproduced in measurements of independently prepared samples. In the end we decided to prepare gels in the mould described in next paragraph, where the surface of the gel is sealed, and no foreign substance is used.

3.3.6 Alginate hydrogel samples – final preparation

In all measurements presented in Paper II of this thesis, the gels were prepared in moulds created from two glass plates apart from each other giving gel thickness of 1.5 mm as shown in Fig. 3.3.2. Plates were sealed with silicone grease and parafilm to avoid drying of sample during a gelation process. After 24 h the mould was gently opened and smaller pieces of gel were cautiously cut out and moved to petri dishes for examination. The surface of smaller pieces was exposed to ddH₂O three times for 10 min to wash out possible loose alginate chains and equilibrate hydrogel. Special attention was taken to keep water on the surface of the sample and not elsewhere, to avoid further sliding of the sample during the measurements.

Following this, the sample surface was kept in ddH₂O water all the time prior and during measurements.



Fig. 3.3.2 Mould made as described in next paragraph

3.3.7 Saturations and reduced concentration for samples used during nanoindentation measurements

Table 2 in Paper II shows the fractional saturation F_{sat} calculated according to Eq. (1.4.4)

Table 3.3.1 shows the reduced concentration calculated as $c[\eta]$, where $c = c_{\text{alg}}$ is the concentration of alginate and $[\eta]$ is the intrinsic viscosity of alginate taken from Table 3.1.1. c_{CaEGTA} is the concentration of CaEGTA.

Table 3.3.1 Reduced concentration $c[\eta]$ for the samples used in nanoindentation measurements

concentration		$c[\eta]$		
c_{alg}	c_{CaEGTA}	Alg_{0.53}³¹	Alg_{0.63}³¹	Alg_{0.66}¹¹⁴
mg/mL	mM			
15.5	20	0.47	0.53	2.16
23.2	20	0.94	1.06	4.33

3.4 Preparing samples for SAXS

3.4.1 Alginate and oligogulonate stock solutions

Alginate stock solutions were prepared by dissolving alginate powder ddH₂O over night to achieve final concentration of 15 mg/ml. The oligogulonates were mixed with alginate stock solution in ratios 0:1, 1:2 and 1:1 oligogulonates to alginate. Alginate stock solutions were filtered using cartridge filters with pore size of 0.8 μ m.

3.4.2 CaEGTA stock solution

CaEGTA solutions were prepared with concentrations 100 and 200 mM and pH = 7.0.

3.4.3 Preparing sample for SAXS measurements

The alginate/oligogulonates stock solution and CaEGTA were mixed to achieve final concentration of alginate 10 mg/mL and CaEGTA 10, 20 and 40 mM. Then to this mixture was added freshly dissolved GDL. Sample was immediately poured into flat cell of 0.2 cm path-length made of thin mica windows (see Fig. 3.4.1). In case of measurements carried at the Photon Factory, the sample was left for 24h before measurements begin, whereas the time resolved SAXS measurements done at SPring-8 facility were done by appropriate time intervals before 24 h.

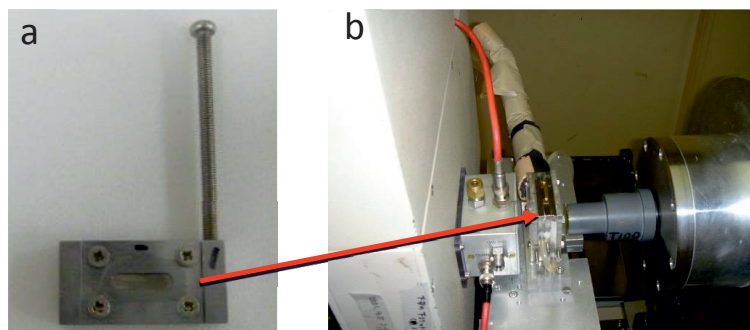


Fig. 3.4.1 a) Flat cell. b) Sample holder. Pictures provided by courtesy of professor Yoshiaki Yuguchi.

3.4.4 Saturations and reduced concentration for samples used during SAXS measurements

Tables 3.4.1 and 3.4.2 show the fractional saturation F_{sat} calculated according to Eq. (1.4.4) and the reduced concentration calculated as $c[\eta]$, where $c = c_{\text{alg}}$ is the concentration of alginate and $[\eta]$ is the intrinsic viscosity of alginate taken from Table 3.1.1. c_{CaEGTA} is the concentration of CaEGTA.

Table 3.4.1 Fractional Ca²⁺ saturation F_{sat} of guluronic residues belonging to alginate and oligoguluronates for the samples used in SAXS measurements

c _{alg}	c _{CaEGTA}	0:1 oligoG:Alg ratio		1:2 oligoG:Alg ratio		1:1 oligoG:Alg ratio	
mg/mL	mM	Alg _{0.53} ³¹	Alg _{0.66} ¹¹⁴	Alg _{0.53} ³¹	Alg _{0.66} ¹¹⁴	Alg _{0.53} ³¹	Alg _{0.66} ¹¹⁴
		F _{SAT}					
10	10	0.74	0.6	0.4	0.35	0.28	0.25
10	20	1.49	1.19	0.8	0.71	0.55	0.51
10	40	2.97	2.39	1.61	1.42	1.1	1.01

oligoGs without alginate		
OligoG	c _{CaEGTA}	oGs _{0.90} ²⁰
mg/mL	mM	F _{SAT}
10	20	0.88
5	20	1.75

Table 3.4.2 Reduced concentration c[η] for the samples used in SAXS measurements

sample	Alg _{0.53} ³¹	Alg _{0.66} ¹¹⁴
c _{alg} mg/mL	c[η]	
10.00	1.02	4.71

3.5 Preparing samples for rheology

Rheology measurements were done with three different sets of sample conditions. The first set of measurements were done at 19.3 mM CaEGTA and final pH = 3.44, second set at 20 mM CaEGTA and pH = 4.0 and third set was done at 40 mM CaEGTA and pH = 4.0. All measurements were carried out without oligoguluronates.

3.5.1 Alginate gels prepared at 19.3 mM CaEGTA with final pH 3.44

3.5.1.1. Stock solutions

Alginate stock solutions were prepared by dissolving alginate powder in ddH₂O over night to achieve concentration of 21.78 and 32.67 mg/ml. CaEGTA solution was prepared dissolving 300 mM CaEGTA stock solution to stock solutions with concentration of 108.9 mM, and adjusting pH to 7.0.

3.5.1.2 Preparing sample for rheology measurements

The alginate stock solution and CaEGTA were mixed to achieve final concentration of alginate 15.5 and 23.2 mg/mL and CaEGTA 19.3 mM. The concentration of GDL was

calibrated so that the solution after 24 hours reaches pH 3.44. After mixing CaEGTA-alginate solution with GDL, the sample was right away poured onto the serrated plate of rheology setup. 20 minutes after mixing, sample was sealed with low-viscosity silicon oil to prevent drying of the sample. Measurement was started after sample reach gel point and carried out for 25 h.

3.5.2 Alginate gels prepared at 20 mM CaEGTA with final pH 4.0

3.5.2.1 Stock solutions

Concentrations of alginate stock solutions were 21.78 and 32.67 mg/ml. CaEGTA stock solutions had concentration of 112.9 mM and pH = 7.0. Prepared similarly as for the previous condition.

3.5.2.2 Preparing sample for rheology measurements

Final concentration of alginate was 15.5 and 23.2 mg/mL and CaEGTA 20 mM. The concentration of GDL was calibrated so that the solution after 24 hours reaches pH 4.0. After mixing with freshly dissolved GDL, the sample was immediately poured onto the serrated plate. 20 minutes after mixing, sample was sealed with low-viscosity silicon oil to prevent drying of the sample. Measurement was started after sample reach gel point and carried out for 25 h.

3.5.3 Alginate gels prepared at 40 mM CaEGTA with final pH 4.0

3.5.3.1 Stock solutions

Concentrations of stock solutions were 21.78 and 32.67 mg/ml for alginate and 225.7 mM for CaEGTA (pH = 7.0). Prepared similarly as for the previous condition.

3.5.3.2 Preparing sample for rheology measurements

Final concentrations were 15.5 and 23.2 mg/mL for alginate and 40 mM for CaEGTA. The concentration of GDL was calibrated that the solution after 24 hours reaches pH 4.0 Right after mixing CaEGTA-alginate solution with freshly dissolved GDL, the sample was poured onto the serrated plate of rheology setup. 20 minutes after mixing, sample was sealed with low-viscosity silicon oil to prevent drying of the sample. Measurement was started after sample reach gel point and carried out for 25 hours.

3.5.4 Issues with sample preparation

At the first measurements we experienced problems with reproducibility of the results. The factor causing this issue was found to be the concentration of GDL. In the first measurements GDL was dissolved in small amount of water. When mixing freshly dissolved GDL with alginate-CaEGTA solution, we could see that the top part of solution got gelled, whereas the

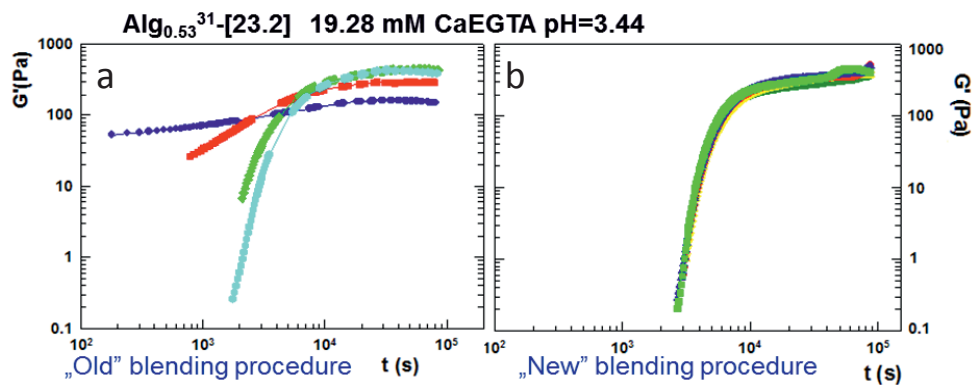


Fig. 3.5.1 Experimental data showing difference in G' reproducibility of the two preparation techniques: a) old blending procedure, b) new blending procedure.

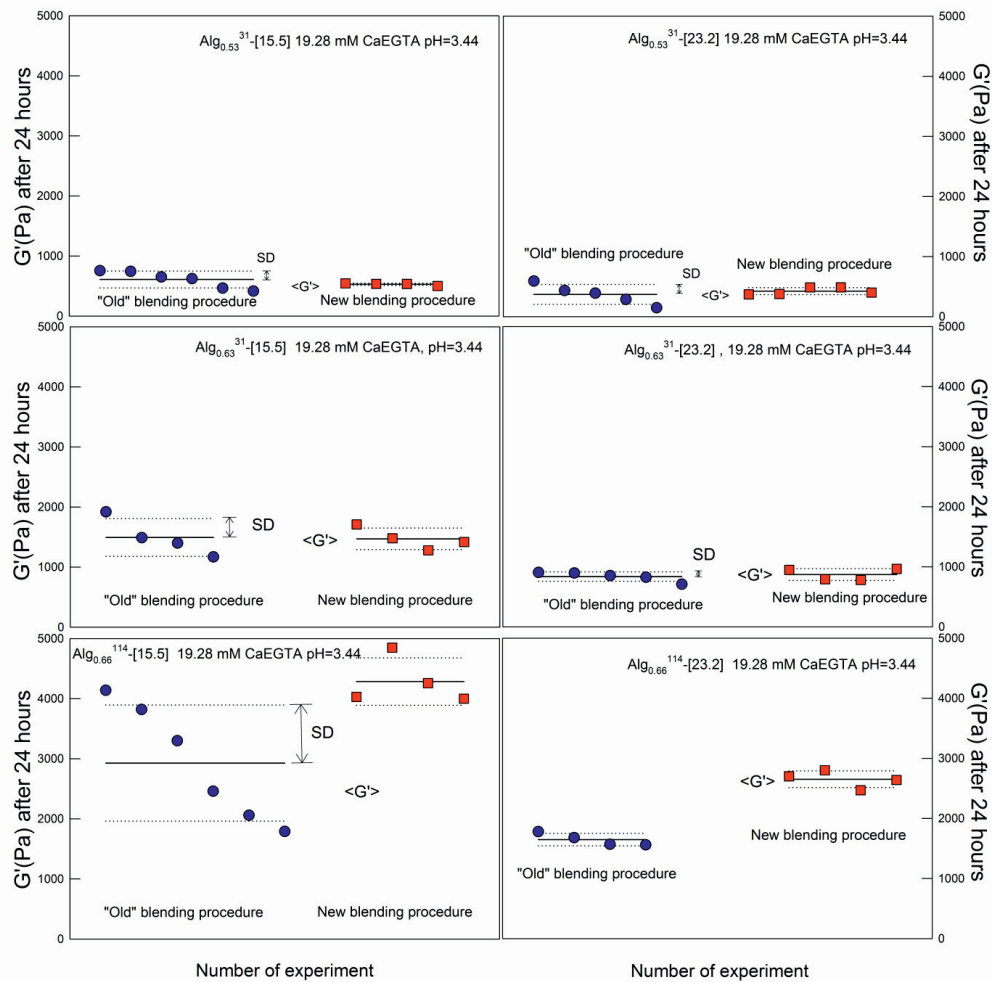


Fig. 3.5.2 Experimental data showing difference in G' reproducibility of the two preparation techniques.

bottom part remained liquid, creating so called “fish eyes”. The problem was solved when we began to dissolve GDL in more water (in our case 3.57x more). The amount of water added to GDL was subtracted from alginate stock solution, leaving final gel concentration the same. All recipes presented here and data presented in chapter 4 are for this latter established technique. The improvement with this latter technique compared to the first preparation technique, is documented in Figs. 3.5.1 and 3.5.2.

3.5.5 Saturations and reduced concentration for samples used during rheology measurements

Table 3.5.1 Fractional Ca^{2+} saturation F_{sat} of guluronic residues belonging to alginate for the samples used in rheology measurements

c_{alg}	$c_{\text{CaEGTA}} = 19.3 \text{ mM pH}=3.44$		
	Alg0.53³¹	Alg0.63³¹	Alg0.66¹¹⁴
mg/mL	F_{sat}		
15.5	0.93	0.78	0.75
23.2	0.62	0.52	0.5
c_{alg}	$c_{\text{CaEGTA}} = 20 \text{ mM pH}=4.0$		
	Alg0.53³¹	Alg0.63³¹	Alg0.66¹¹⁴
mg/mL	F_{sat}		
15.5	0.96	0.81	0.77
23.2	0.64	0.54	0.52
c_{alg}	$c_{\text{CaEGTA}} = 40 \text{ mM pH}=4.0$		
	Alg0.53³¹	Alg0.63³¹	Alg0.66¹¹⁴
mg/mL	F_{sat}		
15.5	1.92	1.62	1.55
23.2	1.28	1.08	1.03

Table 3.5.2 Reduced concentration $c[\eta]$ for the samples used in rheology measurements

c_{alg}	$c[\eta]$		
	Alg0.53³¹	Alg0.63³¹	Alg0.66¹¹⁴
mg/mL			
15.5	0.47	0.53	2.16
23.2	0.94	1.06	4.33

4. Rheology results

Rheology results were not and probably will not be published. Therefore they are presented here as a separate chapter in my thesis. Conditions for which the samples were prepared are described in chapter 3.5.

4.1 Alginate gels prepared at 19.3 mM CaEGTA with final pH 3.44

The time course of the shear storage modulus G' and loss modulus G'' during gelling are shown in Fig. 4.1.1. We measured six different alginate samples gelling in 19.3 mM CaEGTA and reaching pH = 3.44 at the 24 hours from mixing point. The time 86 400 s = 24 hours is marked in the graphs and the final values (at $t = 24$ h) for G' and G'' for all alginate samples are shown in Fig. 4.1.2.

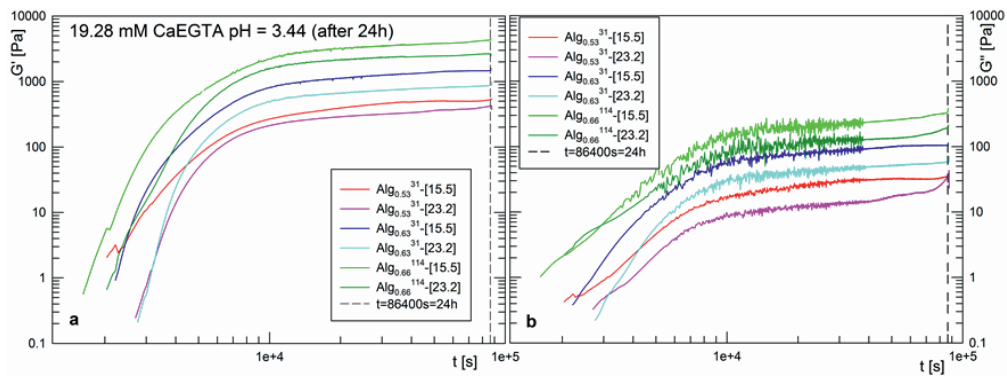


Fig. 4.1.1 G' and G'' as function of time for alginate gelling in 19.3 mM CaEGTA and final pH = 3.44. The vertical line represents $t = 24 \text{ h} = 86400 \text{ s}$. a) Storage modulus G' . b) Loss modulus G'' .

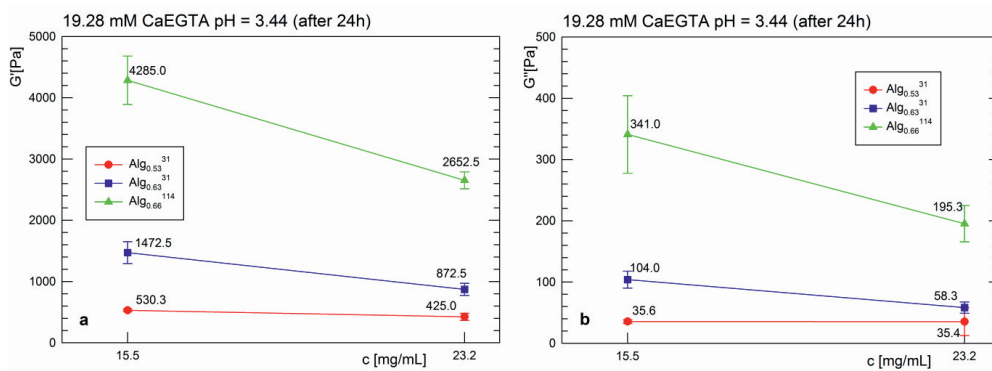


Fig. 4.1.2 Final ($t = 24 \text{ h}$) values for 19.3 mM CaEGTA and final pH = 3.44. a) Storage modulus G' . b) Loss modulus G'' .

Fig. 4.1.2 shows that both G' and G'' increases both with molecular weight and higher guluronic content, whereas decreases with alginate concentration.

4.2 Alginate gels prepared at 20 mM CaEGTA with final pH 4.0

In the same manner as above, the time resolved and final values of G' and G'' during gelling in 20 mM CaEGTA and at a final pH = 4.00 is shown in Fig. 4.2.1.

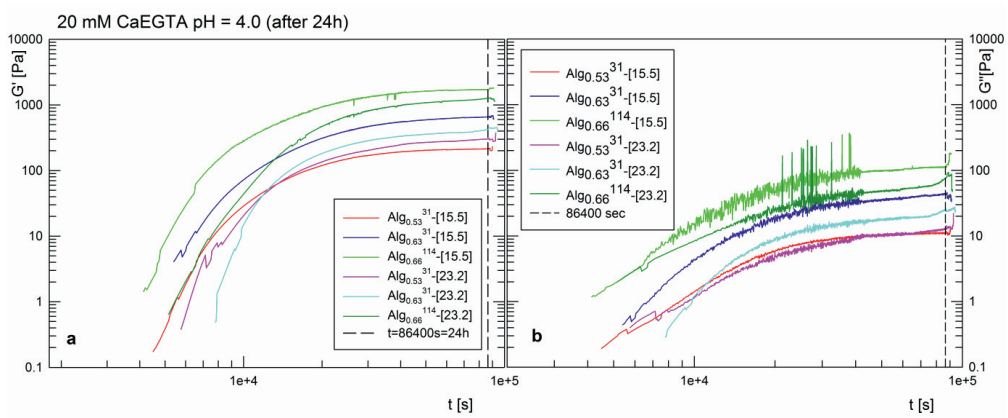


Fig. 4.2.1 G' and G'' as function of time for alginate gelling in 20 mM CaEGTA and final pH = 4.0, vertical line represents $t = 24 \text{ h} = 86400 \text{ s}$. a) Storage modulus G' . b) Loss modulus G'' .

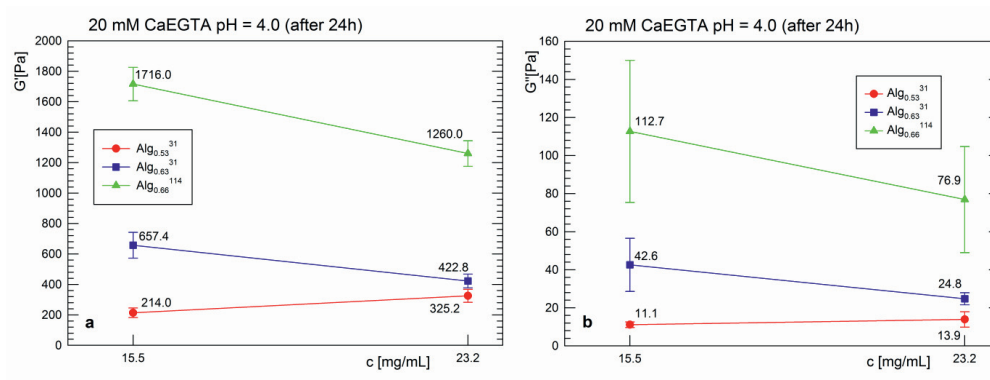


Fig. 4.2.2 Final ($t=24\text{h}$) values for 20 mM CaEGTA and final pH = 4.0. a) Storage modulus G' . b) Loss modulus G'' .

As for pH = 3.44 the storage modulus increases both with molecular weight and higher guluronic content, whereas decrease with alginate concentration as expected [23, 24]. Storage moduli for hydrogels with final pH = 4.00 are lower than in pH=3.44. That is due to protonation of latter one (see chapter xx).

4.3 Alginate gels prepared at 40 mM CaEGTA with final pH 4.0

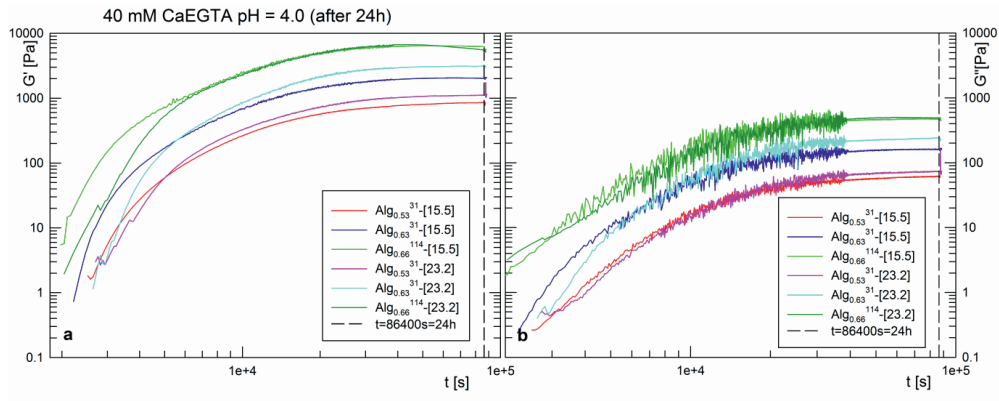


Fig. 4.3.1 G' and G'' as function of time for alginate gelling in 40 mM CaEGTA and final pH = 4.0. Vertical line represents $t = 24 \text{ h} = 86400 \text{ s}$. a) Storage modulus G' . b) Loss modulus G'' .

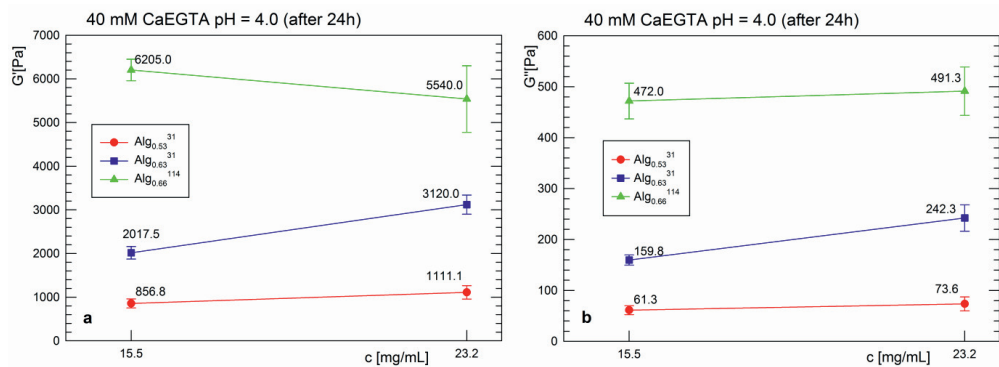


Fig.4.3.2 Final ($t = 24\text{h}$) values for 40 mM CaEGTA and final pH = 4.0. a) Storage modulus G' . b) Loss modulus G'' .

Fig. 4.3.2 shows that the storage and loss moduli of the hydrogels for pH = 4.0 and 40 mM CaEGTA increase both with molecular weight and higher guluronic content. However G' and G'' increase with alginate concentration (except for one sample). This is the opposite of the two cases presented above, and is expected as with 40 mM CaEGTA the sample is in the saturated regime (see Table 3.5.1) [23]. The storage moduli for hydrogels with 40 mM CaEGTA are higher than for ones with 20 mM CaEGTA.

5. Summary of results

Four successfully used techniques in our measurement provided us with complementary results.

Comparing results of nanoindentation and rheology, we can see that in both cases we measure on gelled samples, with exactly the same concentrations of alginate. However measurements done by nanoindentation had not been done for 40 mM CaEGTA and rheology measurements was done without oligoguluronates.

When trying to compare measurements of DLS and SAXS, we can see that in both cases we measure on gelling samples. DLS measurements were done only at saturated regime with two different concentrations, and keeping ratio F_{sat} constant, while measurements done by SAXS were done with different F_{sat} and the same alginate concentration.

Due to that, this chapter briefly summarizes the main finding of each technique and as each paper attached to this thesis presents one technique, sub-chapters are organized and titled in the same manner as papers included in this thesis.

5.1 Paper I: Delaying cluster growth of ionotropic induced alginate gelation by oligogulonate.

Here we study cluster growth during Ca^{2+} induced alginate gelation by dynamic light scattering. Measurements were done on alginate samples with and without oligogulonate (details in chapter 3.2).

During the gelation process, as a result of polymer cluster growth, the transition from liquid to solid state can be observed. Gelation threshold can be characterized by four features introduced by Shibayama [41, 42]: (1) the steep increase in the scattering intensity $\langle I \rangle$; (2) a power-law in the intensity–time correlation function (ICF); (3) a specific broadening of the distribution function, and (4) a noticeable lowering of the initial amplitude of ICF.

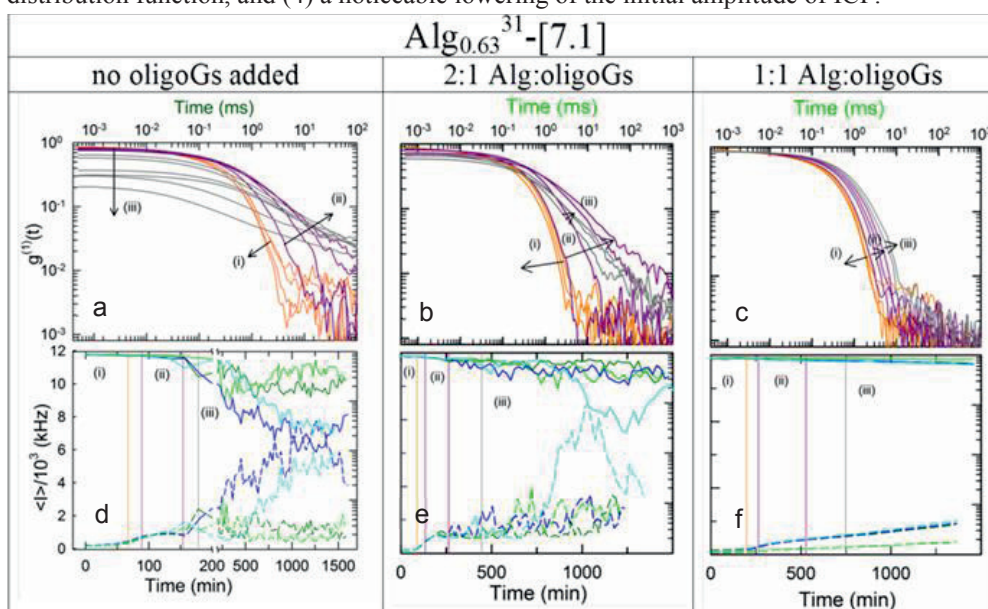


Fig. 5.1.1 The upper row represents ICF for one of parallel experiment, the bottom row represents scattering intensity $\langle I \rangle$ and initial amplitude of ICF for four parallel experiments for $\text{Alg}_{0.63}^{31}\text{-}[7.1]$: a) no oligogulonate b) 2:1 Alg:oligoG c) 1:1 Alg:oligoG d) no oligogulonate e) 2:1 Alg:oligoG f) 1:1 Alg:oligoG. The exact data from graph a are represented on graph d by dark green curve. Data from graph b are represented on graph e by light green curve. whereas data from graph c are represented on graph f by light green curve.

As can be seen in Fig. 5.1.1, our samples fulfil the Shibayama features. The reproducibility in the sample is higher the later the gelation occurs. Detailed study of the parameters from Eq. 2.1.5 and Eq. 2.1.6 enables us to describe the gelation process with the mean relaxation time of the fast mode τ_f shown in Fig. 5.1.2.

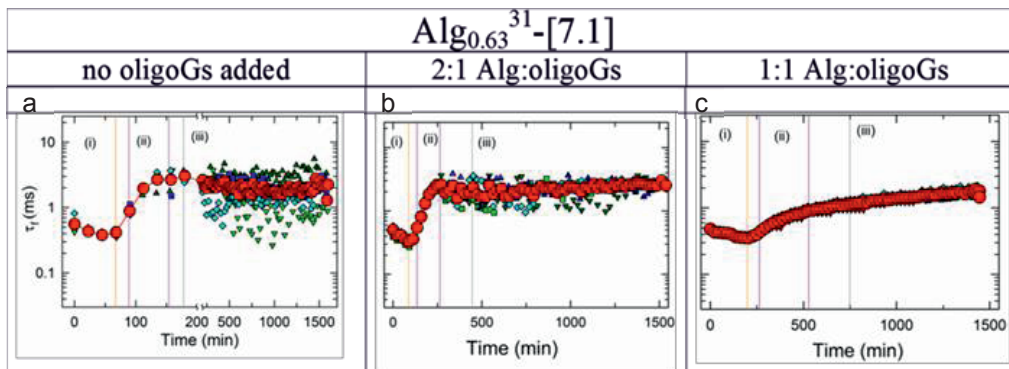


Fig. 5.1.2 Mean relaxation time of the fast relaxation τ_f vs. time after adding GDL, for the four parallel experiments (small \blacktriangle \blacktriangledown \blacklozenge) and the mean of this four parallel (large \bullet).

Fig. 5.1.3 presents data of $\langle\tau_f\rangle$, and it can be observed that addition of oligogulonates delays the gelation. The higher the concentration of oligogulonate, the bigger delay in gelation, when comparing samples without oligogulonate. Detailed study of Fig. 5.1.3 shows that an increase in M_w , increased F_G and increased polymer concentration all lead to a faster increase in τ_f .

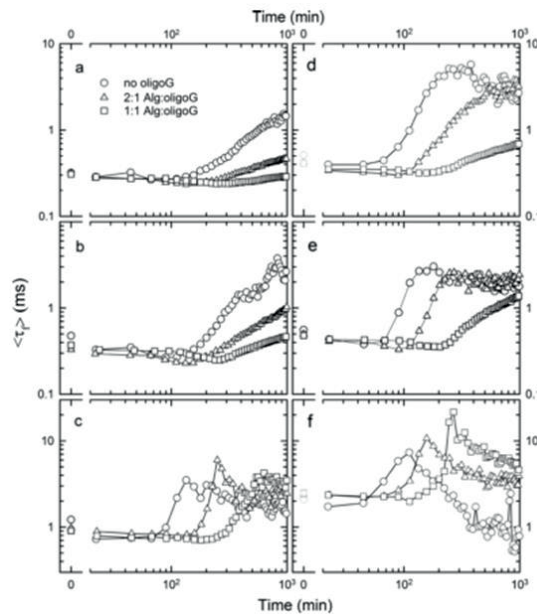


Fig. 5.1.3 Reproduced with permission from the Elsevier from Carbohydrate Polymers (2015) Vol 133, p.126-134 (Fig. 4) [15]. Figure presents: mean relaxation time $\langle\tau_f\rangle$ vs time after inducing Ca^{2+} release for alginates samples without and with oligoG (1:2 and 1:1 oligoG to alginate ratios) for a) $\text{Alg}_{0.53}^{31}\text{-}[3.6]$ b) $\text{Alg}_{0.63}^{31}\text{-}[3.6]$ c) $\text{Alg}_{0.66}^{114}\text{-}[3.6]$ d) $\text{Alg}_{0.53}^{31}\text{-}[7.1]$ e) $\text{Alg}_{0.63}^{31}\text{-}[7.1]$ f) $\text{Alg}_{0.66}^{114}\text{-}[7.1]$

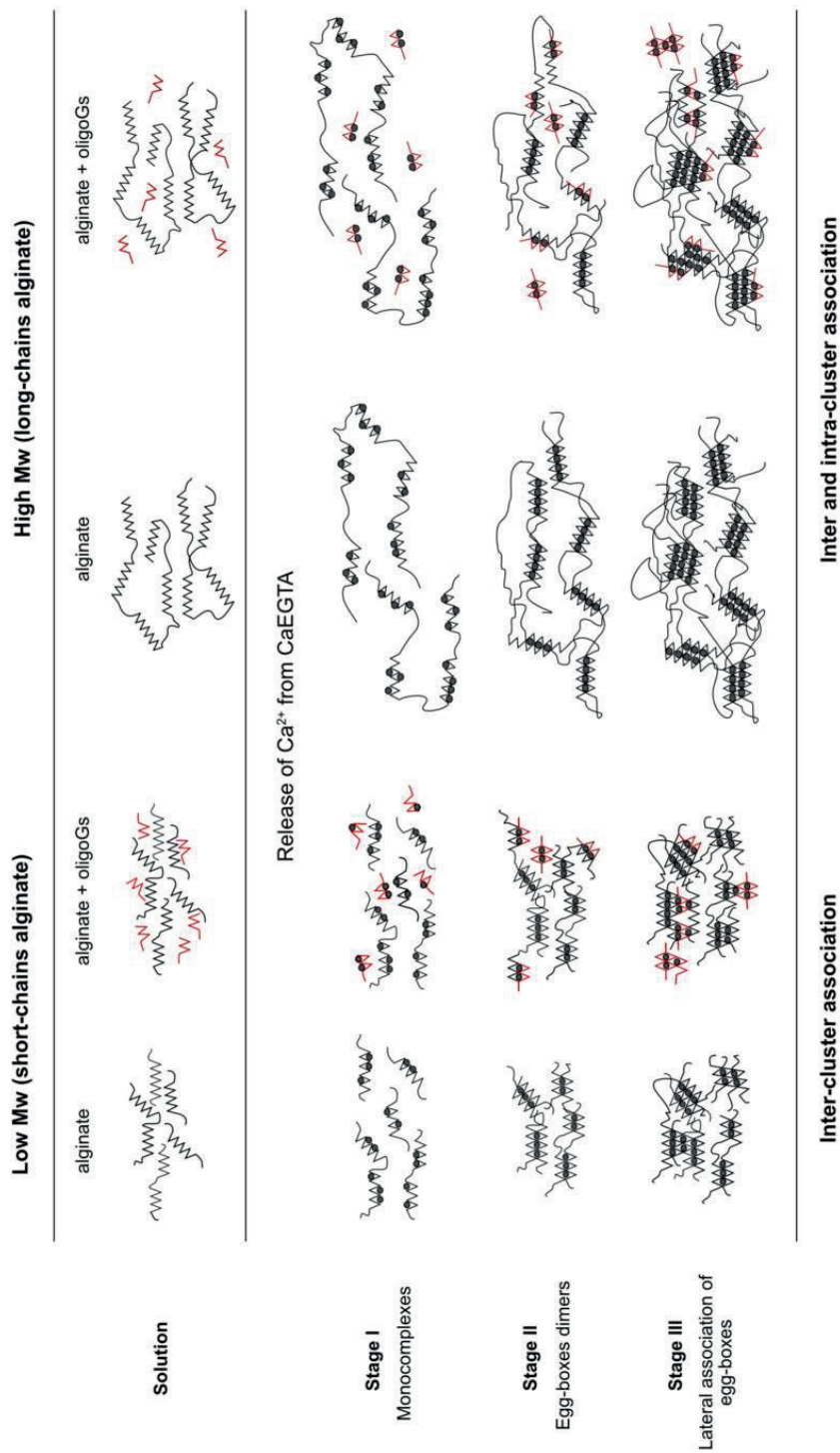


Fig. 5.1.4 Schematic illustration of the effect of adding oligoGs to alginate solutions on the Ca-induced cluster growth at low M_w (short-chains alginate, e.g. Alg_{0.63}³¹ and Alg_{0.53}³¹) and high M_w (long-chains alginate, e.g. Alg_{0.66}¹¹⁴). Symbols: black \blacktriangle is the G-blocks internal in alginate chains, — is the M-blocks, • is Ca²⁺ and red \blacktriangle is oligoGs.

Trying to explain which attributes in the structure in the sample different values of $\langle\tau_f\rangle$ accounts for, we concluded that there are three stages during the alginate/oligoguluronate gelation. We try to present those in Fig.5.1.4.

Stage I: An initial decrease in τ_f suggests formation of less extended structure – monocomplexes [38].

Stage II: A further increase in τ_f suggests creation of egg-boxes dimers.

Stage III: Creation of lateral association of egg-box dimers. However, comparing Fig. 5.1.3 a,b,d,e with Fig. 5.1.3.c,f we can see that $\langle\tau_f\rangle$ for the sample with high molecular weight has a different trend than for the sample with low molecular weight. We believe that for low M_w samples, which are short-chain alginates, lateral association of eggs-boxes dimers leads to inter-cluster compaction and further cluster growth. Whereas for high M_w samples, which are long-chain alginates, lateral association of egg-box dimers leads to intra-cluster compaction and some decrease in cluster size.

5.2 Paper II: Effects of added oligoguluronate on mechanical properties of Ca-alginate-oligoguluronate hydrogels depend on chain length of the alginate.

In this paper we the study effects of oligoguluronates addition on the mechanical properties (Young's modulus) of final Ca-alginate gels by nanoindentation. Measurements were done on alginate samples with and without oligoguluronate (details in chapter 3.3).

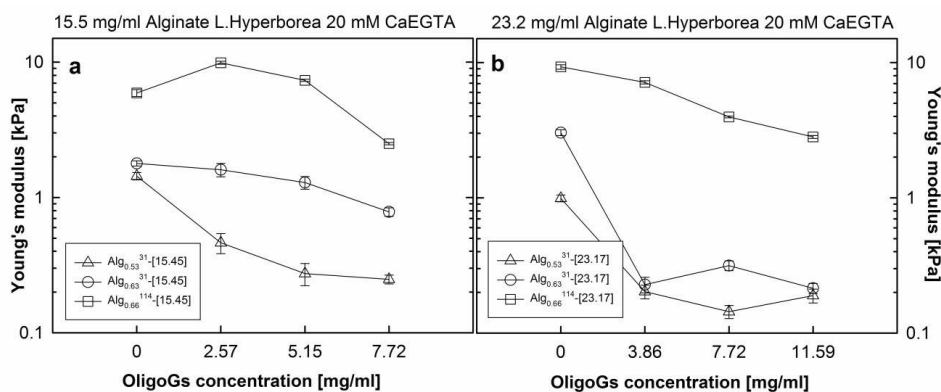


Fig. 5.2.1 Young's modulus vs OligoG concentration, for (a) 15.5 mg/ml alginate and (b) 23.2 mg/mL alginate sample

From previous rheology results of our group [24] and my previous results on the same alginate sample without oligoguluronates (chapter 4), we expected that adding oligoguluronates to an alginate solution prior to gelling initiated by CaEGTA, would result in a decrease in Young's modulus. The decrease is explained by a competition between the added oligoguluronate and the G-blocks belonging to the alginate chains, for Ca^{2+} . Additionally it was known from the same measurements on the same samples that an increase of alginate concentration in case of pure alginate gels resulted in a decrease in the shear modulus, and thus also a decrease in Young's modulus was expected. Our results however do not obey all those expectations, see Fig. 5.2.1.

The minimum consecutive number of guluronic acid residues needed to support Ca^{2+} mediated junctions is 8 ± 2 [36]. Different alginates, with different composition will possess different capacities to support junction zone formation. The average number of junction zones per chain N_{junc} was estimated to be 16.6 ($\text{Alg}_{0.66}^{114}$), 4.0 ($\text{Alg}_{0.63}^{31}$) and 2.6 ($\text{Alg}_{0.53}^{31}$). This suggests that the sample $\text{Alg}_{0.53}^{31}$ is on the borderline ($N_{\text{junc}}=2$) of being able to form a gel.

Table 5.2.1 Estimated alginate chain parameters. The weight average degree of polymerization DP_w was estimated using a molar mass of 198 g/mol (Na-form) for each uronic acid residue. Parameters L_j and L_e are the average number of residues in the junction zones and elastic segments, respectively. The parameters were interpolated to the values for the given samples represented by $N_{G>1}$ based on the empirical correlation between L_e and L_j on one hand, and $N_{G>1}$, on the other, using the reported numerical estimates [69]. The number of junction zone supported per chain (of chain length DP_w) were estimated as $\text{DP}_w / (L_e + L_j)$.

Alginate source:	Sample notation	M_w kg/mol	$N_{G>1}$	DP_w	L_j	L_e	N_{junc}
<i>L. Hyperborea</i> – leaf	$\text{Alg}_{0.53}^{31}$	31	8	160	14	48	2.6
<i>L. Hyperborea</i> –stem	$\text{Alg}_{0.63}^{31}$	31	11	160	17	23	4.0
<i>L. Hyperborea</i> - stem	$\text{Alg}_{0.66}^{114}$	114	13	385	19	16	16.6

When introducing oligoguluronate to the lower M_w samples there is a decrease in the Young's modulus for both concentrations (Fig. 5.2.1). This decrease is expected to be caused by decrease of N_{junc} , and ensuing increased fraction of the sample being in loose end state and increased sol-fraction. For high M_w samples it seems that longer G-blocks are being selectively more involved in the junction zones. At the same time shorter G-blocks are less likely to be engaged in the network.

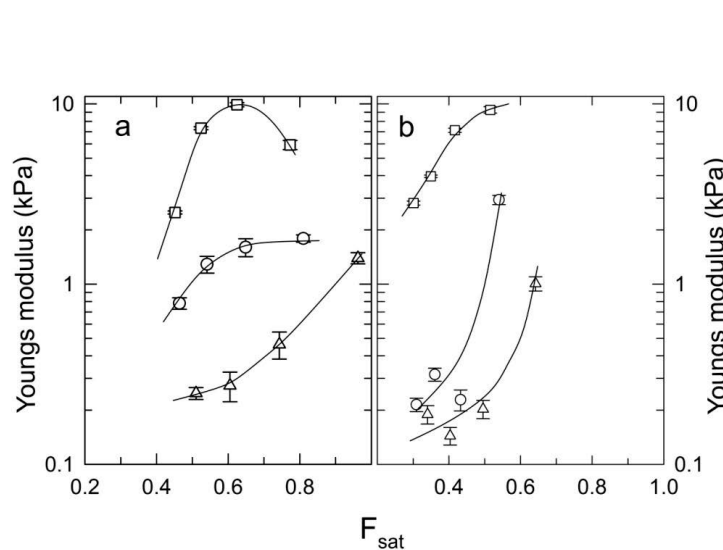


Fig. 5.2.2 Young's modulus vs F_{sat} induced by adding oligoG to the samples, for (a) 15.5 mg/ml alginate and (b) 23.2 mg/mL alginate sample. Squares represent $\text{Alg}_{0.66}^{114}$, circles are $\text{Alg}_{0.63}^{31}$ and triangles are $\text{Alg}_{0.53}^{31}$. The figure is from Paper II.

It was reported by Liao et al. [37], that oligoguluronate can promote junction zone aggregation at $F_{\text{sat}} > 1.2$, and result in an increase in elasticity when the concentration of oligoguluronate is increased. Whereas for $F_{\text{sat}} < 1.2$ decreasing elasticity was reported due to competition for Ca^{2+} of oligoguluronate and the G-blocks belonging to alginate chain [24, 37, 70]. Our present findings in Paper II indicate that the M_w of the alginate chain has also an influence on the mechanical properties. Suggesting that if alginate chain contain sufficient number of G-block sequences, addition of oligoguluronates may actually increase the network connectivity and though the elasticity of gel.

5.3 Paper III: Local structure of Ca induced hydrogels of alginate – oligoguluronate blends.

Here we study the local structure of Ca^{2+} induced alginate gels by small angle X-ray scattering. In static measurements samples were left for gelation in 24 hours before measurement was performed. In time-resolved measurements the sample was measured at appropriate time intervals the first 24 hours after gelation was initiated. Samples were prepared from alginate with and without oligoguluronate (details in chapter 3.4). Scattering curves obtained from SAXS measurements were plotted as Guinier and Kratky plots (details in chapter 2.3.4).

Static measurements

The $R_{G,c}$ values for alginate and oligogulonate in solution can be estimated from a rod-like model using a Guinier plot as described in chapter 2.3.4. Whereas gelling alginate with and without oligogulonates can be described by broken rod model using a Kratky plot as described in the same chapter.

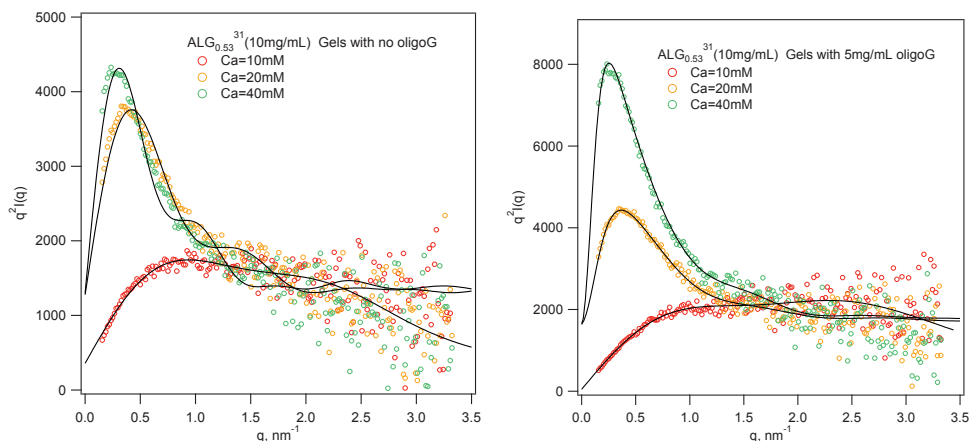


Fig. 5.3.1 Kratky plots for static SAXS measurements from $\text{Alg}_{0.53}^{31}$ -[10] at $\text{Ca}=10, 20$ and 40 mM (a) without oligoG and (b) 1:2 oligoG to alginate ration. Data (symbols) and the corresponding model fits (curves) are depicted.

Table 5.3.2 Cross-sectional radii R_{Gci} and a , a measure of the extension of the inhomogeneities obtained from SAXS analysis for $\text{Alg}_{0.53}^{31}$, $\text{Alg}_{0.66}^{114}$ solution and gels with and without oligoG and for oligoG without alginate.

$\text{Alg}_{0.53}^{31}$		no oligoG			1:2 oligoG:Alginate							
C_{alg}	C_{CaEGTA}	F_{sat}	R_{Gc1}	R_{Gc2}	F_{sat}	R_{Gc1}	R_{Gc2}	a				
mg/mL	mM		nm	nm		nm	nm	nm				
10	0	0	0.41		0							
10	10	0.74	0.87	2.22	0.40	0.64	2					
10	20	1.49	1.69	3.53	0.80	0.73	1.73	4.33				
10	40	2.97	2.18	4.88	1.61	0.83	1.86	5.37				
$\text{Alg}_{0.66}^{114}$		no oligoG			1:2 oligoG:Alginate				1:1 oligoG:Alginate			
C_{alg}	C_{CaEGTA}	F_{sat}	R_{Gc1}	R_{Gc2}	F_{sat}	R_{Gc1}	R_{Gc2}	a	F_{sat}	R_{Gc1}	R_{Gc2}	a
mg/mL	mM		nm	nm		nm	nm	nm		nm	nm	nm
10	0	0	0.49	-								
10	10	0.6	0.83	2.12	0.35	0.64	1.99	-	0.25	0.56	1.74	-
10	20	1.19	1.63	2.97	0.71	1.74	3.02	3.03	0.51	1.13	2.64	5.84
10	40	2.39	1.93	3.91	1.42	1.67	3.25	4.29	1.01	1.54	3.13	5.72

Data obtained from static SAXS measurements for both $\text{Alg}_{0.53}^{31}$ and $\text{Alg}_{0.66}^{114}$ gels with no oligoguluronates, show that both values of $R_{\text{Ge}1}$ and $R_{\text{Ge}2}$ increase with increasing calcium concentrations (Table 5.3.2). At the same time the $R_{\text{Ge}1}$ and $R_{\text{Ge}2}$ of $\text{Alg}_{0.53}^{31}$ gels seems to be larger than for the $\text{Alg}_{0.66}^{114}$ gels. In case of alginate-oliguluronate gels we see an increase in the value of a when increasing the oligoG concentration, and the same when increasing the Ca concentration. This means that the size of the inhomogeneities increases. The values of a for the $\text{Alg}_{0.53}^{31}$ gels tend to be bigger than for $\text{Alg}_{0.66}^{114}$, indicating that a sample with lower F_{G} have more expanded aggregation.

Our data suggest that alginate sample with oligoG yields larger $R_{\text{Ge}1}$ and $R_{\text{Ge}2}$ in the range $0.5 < F_{\text{sat}} < 1.0$ than without oligoG added. However, this is in disagreement with Liao et al. [37]

Dynamic measurements (time-resolved SAXS)

Fig. 5.3.2 shows the time variation of Kratky plots for gelation of alginate without and with oligoG added. In the time-resolved SAXS measurements all curves were fitted with the broken rod-like model using the Debye-Bueche function. The results of fitting the data using the Debye-Bueche type scattering function is shown in Tab. 5.3.3 In the beginning of the gelling process the one component model ($R_{\text{Ge}1}$) was adequate, whereas later in the process the two component rods model ($R_{\text{Ge}1}$ and $R_{\text{Ge}2}$) had to be used. For the alginate-oligoguluronate sample the broken rod-like model with Debye-Bueche function was also used in later time frames.

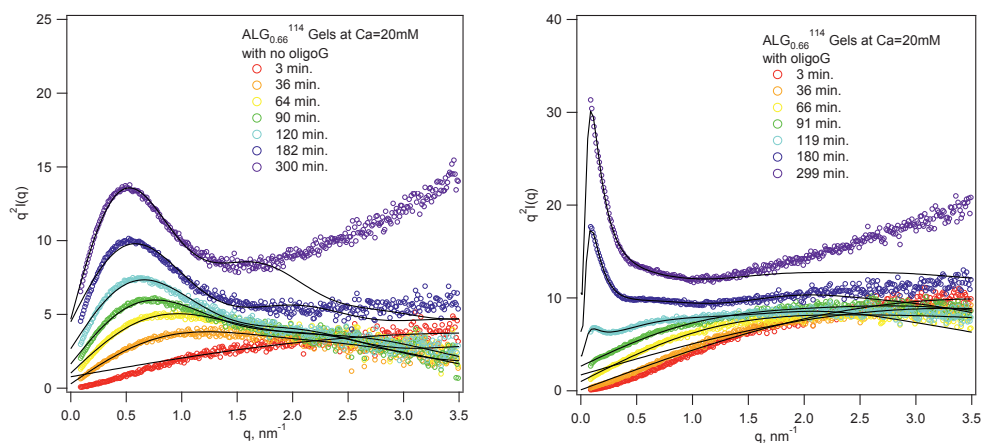


Fig. 5.3.2 Time variation of Kratky plots for time resolved SAXS for gelation of alginate $\text{Alg}_{0.66}^{114}$ -[10] $\text{Ca} = 20 \text{ mM}$. (a) no oligoG, (b) 1:1 oligoG to alginate. Data (symbols) and fit to the data (lines) are shown.

Table 5.3.3 Time-course of cross-sectional radius and an obtained from time resolved SAXS for Alg_{0.66}¹¹⁴ (10.0 mg/mL) with and without oligoG (10.0 mg/mL).

Alg _{0.66} ¹¹⁴ (10.0 mg/mL)			Alg _{0.66} ¹¹⁴ (10.0 mg/mL) + oligoG (10.0 mg/mL)			
C _{CaEGTA} = 20 mM			C _{CaEGTA} = 20 mM			
$F_{sat} = 1.19$			$F_{sat} = 0.51$			
Time	R_{Gc1}	R_{Gc2}	Time	R_{Gc1}	R_{Gc2}	a
(min)	(nm)	(nm)	(min)	(nm)	(nm)	(nm)
3	0.37	-	3	0.38	-	-
36	0.74	1.7	36	0.41	-	-
64	0.75	1.82	66	0.45	1.17	-
90	0.93	2.14	91	0.5	1.47	-
120	1.17	2.35	119	0.68	2.28	10.6
182	1.13	2.47	180	0.63	2.62	11.2
300	1.15	2.92	299	0.55	2.91	10.9

Tab. 5.3.3 shows that oligogulonates added to alginate sample delay the gelation. It can also be seen that alginate samples without oligoG are stiffer and less turbid and that R_{Gc1} , R_{Gc2} and a all were increasing with gelation time.

5.4 Rheology

For alginate samples in unsaturated regime (19.3 and 20 mM CaEGTA) both G' and G'' increases both with M_w and higher F_G , whereas decreases with alginate concentration as expected [23, 24].

For alginate samples in saturated regime (40 mM CaEGTA) storage and loss moduli of the hydrogels increase with M_w , higher F_G and with alginate concentration as expected [23], (except for sample Alg_{0.66}¹¹⁴).

Storage moduli for hydrogels with final pH=4.00 are lower than in pH=3.44. That is due to protonation. The storage moduli for hydrogels with 40 mM CaEGTA are higher than for ones with 20 mM CaEGTA.

Discrepancy with nanoindentation

Data for 20 mM CaEGTA without oligogulonate (rheology results presented in chapter 4 and nanoindentation results presented in Paper I) and data for 19.3 mM CaEGTA without oligogulonate (rheology results presented in chapter 4 and nanoindentation results not presented due to different technique of moulding) have opposite trends in relation of alginate concentration. Rheology measurements shows that stiffness of gel decrease with increasing concentration, whereas nanoindentation results shows increase of gel stiffness with increasing concentration.

References:

- [1] E.C.C. Stanford, British Patent no.142 (1881).
- [2] W.L. Nelson, L.H. Cretcher, THE ALGINIC ACID FROM MACROCYSTIS PYRIFERA1, 2, Journal of the American Chemical Society 51 (1929) 1914-1922.
- [3] W.L. Nelson, L.H. Cretcher, The isolation and identification of d-mannuronic acid lactone from the *Macrocystis pyrifera*, Journal of the American Chemical Society 52 (1930) 2130-2132.
- [4] W.L. Nelson, L.H. Cretcher, The properties of d-mannuronic acid lactone, Journal of the American Chemical Society 54 (1932) 3409-3412.
- [5] G.M. Bird, P. Haas, On the nature of the cell wall constituents of *Laminaria* spp. Mannuronic acid, Biochemical Journal 25 (1931) 403.
- [6] T. Miwa, Alginic acid, Jour. Chem. Soc. Japan 51 (1930) 738-745.
- [7] A. Haug, B.R. Larsen, A study on the constitution of alginic acid by partial acid hydrolysis, Proc Int Seaweed Symp 5 (1965) 271-273.
- [8] K.I. Draget, O. Smidsrød, G. Skjåk-Bræk, in: Biopolymers Online, (Wiley-VCH Verlag GmbH & Co. KGaA, 2005).
- [9] S.T. Moe, K.I. Draget, G. Skjåk-Bræk, O. Smidsrød, in: Food Science and Technology, ed A.M. Stephen (1995).
- [10] F.G. Fischer, H. Dörfel, Die Polyuronsäuren der Braunalgen, Z. Physiol. Chem 302:186 (1955).

- [11] T.M. Bjerkan, B.E. Lillehov, W.I. Strand, G. Skjåk-Braek, S. Valla, H. Ertesvag, Construction and analyses of hybrid *Azotobacter vinelandii* mannuronan C-5 epimerases with new epimerization pattern characteristics, *Biochemical Journal* 381 (2004) 813-821.
- [12] B.I.G. Svanem, G. Skjåk-Bræk, H. Ertesvåg, S. Valla, Cloning and Expression of Three New *Azotobacter vinelandii* Genes Closely Related to a Previously Described Gene Family Encoding Mannuronan C-5-Epimerases, *Journal of bacteriology* 181 (1999) 68-77.
- [13] H.K. Høidal, H. Ertesvåg, G. Skjåk-Bræk, B.T. Stokke, S. Valla, The recombinant *Azotobacter vinelandii* mannuronan C-5-epimerase AlgE4 epimerizes alginate by a nonrandom attack mechanism, *Journal of Biological Chemistry* 274 (1999) 12316-12322.
- [14] Y.A. Mørch, S. Holtan, I. Donati, B.L. Strand, G. Skjåk-Bræk, Mechanical properties of C-5 epimerized alginates, *Biomacromolecules* 9 (2008) 2360-2368.
- [15] A.M. Padoł, G. Maurstad, K.I. Draget, B.T. Stokke, Delaying cluster growth of ionotropic induced alginate gelation by oligoguluronate, *Carbohydrate Polymers* 133 (2015) 126-134.
- [16] I. Donati, S. Paoletti, in: *Alginates: Biology and Applications*, ed B.H.A. Rehm (Springer Berlin Heidelberg, 2009).
- [17] P. de Vos, M.M. Faas, B. Strand, R. Calafiore, Alginate-based microcapsules for immunoisolation of pancreatic islets, *Biomaterials* 27 (2006) 5603-5617.
- [18] K.I. Draget, K. Ostgaard, O. Smidsrød, Alginate-Based Solid Media for Plant-Tissue Culture, *Applied Microbiology and Biotechnology* 31 (1989) 79-83.
- [19] K.Y. Lee, D.J. Mooney, Alginate: Properties and biomedical applications, *Progress in Polymer Science* 37 (2012) 106-126.
- [20] A. Haug, B. Larsen, O. Smidsrød, Studies on the sequence of uronic acid residues in alginic acid, *Acta Chem Scand* 21 (1967) 691-704.
- [21] Y.A. Mørch, Novel Alginate Microcapsules for Cell Therapy – A study of the structure-function relationships in native and structurally engineered alginates, Doctoral Thesis at NTNU (2008).
- [22] O. Smidsrød, R.M. Glover, S.G. Whittington, The relative extension of alginates having different chemical composition, *Carbohydrate Research* 27 (1973) 107-118.
- [23] M. Sletmoen, K.I. Draget, B.T. Stokke, in: *Macromolecular Symposia*, (Wiley Online Library, 2010).
- [24] T.E. Jorgensen, M. Sletmoen, K.I. Draget, B.T. Stokke, Influence of oligoguluronates on alginate gelation, kinetics, and polymer organization, *Biomacromolecules* 8 (2007) 2388-2397.
- [25] O. Smidsrød, Molecular basis for some physical properties of alginates in the gel state, *Faraday discussions of the Chemical Society* 57 (1974) 263-274.
- [26] A. Haug, Composition and properties of alginates (Norwegian Institute of Seaweed Research (Norsk institutt for tang- og tareforskning), [Trondheim, Norvège], 1964).
- [27] K.I. Draget, G. Skjåk Bræk, O. Smidsrød, Alginic acid gels: the effect of alginate chemical composition and molecular weight, *Carbohydrate Polymers* 25 (1994) 31-38.
- [28] K.I. Draget, G. Skjåk-Braek, B.T. Stokke, Similarities and differences between alginic acid gels and ionically crosslinked alginate gels, *Food Hydrocolloids* 20 (2006) 170-175.
- [29] O. Smidsrød, K.I. Draget, Alginate gelation technologies, *Special Publications of the Royal Society of Chemistry* 192 (1997) 279-293.
- [30] G.T. Grant, E.R. Morris, D.A. Rees, P.J.C. Smith, D. Thom, Biological interactions between polysaccharides and divalent cations: The egg-box model, *FEBS Letters* 32 (1973) 195-198.
- [31] B.T. Stokke, K.I. Draget, O. Smidsrød, Y. Yuguchi, H. Urakawa, K. Kajiwara, Small-angle X-ray scattering and rheological characterization of alginate gels. 1. Ca-alginate gels, *Macromolecules* 33 (2000) 1853-1863.
- [32] A. Mikkelsen, A. Elgsaeter, Density distribution of calcium-induced alginate gels. A numerical study, *Biopolymers* 36 (1995) 17-41.
- [33] G. Maurstad, Y.A. Mørch, A.R. Bausch, B.T. Stokke, Polyelectrolyte layer interpenetration and swelling of alginate-chitosan multilayers studied by dual wavelength reflection interference contrast microscopy, *Carbohydrate Polymers* 71 (2008) 672-681.

- [34] H. Grasdalen, B. Larsen, O. Smidsrød, A p.m.r. study of the composition and sequence of uronate residues in alginates, *Carbohydrate Research* 68 (1979) 23-31.
- [35] H. Grasdalen, B. Larsen, O. Smisrod, ¹³C-n.m.r. studies of monomeric composition and sequence in alginate, *Carbohydrate Research* 89 (1981) 179-191.
- [36] B.T. Stokke, O. Smidsrød, F. Zanetti, W. Strand, G. Skjåk-Bræk, Distribution of uronate residues in alginate chains in relation to alginate gelling properties — 2: Enrichment of β -d-mannuronic acid and depletion of α -l-guluronic acid in sol fraction, *Carbohydrate Polymers* 21 (1993) 39-46.
- [37] H. Liao, W. Ai, K. Zhang, M. Nakauma, T. Funami, Y. Fang, K. Nishinari, K.I. Draget, G.O. Phillips, Mechanisms of oligoguluronate modulating the calcium-induced gelation of alginate, *Polymer* 74 (2015) 166-175.
- [38] Y. Fang, S. Al-Assaf, G.O. Phillips, K. Nishinari, T. Funami, P.A. Williams, L. Li, Multiple Steps and Critical Behaviors of the Binding of Calcium to Alginate, *The Journal of Physical Chemistry B* 111 (2007) 2456-2462.
- [39] Y. Fang, S. Al-Assaf, G.O. Phillips, K. Nishinari, T. Funami, P.A. Williams, Binding behavior of calcium to polyuronates: Comparison of pectin with alginate, *Carbohydrate Polymers* 72 (2008) 334-341.
- [40] D. Larobina, L. Cipelletti, Hierarchical cross-linking in physical alginate gels: a rheological and dynamic light scattering investigation, *Soft Matter* 9 (2013) 10005-10015.
- [41] M. Shibayama, T. Norisuye, Gel formation analyses by dynamic light scattering, *Bulletin of the Chemical Society of Japan* 75 (2002) 641-659.
- [42] M. Shibayama, Universality and Specificity of Polymer Gels Viewed by Scattering Methods, *Bulletin of the Chemical Society of Japan* 79 (2006) 1799-1819.
- [43] S. Richter, in: *Macromolecular Symposia*, (Wiley Online Library, 2007).
- [44] T. Matsunaga, M. Shibayama, Gel point determination of gelatin hydrogels by dynamic light scattering and rheological measurements, *Physical Review E* 76 (2007) 030401.
- [45] S.K. Kundu, N. Osaka, T. Matsunaga, M. Yoshida, M. Shibayama, Structural Characterization of Ionic Gelator Studied by Dynamic Light Scattering and Small-Angle Neutron Scattering, *The Journal of Physical Chemistry B* 112 (2008) 16469-16477.
- [46] A. Maleki, A.L. Kjoniksen, B. Nystrom, Characterization of the chemical degradation of hyaluronic acid during chemical gelation in the presence of different cross-linker agents, *Carbohydr Res* 342 (2007) 2776-2792.
- [47] J.E. Martin, J. Wilcoxon, J. Odinek, Decay of density fluctuations in gels, *Phys Rev A* 43 (1991) 858-872.
- [48] M. Prasad, M. Kopycinska, U. Rabe, W. Arnold, Measurement of Young's modulus of clay minerals using atomic force acoustic microscopy, *Geophysical Research Letters* 29 (2002) 13-11-13-14.
- [49] K. Miyake, N. Satomi, S. Sasaki, Elastic modulus of polystyrene film from near surface to bulk measured by nanoindentation using atomic force microscopy, *Applied Physics Letters* 89 (2006) 031925.
- [50] C.d.L. Davies, B.T. Stokke, in: *Biophysical Microtechniques*, ed N.U.o.S.a. Technology (2008).
- [51] Y.H. Hu, X.H. Zhao, J.J. Vlassak, Z.G. Suo, Using indentation to characterize the poroelasticity of gels, *Applied Physics Letters* 96 (2010) 121904.
- [52] B.J. Briscoe, K.S. Sebastian, M.J. Adams, The Effect of Indenter Geometry on the Elastic Response to Indentation, *Journal of Physics D-Applied Physics* 27 (1994) 1156-1162.
- [53] C.T. McKee, J.A. Last, P. Russell, C.J. Murphy, Indentation versus tensile measurements of Young's modulus for soft biological tissues, *Tissue Engineering Part B: Reviews* 17 (2011) 155-164.
- [54] M.L. Oyen, R.F. Cook, A practical guide for analysis of nanoindentation data, *Journal of the mechanical behavior of biomedical materials* 2 (2009) 396-407.
- [55] C.X. Wang, C. Cowen, Z. Zhang, C.R. Thomas, High-speed compression of single alginate microspheres, *Chemical Engineering Science* 60 (2005) 6649-6657.

- [56] L.A. Pfister, M. Papaloizos, H.P. Merkle, B. Gander, Hydrogel nerve conduits produced from alginate/chitosan complexes, *Journal of Biomedical Materials Research Part A* 80A (2007) 932-937.
- [57] M. Moresi, M. Bruno, Characterisation of alginate gels using quasi-static and dynamic methods, *Journal of Food Engineering* 82 (2007) 298-309.
- [58] A. Oleś, *Metody doświadczalne fizyki ciała stałego*, 1998).
- [59] W. Łuźny, *Wstęp do nauki o polimerach* (Akademia Górniczo-Hutnicza, Kraków, 1999).
- [60] A. Guinier, G. Fournet, *Small angle scattering of X-rays*, 1955).
- [61] K. Høydalsvik, Nanostructure of dip-coated Yttria-doped Zirconia Sol-Gel coatings studied by grazing-incidence small-angle x-ray scattering, Aberystwyth University PhD thesis or dissertation (2010).
- [62] (BL-10C: Small-angle X-ray scattering <http://pfweis.kek.jp/~saxs/BeamLine/BL10C/bl10c.html> Photon Factory).
- [63] K. Kajiwara, Y. Hiragi, in: *Analytical Spectroscopy Library*, eds H. Saisho, Y. Gohshi (Elsevier, 1996).
- [64] (BL45XU OUTLINE http://www.spring8.or.jp/wkg/BL45XU/instrument/lang-en/INS-0000000334/instrument_summary_view, RIKEN Harima Institute Spring-8 Center).
- [65] O. Glatter, O. Kratky, *Small Angle X-ray Scattering*, 1982).
- [66] B. Hammouda, (National Institute of Standards and Technology - Center for Neutron Research 2011).
- [67] Y. Yuguchi, H. Urakawa, K. Kajiwara, K.I. Draget, B.T. Stokke, Small-angle X-ray scattering and rheological characterization of alginate gels. 2. Time-resolved studies on ionotropic gels, *Journal of Molecular Structure* 554 (2000) 21-34.
- [68] F. Chambon, H.H. Winter, Linear Viscoelasticity at the Gel Point of a Crosslinking PDMS with Imbalanced Stoichiometry, *Journal of Rheology* (1978-present) 31 (1987) 683-697.
- [69] B.T. Stokke, O. Smidsrød, P. Bruheim, G. Skjåk-Bræk, Distribution of Uronate Residues in Alginate Chains in Relation to Alginate Gelling Properties, *Macromolecules* 24 (1991) 4637-4645.
- [70] K. Draget, O. Smidsrød, Modification of gelling kinetics and elastic properties by nano structuring of alginate gels exploiting the properties of polyguluronate, *SPECIAL PUBLICATION-ROYAL SOCIETY OF CHEMISTRY* 303 (2007) 227.

Delaying cluster growth of ionotropic induced alginate gelation by oligoguluronate

A.M.Padoł, G.Maurstad, K.I.Draget, B.T.Stokke,
Carbohydrate Polymers Vol.133, 2015, 126–134



Contents lists available at ScienceDirect

Carbohydrate Polymers

journal homepage: www.elsevier.com/locate/carbpol

Delaying cluster growth of ionotropic induced alginate gelation by oligoguluronate



Anna Maria Padoł^a, Gjertrud Maurstad^a, Kurt Ingar Draget^b, Bjørn Torger Stokke^{a,*}

^a Biophysics and Medical Technology, Department of Physics, The Norwegian University of Science and Technology, NTNU, NO-7491 Trondheim, Norway

^b Department of Biotechnology, The Norwegian University of Science and Technology, NTNU, NO-7491 Trondheim, Norway

ARTICLE INFO

Article history:

Received 28 April 2015

Received in revised form 22 June 2015

Accepted 7 July 2015

Available online 13 July 2015

Keywords:

Alginate

Oligoguluronate

Ionotropic gelation

ABSTRACT

Alginates form gels in the presence of various divalent ions, such as Ca^{2+} that mediate lateral association of chain segments. Various procedures exist that introduce Ca^{2+} to yield alginate hydrogels with overall homogeneous or controlled gradients in the concentration profiles. In the present study, the effect of adding oligomers of α -L-guluronic acid (oligoGs) to gelling solutions of alginate was investigated by determination of the cluster growth stimulated by in situ release of Ca^{2+} . Three different alginate samples varying in fraction of α -L-guluronic acid and molecular weights were employed. The cluster growth was determined for both pure alginates and alginates with two different concentrations of the oligoGs employing dynamic light scattering. The results show that addition of oligoG slows down the cluster growth, the more efficient for the alginates with higher fraction of α -L-guluronic acid, and the higher molecular weight. The efficiency in delaying and slowing the cluster growth induced by added oligoG were discussed in view of the molecular parameters of the alginates. These results show that oligoG can be added to alginate solutions to control the cluster growth and eventually also transition to the gel state. Quantitative relation between the concentration of added oligoG, type and molecular weight of the alginate, and concentration, can be employed as guidelines in tuning alginate cluster growth with specific properties.

© 2015 Elsevier Ltd. All rights reserved.

1. Introduction

Alginates are naturally occurring polysaccharides as cell wall components in brown algae species or produced by *Azobacter vinelandii* and several of *Pseudomonas* species. Commercial alginates are all from algae sources (Moe, Draget, Skjåk-Braek, & Smidsrød, 1995). They are linear heteropolysaccharides of (1 → 4) linked β -D-mannuronic acid, denoted M, and α -L-guluronic acid, denoted G. The monosaccharide fractions and sequence depend on the alginate source as extracted from different algae, between different parts of one algae species as well as the harvesting season. The monomers occur within the alginate molecule as homopolymeric sequences of mannuronic or guluronic acid, denoted as M- and G-blocks, and sequences of a more alternating nature denoted MG-blocks (Moe et al., 1995). In addition to the selection of alginate with sequences obtainable from natural sources, tailor-made alginate sequences can be manufactured by ex

vivo enzymatic modification applying mannuronan C5 epimerases converting mannuronate to guluronate residues (Høidal, Ertesvåg, Skjåk-Braek, Stokke, & Valla, 1999; Svanem, Skjåk-Braek, Ertesvåg, & Valla, 1999). The fraction and properties of the G-blocks are the key structural element in the binding of multivalent ions (most commonly Ca^{2+}) and hence also for the gelling properties of alginates (Smidsrød, 1974).

The mild ionotropic gelation of alginates, combined with alginate's biocompatibility and nontoxicity, have paved the way for various applications (Lim & Sun, 1980; Marijnissen et al., 2002; Miralles et al., 2001; Morch, Donati, Strand, & Skjåk-Braek, 2007) and concomitant research in the structure function relationship of this versatile biopolymer family. Within the food area, alginates functionality as thickeners, stabilizers, film formers and gelling agents are widely explored (Moe et al., 1995). Biomedical and pharmaceutical applications exploit alginate functionality for cell entrapment, immunological isolation barriers between implant and host, and for controlled drug delivery (de Vos, Faas, Strand, & Calafiore, 2006; Draget, Ostgaard, & Smidsrød, 1989; Lee & Mooney, 2012). The use of alginates combined with synthetic polymers to prepare soft materials with enhanced mechanical properties and

* Corresponding author. Tel.: +47 73 59 34 34; fax: +47 73597710.
E-mail address: bjorn.stokke@ntnu.no (B.T. Stokke).

use of alginate derived oligomers as functional building blocks of synthetic polymer materials, e.g., support ionotropic gelation, are other recent examples of exploitation of alginate properties (Ghadban, Albertin, Rinaudo, & Heyraud, 2012; Sun et al., 2012).

Alginate hydrogel formation, following the introduction of multivalent ions, is promoted by formation of junction zones mediating interconnectivity within the network. The junction zones are probably most extensively described for the Ca^{2+} -mediated ones where chelation of Ca^{2+} by guluronic acid sequences has been described by the “egg-box”-model and further detailed (Grant, Morris, Rees, Smith, & Thom, 1973; Sikorski, Mo, Skjak-Braek, & Stokke, 2007; Stokke et al., 2000). This model depicts each divalent ion to interact with two neighbouring G-residues and paired with the same structural motif in the partner chain (Smidsrød, Glover, & Whittington, 1973). The reported minimum number of consecutive guluronic acid residues to support stable divalent cation mediated junctions is reported to 8 ± 2 for Ca^{2+} (Stokke, Smidsrød, Zanetti, Strand, & Skjak-Braek, 1993). Furthermore, the number of chain segments laterally associated to form a junction zone can increase beyond two chains yielding various junction zone multiplicities, as indicated at high Ca^{2+} saturation of the guluronic acid (Stokke et al., 2000). The effective junction zone functionality, i.e. the number of alginate chains extending from a junction zone, can exceed four for alginates supporting this mode of interaction. More recent progress in the relationship between alginate structure and gelation properties include the report of alternating MG sequences supporting calcium induced junction (Donati et al., 2005), and the discovery of long G-blocks in alginate seaweed extracts and their impact of alginate gelation properties (Aarstad, Strand, Klepp-Andersen, & Skjak-Braek, 2013).

Control of alginate hydrogel properties such as gelation kinetics, mechanical properties and syneresis are essential to be able to exploit their valuable properties as gelling or film-formation additives, viscosity enhancers or used to stabilize suspensions or emulsions. Use of oligoguluronates (typically with degree of polymerization $\text{DP} \sim 20$, and more than 90% G) isolated by acid hydrolysis and selective precipitation has recently been suggested as a means to achieve such control using different mixing ratios with a high M_w alginate (Draget & Smidsrød, 2007; Jørgensen, Sletmoen, Draget, & Stokke, 2007). Previous studies of adding oligoguluronates as a modulator for alginate gelling properties have mainly been focusing on rheological properties (Jørgensen et al., 2007). As oligoguluronates are almost entirely built from G-blocks they compete for cations with G-block sequences in alginate chains of higher molecular weight. Due to their low degree of polymerization ($\text{DP} \sim 20$), it is suggested that the oligoguluronates does not mediate network connectivity when mixed with high M_w alginates as they do not contain elastically active segments. Some data on the structure of the in-situ gelling alginate was reported by our group based on multifrequency determination of storage and loss modulus and analysis of the data according to the Winter–Chambon procedure. It was found that gelation was delayed and alginate gel strength decreased with increased concentration of free G-blocks added to the alginate (Jørgensen et al., 2007).

In the present work we study impact of adding free G-blocks on the cluster growth occurring in Ca^{2+} induced alginate gel formation by dynamic light scattering. Thus, assessing the effect of added oligoGs on the cluster growth, consequences of expected competition for Ca^{2+} between the added oligoguluronate and alginate chains can be monitored. We introduce Ca^{2+} induced gelation by release from a Ca^{2+} chelator (CaEGTA), to avoid adverse effect of non-homogeneous gelation occurring when mixing Ca^{2+} solution with aqueous sodium alginate due to the rapidly occurring gelation (Moe et al., 1995; Sletmoen, Draget, & Stokke, 2010).

2. Experimental

2.1. Materials

Three different alginates with various molecular properties were selected for the study. The two samples with low molecular weight were selected with different fraction of α -L-GulA (G), while the high molecular weight sample was selected with similar fraction of α -L-GulA as one of the low molecular weight one. The oligoguluronate sample was obtained by acid hydrolysis of high molecular weight alginate exploiting the different kinetics of the different glycosidic linkages (Haug, Larsen, & Smidsrød, 1966; Haug, Larsen, & Smidsrød, 1967). The weight average molecular weight (M_w) and intrinsic viscosities $[\eta]$ of the three alginate samples were determined as previously reported (Kristiansen, Tomren, & Christensen, 2011; Vold, Kristiansen, & Christensen, 2006). The fractions of the α -L-GulA, F_G , β -D-ManA (M), $F_M = 1 - F_G$, and fraction of diad combinations GG, GM and MM, as well as triad combinations, e.g., GGG (F_{GGG}) were determined using NMR (Grasdalen, Larsen, & Smidsrød, 1979; Grasdalen, Larsen, & Smidsrød, 1981). The three alginate samples are denoted with the Alg_X^Y -[c] sample designation, where the numerical values of X and Y depicts the F_G and M_w (in kg/mol) of the actual sample, respectively, and c is concentration of sample in mg/ml (when denoted). The parameters of the samples are summarized in Table 1.

2.2. Methods

2.2.1. Sample preparation for dynamic light scattering

Alginate stock solutions were prepared by dissolving alginate powder in aqueous 50 mM NaCl over night to a final concentration of 5 and 10 mg/ml. The cluster growth was monitored for the in-situ Ca^{2+} introduction method using release from CaEGTA (pH = 7.0) by lowering the pH as induced by adding required amount of (solid) D-gluconic acid δ -lactone (GDL) freshly dissolved in 0.5 ml of 50 mM NaCl similarly as described (Stokke et al., 2000) and vortexing it for 20 s without delay. CaEGTA was prepared as reported (Jørgensen et al., 2007). The experiments were carried out at constant 40 mM NaCl concentration to reduce possible effects of reduced pH during the GDL hydrolysis on the ionic strength. Double deionized water with resistivity 18.2 M Ω cm obtained using a Millipore setup was used throughout. All alginate stock solutions and CaEGTA were filtered with Acrodisc[®] Syringe Filters with Supor[®] Membrane from PALL before being used for preparation of gels. A 0.2 μm poresize filter was used for the alginates $\text{Alg}_{0.53}^{31}$, $\text{Alg}_{0.63}^{31}$ and CaEGTA whereas a filter with poresize of 0.45 μm was used for the $\text{Alg}_{0.66}^{114}$ sample. In the experimental series including oligoG, this was mixed with the alginate stock solution in ratio 2:1 or 1:1 (w/w) alginate to oligoGs prior to introducing the CaEGTA.

Alginate cluster growth were determined for 3.6 or 7.1 mg/ml alginate and 4.6 or 9.2 mM CaEGTA accordingly, prepared by blending appropriate volume of the stock solutions. The ratio between alginate and Ca^{2+} concentration was kept constant for both alginate concentrations. The fractional saturation of the G-residues of the alginates:

$$F_{\text{SAT}} = \frac{[\text{Ca}^{2+}] Z_{\text{Ca}}}{[G] Z_G} \quad (1)$$

are summarized in Table 2. In Eq. (1), Z_{Ca} and Z_G are the valences of the Ca^{2+} and G-residues, respectively. The in-situ release of Ca^{2+} from CaEGTA was initiated by adding freshly dissolved GDL in aqueous 50 mM NaCl (filtered, 0.2 μm syringe filtered prior GDL addition).

The freshly dissolved GDL was stirred with CaEGTA–alginate mixture, and the sample was transferred to the sample cell for

Table 1

Chemical composition of employed alginates and oligoguluronates. The weight average molecular weight (M_w), intrinsic viscosities $[\eta]$, number average degree of polymerization DPn, the average G-block length larger than 1 $N_{G>1}$, and the fractions of the α -L-GulA, F_G , β -D-ManA (M), $F_M = 1 - F_G$, as well as fraction of diad and triad combinations in samples are depicted.

Alginate source	Sample notation	M_w kg/mol ¹	$[\eta]$ ml/g	DPn	$N_{G>1}$	F_G^2	F_M^2	F_{GG}^2	F_{MG}/F_{GM}^2	F_{MM}^2	F_{MGG}/F_{GGM}^2	F_{MGM}^2	F_{GGG}^2
<i>L. hyperborea</i> –leaf	Alg _{0.53} ³¹ -[c]	31	132	–	8	0.53	0.47	0.35	0.19	0.28	0.05	0.14	0.30
<i>L. hyperborea</i> –stem	Alg _{0.63} ³¹ -[c]	31	149	–	11	0.63	0.37	0.50	0.13	0.24	0.05	0.10	0.46
<i>L. hyperborea</i> –stem	Alg _{0.66} ¹¹⁴ -[c]	114	610	–	13	0.66	0.34	0.55	0.12	0.22	0.05	0.09	0.50
<i>L. hyperborea</i> –stem	OligoGs-[c]	–	–	19	–	0.94	0.06	0.83	0.11	0.05	0.03	0.08	0.8

¹ The weight average molecular weights were determined by SEC-MALLS as stated in the text.

² The fraction monomers, diad and triad combinations of the various alginates and oligoG were determined by NMR as stated in the text.

Table 2

Fractional Ca²⁺ saturation of F_G fraction of alginates and reduced concentration $c[\eta]$ for the various alginate samples at their employed concentration.

Sample	No OligoG added			2:1 Alg:OligoG ratio			1:1 Alg:OligoG ratio		
	ALC _{0.53} ³¹	ALC _{0.63} ³¹	ALC _{0.66} ¹¹⁴	ALG _{0.53} ³¹	ALG _{0.63} ³¹	ALG _{0.66} ¹¹⁴	ALC _{0.53} ³¹	ALC _{0.63} ³¹	ALC _{0.66} ¹¹⁴
c_p (mg/ml)	C_{CaEGTA} (mM)	F_{sat}	F_{sat}	F_{sat}	F_{sat}	F_{sat}	F_{sat}	F_{sat}	F_{sat}
3.6	4.6	0.96	0.81	0.77	0.51	0.46	0.45	0.35	0.33
7.1	9.2	0.96	0.81	0.77	0.51	0.46	0.45	0.35	0.33
		$c[\eta]$							
3.6	4.6	0.47	0.53	2.16					
7.1	9.2	0.94	1.06	4.33					

characterization by dynamic light scattering. The amount of GDL was adjusted to result in a pH of about 4 after 24 h. This final pH was selected to yield a situation where the EGTA chelation of Ca²⁺ is sufficiently reduced to make Ca²⁺ accessible for inducing Ca²⁺-mediate gelation while at the same time not inducing acid gelation of alginate expected to occur at pH below the pK_a values of 3.38 and 3.65 for mannuronic acid and guluronic acid, respectively (Haug, 1964). The change in pH following addition of GDL was determined in parallel experiments without alginate using of conventional pH electrode (data not shown). The final concentration of GDL in the alginate solutions were 14 and 28 mM for the 4.6 and 9.2 mM of CaEGTA final concentrations, respectively.

2.2.2. Dynamic light scattering

Alginate cluster growth induced by Ca²⁺ released homogeneously in the solutions were determined by dynamic light scattering (DLS) (Zetasizer Nano ZS, Malvern, UK) at a wavelength of 633 nm in backscattering mode (scattering angle of 173°) and at a temperature of 25 °C. Each sample was characterized by DLS just after adding GDL to induce reduction of pH, and subsequently every 22nd minute for 24 h. Four independently prepared samples were determined for each set of experimental parameters. Changes in a polymer solution undergoing a sol–gel transition induce changes in the intensity correlation function. We adopted the reported emerging power law part due to the cluster growth and eventual sol–gel transition in the intensity correlation function $g^{(1)}(q,t)$ (Kundu, Osaka, Matsunaga, Yoshida, & Shibayama, 2008; Maleki, Kjoniksen, & Nystrom, 2007; Matsunaga & Shibayama, 2007; Richter, 2007; Shibayama, 2006; Shibayama & Norisuye, 2002) to analyse the data:

$$g^{(1)}(t) = A_f \exp \left[- \left(\frac{t}{\tau_{fe}} \right)^{\beta_f} \right] + \frac{A_s}{(1 + t/V)^d} \quad (2)$$

In Eq. (2), parameter A_f is the amplitude of fast relaxation mode, τ_{fe} the fast relaxation time, β_f is the stretch exponent coefficient and is a measure of the width of the distribution of relaxation times, A_s the amplitude of slow relaxation mode, V is a variable at which power law tail begin and d is power law coefficient. The parameters were extracted using a custom designed least square fitting routine (implemented in the Interactive Data Language, ITT Solutions) to fit the experimentally determined $g^{(1)}(t)$. Residuals not systematically depending on the time were used as guideline in the fit to the

data. The mean relaxation time of the fast mode averaged over the distribution of species is calculated as:

$$\tau_f = \int_0^{\infty} \exp \left[- \left(\frac{t}{\tau_{fe}} \right)^{\beta_f} \right] dt = \left(\frac{\tau_{fe}}{\beta_f} \right) \Gamma \left(\frac{1}{\beta_f} \right) \quad (3)$$

where Γ is the gamma function. In the following, we adopt the notation $\langle \tau_f \rangle$ to depict the average of a property obtained from determination of parallel samples, e.g., $\langle \tau_f \rangle$ depicts the τ_f averaged value from parallel measurements.

3. Results

Fig. 1 shows examples of dynamic light scattering data for monitoring Ca²⁺ induced cluster growth in alginate Alg_{0.63}³¹ at a concentration of 7.1 mg/ml. Data were obtained as function of time after inducing release of Ca²⁺ from CaEGTA by adding GDL to reduce the pH and thereby reducing the stability of the CaEGTA complex. The intensity correlation function $g^{(1)}(t)$ just after initiation release of Ca²⁺, decays with a fast relaxation mode describing the overall decay (Fig. 1a). The experimentally determined $g^{(1)}(t)$ at increasing time following initiation of Ca²⁺ release are characterized by the following trends. Initially, the relaxations are adequately described by one relaxation component (Fig. 1a), with the mean relaxation time of the fast mode τ_f initially being reduced, followed by an increase of τ_f and a second component with power law relaxation emerging (Fig. 1a). The power law decay mode is clearly identified after about 134 min for the particular example depicted in Fig. 1a. The mean intensity $\langle I \rangle$ of the scattered light is found to increase with time in a reproducible way between the parallel experiments up to about 200 min after initiation release of Ca²⁺, followed by more fluctuations with time, and lack of reproducibility of $\langle I \rangle$ between the parallel experiments (Fig. 1b). The initial amplitudes of the correlation function σ_f^2 are observed close to 1 and reproducible among the parallel experiments within the first 2 h, followed by a reduction of this parameter and onset of larger variation among the parallel experiments (Fig. 1b). The mean relaxation time of the fast mode is determined to 0.56 ms, followed by a reduction to 0.38 ms (about 30%) 45 min after initiating the pH reduction and concomitant Ca²⁺ release. The mean relaxation time is subsequently increasing, reaching about 2.6 ms after 140 min. Parameter τ_f within the parallel experiments are highly reproducible within

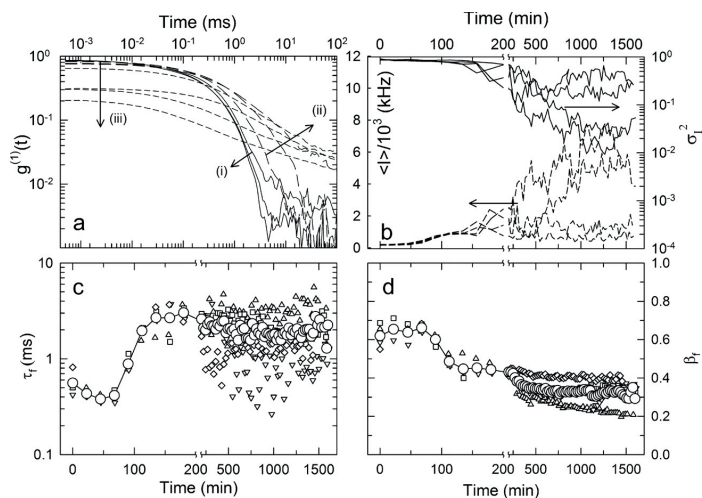


Fig. 1. Dynamic light scattering characterization of ionotropic induced cluster growth of 7.1 mg/ml alginate $\text{Alg}_{0.63}^{31}$ following release of calcium to a final concentration of $[\text{Ca}^{2+}] = 9.2 \text{ mM}$. (a) Intensity correlation function ICF at various time intervals, for one of the four parallel experiments. The arrows depict the $g^{(1)}(t)$ obtained at (i—solid lines) 0, 45 and 67 min (in the direction of the arrow) (ii—long dashed lines) at 89, 111, 154 min (in the direction of the arrow) (iii—short dashed lines) depicts trends in the plateau of the $g^{(1)}(t)$ for 178, 220, 440, 770, 1078 min, after adding GDL. (b) Mean scattering intensity $\langle I \rangle$ (---, left) and initial amplitude of ICF σ_I^2 (—, right) vs. time after adding GDL for the four parallel experiments (small symbols) and the mean of this four parallel (large \circ). (c) Mean relaxation time τ_f of the fast relaxation vs. time after adding GDL, for each of the four parallel experiments (small symbols) and the mean of this four parallel (large \circ). (d) Stretched exponential parameter β_f of the fast relaxation mode of $g^{(1)}(t)$ vs. time after adding GDL, for each of the four parallel experiments (small symbols), and their mean values (large \circ).

the first 140 min, while this is not the case at the longer times (Fig. 1c). This reduced reproducibility of τ_f between the parallel experiments is suggested to arise from onset of non-ergodic nature within the samples similar to that reported for other hydrogels (Shibayama, 2006; Shibayama & Norisuye, 2002).

Parameter β_f of the stretched exponential is 0.65 initially and nearly constant up to 70 min, followed by a decrease reaching 0.4 after 3 h, and is apparently levelling out at plateau value of 0.32 for the mean among the experiments from about 10 h (Fig. 1d). There is an increasing spread of the β_f parameter from about 3 h onwards. Preliminary fits using $\beta_f = 1$ to the experimental determined $g^{(1)}(t)$ at the initial state, yielded residuals systematically depending on time and were for this reason not pursued.

In situ release of Ca^{2+} in solutions of alginates with oligogulonuronate was observed to slow down the trends described above. For the alginate:oligoG ratio of 2:1 for the $\text{Alg}_{0.63}^{31}$, the intensity correlation functions change from initially being described by a fast relaxation mode to the emergence of an additional power law relaxation with increasing time after adding GDL (Fig. 2a). The time required for the power law relaxation mode to develop is longer in the presence of the oligoG than without (Figs. 1a and 2a). Increasing the oligoG content to an alginate:oligoG ratio 1:1 for $\text{Alg}_{0.63}^{31}$ results in $g^{(1)}(t)$ that mainly can be explained by one fast relaxation mode with increasing mean relaxation time (Fig. 2b). For the sample of oligoG at 7.1 mg/ml subjected to release of Ca^{2+} similar to the alginates, the changes from the initial $g^{(1)}(t)$ characterized by one fast component was observed to be different from that of the alginate samples. The initial, single fast mode, was first found to be even faster followed by a slowing down, reduction of the initial amplitude σ_I^2 (Fig. 2c), but less clear possible power law relaxation mode compared to the higher molecular weight samples.

For the alginate:oligoGs ratio 2:1, the mean intensity of the scattered light $\langle I \rangle$ is found to increase with time in a reproducible way between the parallel experiments up to about 250 min followed by more fluctuations with time after initiation release of Ca^{2+} , and lack of reproducibility of $\langle I \rangle$ between the parallel experiments (Fig. 2d).

Adding oligoG also affect the initial amplitude of $g^{(1)}(t)$ being reproducible and only slightly reduced up to 200 min, and throughout the data collection period for the 2:1 and 1:1 alginate:oligoGs ratios, respectively (Fig. 2d and e). Inverting the sample cuvette for the 1:1 alginate:oligoGs case (Fig. 2b) following completion of the DLS data collection period (about 24 h) showed that the sample had not gelled. The initial value of the intensity correlation function for the oligoGs sample was observed to be constant close to 1 up to 100 min after initiating the Ca release, followed by a reduction to about 0.1 within the time interval 100 to 400 min, and the levelling out at this value (Fig. 2f). The scattered mean intensity was observed to increase in the period of decreasing amplitude of the ICF.

Similar trends as observed for the mean relaxation time and stretched exponential parameter β_f in the case of no added oligoG were found when adding oligoG, but with slower development trends with increasing oligoG. Parameter τ_f were observed to be reproducible for time up to 220 min and for more than 20 h for the alginate/oligoG ratio of 2:1 and 1:1 (Fig. 3a and b). The data show that τ_f initially decrease with reaction time towards a minimum value of 0.33 ms at 90 min and 0.36 ms at 205 min for these two ratios of alginate to oligoG (Fig. 3a and b). Further increase of the reaction time yields an increase in parameter τ_f , with rate of increase slower the larger the oligoG concentration. Similar trends are observed for parameter τ_f for a concentration of 3.6 mg/ml and the other alginates (Table 3). The initial value of τ_f of the oligoG sample was determined to 0.06 ms (Fig. 3c). This parameter was determined nearly constant, or slightly reduced (to 0.04–0.05 ms) up to 120 min after adding GDL, followed by an increase reaching about 6 ms at 500 min and a subsequent apparent slower increase in τ_f (Fig. 3c). Parameter β_f of the stretched exponential is initially observed to be 0.65 at an alginate:oligoG ratio of 2:1 for the $\text{Alg}_{0.63}^{31}$, and nearly constant up to 150 min, followed by a decrease reaching 0.5 after 3 h (data not shown). Increasing the oligoG content yields a β_f parameter that is less dependent on time after inducing the Ca^{2+} release (data not shown). The τ_f averaged value from parallel measurements, $\langle \tau_f \rangle$, versus time for the

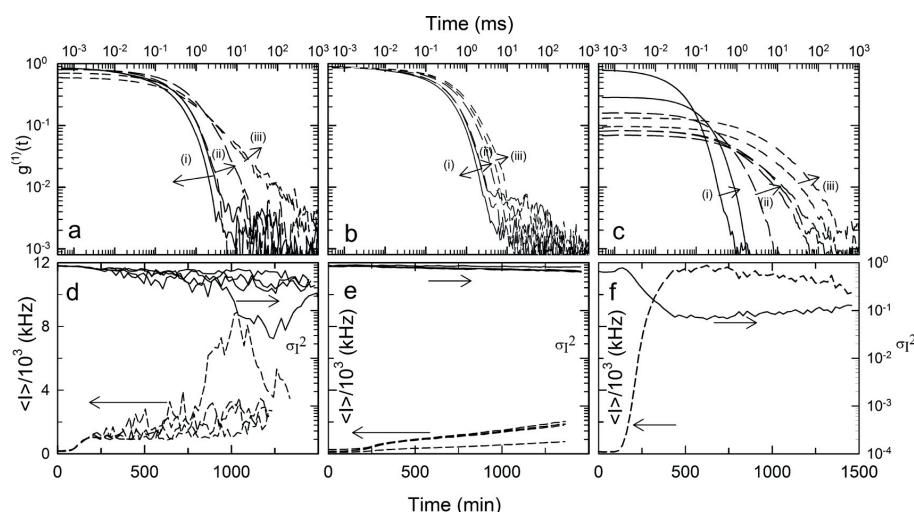


Fig. 2. Intensity correlation function at various time intervals after initiating the in-situ release of Ca by adding GDL to (a) $\text{Alg}_{0.63}^{31}$ -[7.1] with 2:1 Alginate:OligoGs (b) $\text{Alg}_{0.63}^{31}$ -[7.1] with 1:1 Alginate:OligoGs (c) $\text{OligoG}_{0.94}$ -[7.1] without additional alginate. In (a), arrows depicts $g^{(1)}(t)$ vs time after addition of GDL: (i—continuous line) for 0, 88 min, (ii—long dashed lines) for 132 and 176 min; (iii—short dashed lines) for 440 and 836 min. In (b), the arrows represents $g^{(1)}(t)$ for (i) 0 and 132 min, (ii) 198 and 352 min (iii) for 440 and 528 min and (c) (i) 44, 154 min, (ii) 220, 352, 418 and 616 min, (iii) for 836 and 1276 min. (l) and σ_l^2 vs. time after adding GDL to (d) $\text{Alg}_{0.63}^{31}$ -[7.1] with 2:1 Alginate:OligoGs (e) $\text{Alg}_{0.63}^{31}$ -[7.1] with 1:1 Alginate:OligoGs (f) $\text{OligoG}_{0.94}^{\text{DPh19}}$ -[7.1] without additional alginate.

Table 3

Initial value of mean relaxation time $\langle \tau_f \rangle_0$, and minimum relaxation time $\langle \tau_f \rangle_{\text{min}}$ and time t_{min} to reach minimum relaxation time for Ca^{2+} induced cluster growth in alginates.

Sample	Parameter	No OligoG added			2:1 Alg:OligoG ratio			1:1 Alg:OligoG ratio		
		$\text{ALG}_{0.53}^{31}$	$\text{ALG}_{0.63}^{31}$	$\text{ALG}_{0.66}^{114}$	$\text{ALG}_{0.53}^{31}$	$\text{ALG}_{0.63}^{31}$	$\text{ALG}_{0.66}^{114}$	$\text{ALG}_{0.53}^{31}$	$\text{ALG}_{0.63}^{31}$	$\text{ALG}_{0.66}^{114}$
3.6	c_p (mg/ml)									
	$\langle \tau_f \rangle_0$ (ms)	0.32	0.48	1.11	0.32	0.31	0.97	0.31	0.37	0.91
	$\langle \tau_f \rangle_{\text{min}}$ (ms)	0.27	0.27	0.73	0.24	0.23	0.77	0.24	0.25	0.708
	t_{min} (min)	67	89	22	134	132	113	313	263	181
7.1	$\langle \tau_f \rangle_0$ (ms)	0.51	0.56	2.09	0.42	0.50	2.38	0.41	0.48	2.50
	$\langle \tau_f \rangle_{\text{min}}$ (ms)	0.40	0.38	1.73	0.30	0.33	2.29	0.32	0.36	1.99
	t_{min} (min)	45	45	22	89	90	67	134	205	112

various alginates, the two alginate concentrations and with added oligoG are shown in Fig. 4. This shows generally that $\langle \tau_f \rangle$ increases more rapidly with increasing alginate concentration and molecular weight of the alginate.

Differences in changes of the mean relaxation time are summarized by the time needed to reach two times the initial value of $\langle \tau_f \rangle$ (Fig. 5). This indicated that oligoG is more efficient in slowing down the growth of $\langle \tau_f \rangle$ for the lower molecular weight alginates than the higher molecular weight ones. The data indicate that the samples with higher guluronic content $\text{Alg}_{0.63}^{31}$ -[7.1] need 90 min, 158 min and 500 min for doubling of $\langle \tau_f \rangle$ compared to the initial value $\langle \tau_f \rangle_0$ at 0, 3.6 and 7.1 mg/ml oligoG added, respectively. This is shorter than the time needed to double $\langle \tau_f \rangle$ for the $\text{Alg}_{0.53}^{31}$ -[7.1] case, observed to be 100, 170 and 1000 min for 0, 3.6 and 7.1 mg/ml oligoG, respectively (Fig. 5). Whereas for the case $\text{Alg}_{0.66}^{114}$ -[7.1], it is observed that this higher M_w sample need less time to double $\langle \tau_f \rangle$ relative to its starting plateau than the lower molecular weight one. The actual times are 66, 120, 223 min for this high M_w sample as compared to 90, 158, 500 min for the lower M_w alginate ($\text{Alg}_{0.63}^{31}$ -[7.1]), with 0, 3.6, and 7.1 mg/ml oligoG added (Fig. 5b). Adding 3.6 mg/ml oligoG to $\text{Alg}_{0.53}^{31}$ -[3.6] yields a situation with no doubling of the initial $\langle \tau_f \rangle$ within 1 day (Figs. 4a and 5a).

Examples of the estimate exponent of the power law component (Eq. (2)) include values of d in the range 0.7–0.9 observed at 200 min, and d of about 0.6 after 10 h, respectively, for the 2:1

alginate:oligoG sample condition using the $\text{Alg}_{0.63}^{31}$ -[7.1] sample (Fig. 2a). Increasing the oligoG to 1:1 alginate:oligoG yielded almost complete suppression of the power law relaxation component (Fig. 2b). However, systematic trends in the power law coefficients depending on sample and added oligoG were not clearly evident.

4. Discussion

The observed changes in the light scattering parameters of the three alginate samples, including also various amounts of oligoG added are rationalized in terms of molecular properties of the samples, the actual concentration relative to the overlap concentration and general trends of polymer cluster growths during a sol–gel transition as outlined in the following. We proceed by relating the trends observed during the phase where the initial amplitude of the intensity correlation function is reproducible (Figs. 1b and 2d and e) to molecular properties. This regime appear to be in the region where the samples conform to the ergodic assumption, while the present scattering data observed beyond this point indicate that signatures due to the non-ergodic effect is emerging. In general, the trends observed of a steep increase in the mean scattered intensity, emergence of a power law relaxation mode in the intensity correlation function, and reduction of the initial amplitude of the ICF (Figs. 1 and 2) all conform to that expected

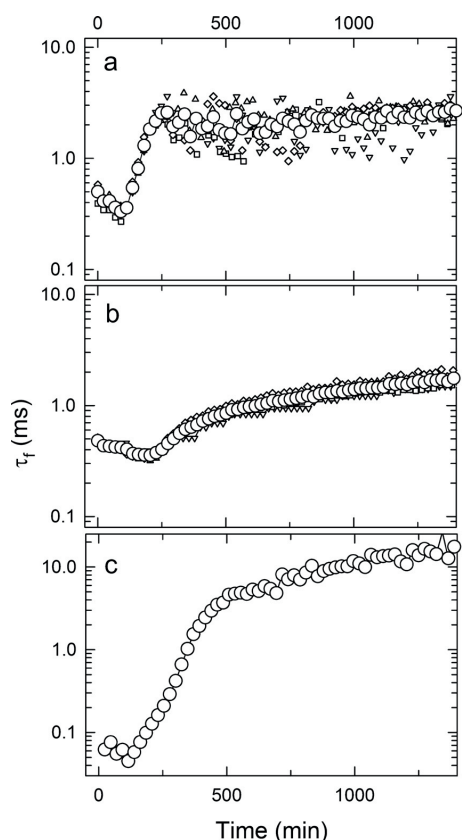


Fig. 3. Mean relaxation times of the fast relaxation τ_f versus time after adding GDL to characterization of ionotropic induced cluster growth of 7.1 mg/ml alginate $\text{Alg}_{0.63}^{31}$ –oligoG solutions for 2:1 (a) and 1:1 (b) alginate:oligoG concentration ratios and (c) 7.1 mg/ml oligoG solution without alginate. Data are shown for the individual parallel experiments as well as the averaged values.

for a sol–gel transition (Kundu et al., 2008; Maleki et al., 2007; Matsunaga & Shibayama, 2007; Richter, 2007; Shibayama, 2006; Shibayama & Norisuye, 2002). On a general and qualitative basis it can be deduced from Fig. 4 that an increase in M_w , increased F_G and increased polymer concentration all lead to a faster increase in $\langle\tau_f\rangle$. A possible explanation for the difference in $\langle\tau_f\rangle$ as function of molecular weight is that an increased M_w at comparable guluronic content of the polymer (e.g. $\text{Alg}_{0.63}^{31}$ and $\text{Alg}_{0.66}^{114}$, compare Fig. 4b with c and Fig. 4e with f) and Ca^{2+} concentrations will inevitably lead to an increase in intermolecular crosslinking, increased viscosity and eventually percolation (Jorgensen et al., 2007); all parameters that will increase the mean relaxation time. This argument is also valid for an increased polymer concentration. But the larger relative increase of $\langle\tau_f\rangle$ for increasing concentration from 3.6 to 7.1 mg/ml for the $\text{Alg}_{0.66}^{114}$ compared to the other alginate sample is suggested to arise from the latter concentration being larger than the overlap concentration. The associated increase in $[\eta]$ is from 2.16 to 4.33 (Table 2), where the latter is above 4 generally considered to represent onset of the semidilute regime (Robinson, Ross-Murphy & Morris, 1982). Upon increasing F_G content, the fraction of long G-blocks able to support stable static intermolecular junction zones increases. This can be seen as an increase in average G-block length larger than 1 ($N_{G>1}$) from about 8 to ~13 (Table 1). The alginates with F_G 0.63 and 0.66 supports

more stable intermolecular junction zones as compared to a more dynamic and reversible situation expected for the F_G 0.53 alginate. Addition of oligoguluronates leads to a concentration dependent delay in the onset of an increase in $\langle\tau_f\rangle$ in all cases.

Parameter τ_f shows in general a trend of first being reduced by about 20–35% followed an increase with time. The initial decrease in τ_f is suggested to arise from formation of less extended structures by Ca^{2+} -induced intramolecular interactions coined monocomplexes (Fig. 6a, ii and c, ii) by Williams and coworkers (Fang et al., 2007, 2008). The occurrence of this reduction τ_f appears from 22 min ($\text{Alg}_{0.66}^{114}$ –[7.1]) to 313 min ($\text{Alg}_{0.53}^{31}$ –[3.6]) (Table 3), which correspond to a pH in the range 5.4 till 4.4. This is at least 1 pH unit above the pK_a of the carboxyl groups of the alginate molecule, and a reduced chain expansion due to protonation (Sletmoen et al., 2010) appear thus not as a possible mechanism explaining the observed reduction in $\langle\tau_f\rangle$.

In all samples, the initial reduction τ_f is followed by temporal growth τ_f value which could be attributed to further lateral association of G-blocks mediating connectivity within and between the clusters (Fig. 6a, iii and c, iii) (Fang et al., 2007). The non-linear temporal dependence of τ_f (e.g. Fig. 3) in this phase before the maximum or plateau is reached, arises from inter-cluster associations yielding an increase in the average size that is non-linear with time, typical for association reaction from sol to gel state (Stepho, 1998).

After reaching maximum $\langle\tau_f\rangle$ two different trends are observed. The mean relaxation times (τ_f) are nearly constant for the samples $\text{Alg}_{0.63}^{31}$ and $\text{Alg}_{0.53}^{31}$ while some decrease is observed for $\text{Alg}_{0.66}^{114}$. These trends appear to arise from the different M_w of the alginates (Table 1). Samples $\text{Alg}_{0.63}^{31}$ and $\text{Alg}_{0.53}^{31}$ being short-chains alginates probably continues formation of cluster by via inter-cluster association leading to small but continues growth in particle size and thus mean relaxation time τ_f (Fig. 6a, iv). The reduced $\langle\tau_f\rangle$ indicated at longer time for the $\text{Alg}_{0.66}^{114}$ sample, a longer chains alginate, could arise from preferential inclusion of the largest cluster into the gel fraction resulting in reduced mean size of the fraction of mobile clusters. Additionally, further lateral association within an individual cluster driving compaction and reduction in particle size and thus decrease in mean relaxation time τ_f (Fig. 6c, iv) (Fang et al., 2007) could also contribute.

Addition of oligoG to the three different alginates (Fig. 6) imply including a component that generally is slowing down the cluster growth (Jorgensen et al., 2007; Sletmoen et al., 2010). The slowing down of the cluster growth is larger for the alginates with shorter chain length and with smaller fraction of G-blocks (Fig. 4). There is various possible molecular effect of the added oligoG, where alignment of the oligoG distribution with that corresponding to the internal G-blocks of the alginates, and total concentration ratios of these appear to be key elements. Thus for the sample $\text{Alg}_{0.53}^{31}$ the oligoG competing with association modes leading to increased τ_f is nearly suppressing the cluster growth totally. The observed non-linear tendency to divergence of the time to yield a two fold increase in τ_f with increasing oligoG concentration for the $\text{Alg}_{0.53}^{31}$ at 7.1 mg/ml is reflecting the conditions similar to a critical concentration needed for macroscopic interconnectivity resulting in gelation. The critical concentration similar to reported in other gelling (bio)polymers (Guo, Elgsaeter, & Stokke, 1998; te Nijenhuis, 1997) is in the present system suggested to be affected by the concentration of oligoG. The oligoG–G-block interaction reducing the effective mean functionality of the alginate chains is the underlying molecular mechanism in this interpretation. Adding oligoG is found to increase the time for two fold increase in τ_f more substantially, typically 100% at alginate:oligoG 2:1 (Fig. 5), than the effect of added oligoG on the relative increase in gelation time reported previously (Jorgensen et al., 2007). The larger relative change observed here is suggested to arise from the lower alginate

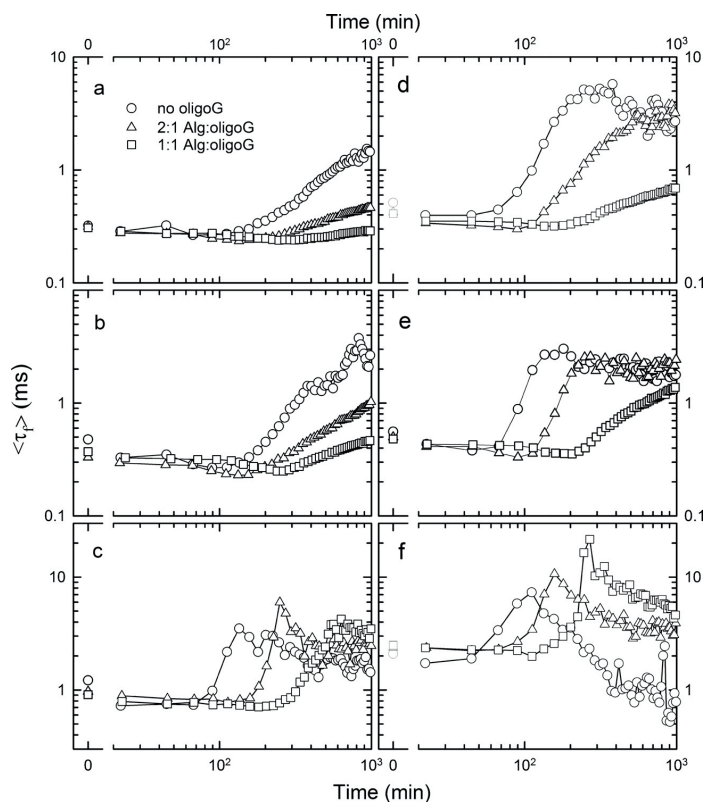


Fig. 4. Mean relaxation time (τ_r) versus time after inducing Ca^{2+} release for Alginates: (a) 3.6 mg/ml $\text{Alg}_{0.53}^{31}$ with added oligogulonates 0, 1.8, 3.6 mg/ml (b) 3.6 mg/ml $\text{Alg}_{0.63}^{31}$ with added oligogulonates 0, 1.8, 3.6 mg/ml (c) 3.6 mg/ml $\text{Alg}_{0.66}^{114}$ with added oligogulonates 0, 1.8, 3.6 mg/ml (d) 7.1 mg/ml $\text{Alg}_{0.53}^{31}$ with added oligogulonates 0, 3.6, 7.1 mg/ml (e) 7.1 mg/ml $\text{Alg}_{0.63}^{31}$ with added oligogulonates 0, 3.6, 7.1 mg/ml (f) 7.1 mg/ml $\text{Alg}_{0.66}^{114}$ with added oligogulonates 0, 3.6, 7.1 mg/ml.

concentrations in the present case, although there are differences in the molecular parameters of the alginates employed. Various association modes can be foreseen that is suppressing cluster growth towards to network formation. A simplistic scenario is that pairing up of a particular G-block within and alginate chain with an oligoG, yield a structure that is not propagating connectivity,

and thereby suppress cluster growth (Fig. 6b, iv). In this particular alginate sample, $\text{Alg}_{0.53}^{31}$, it appear that there is only a small fraction of G-blocks sequences available for mediating a connectivity transition following the Ca^{2+} mediated pairing with the oligoGs. Increasing the F_G to 0.63 yields some excess oligoG saturated G-

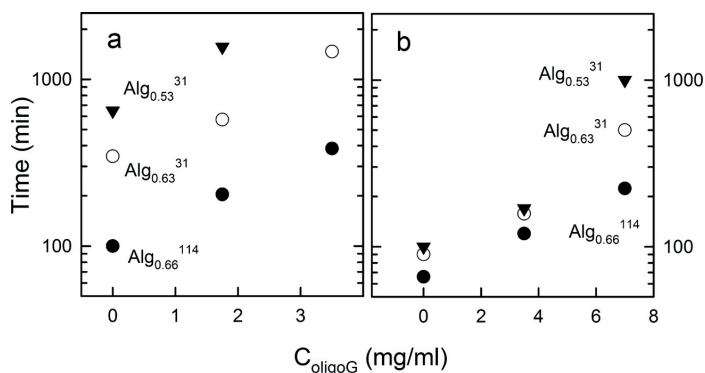


Fig. 5. The time required to reach a two-fold increase of the mean relaxation time (τ_r) from the initial value versus concentration of added oligogulonate at 3.6 mg/ml (a) and 7.1 mg/ml (b) alginate in 40 mM NaCl aqueous solution. Data were obtained for three alginates with fraction on guluronic acid and molecular weights as indicated by the sample identifiers (Table 1).

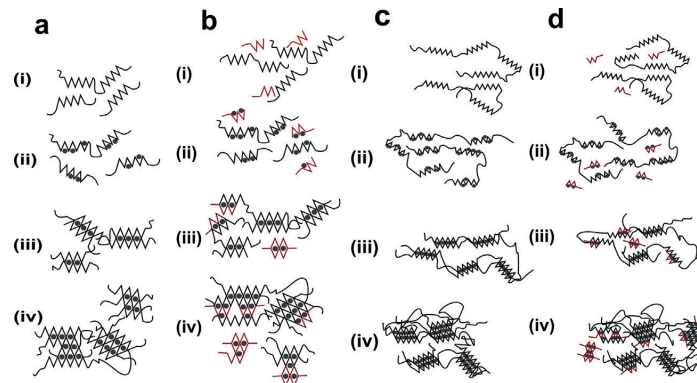


Fig. 6. Schematic illustration of effect of adding oligoGs to alginate solutions on the Ca-induced cluster growth at low M_w /short-chains alginate e.g. Alg_{0.63}³¹ and Alg_{0.53}³¹ (a—pure alginate, b—blend of alginate and oligoGs) and high M_w /long-chains alginate e.g. Alg_{0.66}¹¹⁴ (c—pure alginate, d—blend of alginate and oligoGs). The schematic illustrations depicted in the order (i), (ii), (iii) and (iv) represents possible association modes in progression of cluster growth ultimately yielding a hydrogel. (i) represent the initial solution before the onset of cluster growth, (ii) formation of monocomplexes upon addition of Ca²⁺, (iii) formation of egg-box dimers, (iv) lateral association of egg-box dimers possibly leading to inter- and intra-cluster mediated progression of crosslinking and possible compaction. Symbols represents: black \wedge/\wedge G-blocks internal in alginate chains, —M-blocks, •—Ca²⁺, red \wedge/\wedge oligoGs. (For interpretation of the references to colour in this figure legend, the reader is referred to the web version of this article.)

blocks, while increasing the molecular weight reduces the impact of the loose ends in the connectivity transition (Fig. 6d, iv).

The changes observed for the oligoG solution without the alginate is different from those with alginate by the initial smaller relaxation time, the onset of the increase in the $\langle l \rangle$ being earlier and less pronounced power law relaxation mode at the latter stages (compare Figs. 1 and 2). Thus, the behaviour of the Ca-induced changes in the oligoG sample appearing less accentuated when existing in a blend with alginate, suggest also a substantial interaction between the oligoG and alginates.

The lack of reproducibility observed for estimates of τ_f (e.g. Fig. 3) and fluctuations in the intensity can be attributed to the non-ergodic nature of the Ca²⁺-induced gel at later stages. This interpretation is based on the emergence of spatial inhomogeneous structure being formed in gels as reported (De Morais, Pereira, & Fonseca, 2012; Li, Ngai, & Wu, 2010; Shibayama & Norisuye, 2002). Despite the averaging performed here only include a few parallel experiments, it is interesting to note the reduction in $\langle \tau_f \rangle$ observed following the maximum for the highest molecular weight alginate. This could allude to a reduction of the mean size of the mobile fraction of the clusters following integration of the largest clusters in the immobile fraction, consistent with development of cluster size distributions in general through gelation.

5. Conclusions

Polymer cluster growth induced by in situ release of Ca²⁺ in alginate solution reveal that the rate of change reflect general behaviour of a sol–gel transition, and where the specific changes depend on the molecular properties of alginate and concentration. Moreover, data obtained from addition of oligoG to the aqueous solution show that this represents an efficient additive to control the kinetics of the cluster growth, and thereby also the sol–gel transition. The quantitative effect of adding oligoG to the alginate solution depends on the molecular properties of the alginate and their concentration. The clear evidence that the use of oligoG for kinetic control of the sol–gel transition arises from their ability to bind Ca²⁺ in the early phase of cluster growth and therefore reducing the accessible Ca²⁺ for entering into junction structures mediating increased size of the clusters and eventual gelation. Additionally, clear trends of intramolecular Ca²⁺ binding result-

ing in an initially reduced relaxation time indicated the presence also of this binding mode. Additional control can be achieved by choice of molecular weight, alginate type with its specific fraction of guluronic content, and design of specific residue sequence obtainable by epimerization using various enzymes specifically introducing particular sequences.

Acknowledgement

This work is support by the Norwegian Research Council, contract number 1826595/I40.

References

- Aarstad, O., Strand, B. L., Klepp-Andersen, L. M., & Skjåk-Bræk, G. (2013). Analysis of G-block distributions and their impact on gel properties of in vitro epimerized mannanuronan. *Biomacromolecules*, *14*(10), 3409–3416.
- De Morais, W. A., Pereira, M. R., & Fonseca, J. L. C. (2012). Characterization of gelification of chitosan solutions by dynamic light scattering. *Carbohydrate Polymers*, *87*(4), 2376–2380.
- de Vos, P., Faas, M. M., Strand, B., & Calafiore, R. (2006). Alginate-based microcapsules for immunoisolation of pancreatic islets. *Biomaterials*, *27*(32), 5603–5617.
- Donati, I., Holtan, S., Morch, Y. A., Borgogna, M., Dentini, M., & Skjåk-Bræk, G. (2005). New hypothesis on the role of alternating sequences in calcium-alginate gels. *Biomacromolecules*, *6*(2), 1031–1040.
- Draget, K., & Smidsrød, O. (2007). Modification of gelling kinetics and elastic properties by nano structuring of alginate gels exploiting the properties of polyguluronate. *Special Publication—Royal Society of Chemistry*, *303*, 227.
- Draget, K. I., Ostgaard, K., & Smidsrød, O. (1989). Alginate-based solid media for plant-tissue culture. *Applied Microbiology and Biotechnology*, *31*(1), 79–83.
- Fang, Y., Al-Assaf, S., Phillips, G. O., Nishinari, K., Funami, T., & Williams, P. A. (2008). Binding behavior of calcium to polyuronates: Comparison of pectin with alginate. *Carbohydrate Polymers*, *72*(2), 334–341.
- Fang, Y., Al-Assaf, S., Phillips, G. O., Nishinari, K., Funami, T., Williams, P. A., et al. (2007). Multiple steps and critical behaviors of the binding of calcium to alginate. *The Journal of Physical Chemistry B*, *111*(10), 2456–2462.
- Ghadban, A., Albertin, L., Rinaudo, M., & Heyraud, A. (2012). Biohybrid glycopolymer capable of ionotropic gelation. *Biomacromolecules*, *13*(10), 3108–3119.
- Grant, G. T., Morris, E. R., Rees, D. A., Smith, P. J. C., & Thom, D. (1973). Biological interactions between polysaccharides and divalent cations: The egg-box model. *FEBS Letters*, *32*, 195–198.
- Grasdalen, H., Larsen, B., & Smidsrød, O. (1979). A p.M.R. study of the composition and sequence of uronate residues in alginate. *Carbohydrate Research*, *68*, 23–31.
- Grasdalen, H., Larsen, B., & Smidsrød, O. (1981). ¹³C-nmr studies of monomeric composition and sequence in alginate. *Carbohydrate Research*, *89*, 179–191.
- Guo, B., Elgsaeter, A., & Stokke, B. T. (1998). Gelation kinetics of scleraldehyde–chitosan co-gels. *Polymer Gels and Networks*, *6*, 113–135.

- Haug, A. (1964). *Composition and properties of alginates*. Trondheim: Norwegian Institute of Technology (Composition and properties of alginates. Thesis).
- Haug, A., Larsen, B., & Smidsrød, O. (1966). A study of constitution of alginic acid by partial acid hydrolysis. *Acta Chemica Scandinavica*, 20(1), 183–8.
- Haug, A., Larsen, B., & Smidsrød, O. (1967). Studies on sequence of uronic acid residues in alginic acid. *Acta Chemica Scandinavica*, 21(3), 691–8.
- Høidal, H. K., Ertesvåg, H., Skjåk-Braek, G., Stokke, B. T., & Valla, S. (1999). The recombinant *Azotobacter vinelandii* mannuronan c-5-epimerase *algE4* epimerizes alginate by a nonrandom attack mechanism. *Journal of Biological Chemistry*, 274, 12316–12322.
- Jorgensen, T. E., Sletmoen, M., Draget, K. I., & Stokke, B. T. (2007). Influence of oligoguluronates on alginate gelation, kinetics, and polymer organization. *Biomacromolecules*, 8(8), 2388–2397.
- Kristiansen, K. A., Tomren, H. B., & Christensen, B. E. (2011). Periodate oxidized alginates: Depolymerization kinetics. *Carbohydrate Polymers*, 86(4), 1595–1601.
- Kundu, S. K., Osaka, N., Matsunaga, T., Yoshida, M., & Shibayama, M. (2008). Structural characterization of ionic gelator studied by dynamic light scattering and small-angle neutron scattering. *The Journal of Physical Chemistry B*, 112(51), 16469–16477.
- Lee, K. Y., & Mooney, D. J. (2012). Alginate: Properties and biomedical applications. *Progress in Polymer Science*, 37(1), 106–126.
- Li, J. F., Ngai, T., & Wu, C. (2010). The slow relaxation mode: From solutions to gel networks. *Polymer Journal*, 42(8), 609–625.
- Lim, F., & Sun, A. M. (1980). Microencapsulated islets as a bioartificial endocrine pancreas. *Science*, 210, 908–910.
- Maleki, A., Kjoniksen, A. L., & Nystrom, B. (2007). Characterization of the chemical degradation of hyaluronic acid during chemical gelation in the presence of different cross-linker agents. *Carbohydrate Research*, 342(18), 2776–2792.
- Marijnissen, W., van Osch, G., Aigner, J., van der Veen, S. W., Hollander, A. P., Verwoerd-Verhoef, H. L., et al. (2002). Alginate as a chondrocyte-delivery substance in combination with a non-woven scaffold for cartilage tissue engineering. *Biomaterials*, 23(6), 1511–1517.
- Matsunaga, T., & Shibayama, M. (2007). Gel point determination of gelatin hydrogels by dynamic light scattering and rheological measurements. *Physical Review E: Statistical, Nonlinear, and Soft Matter Physics*, 76(3), 030401.
- Miralles, G., Baudoin, R., Dumas, D., Baptiste, D., Hubert, P., Stoltz, J. F., et al. (2001). Sodium alginate sponges with or without sodium hyaluronate: In vitro engineering of cartilage. *Journal of Biomedical Materials Research*, 57(2), 268–278.
- Moe, S. T., Draget, K. I., Skjåk-Braek, G., & Smidsrød, O. (1995). Alginates. In A. M. Stephen (Ed.), *Food polysaccharides, their applications. Food science and technology* (Vol. 67) (pp. 245–286). New York: Marcel Dekker Inc.
- Morch, Y. A., Donati, I., Strand, B. L., & Skjåk-Braek, G. (2007). Molecular engineering as an approach to design new functional properties of alginate. *Biomacromolecules*, 8(9), 2809–2814.
- Richter, S. (2007). Comparison of critical exponents determined by rheology and dynamic light scattering on irreversible and reversible gelling systems. *Macromolecular Symposia*, 256, 88–94.
- Robinson, G., Ross-Murphy, S. B., & Morris, E. R. (1982). Viscosity-molecular weight relationships, intrinsic chain flexibility, and dynamic solution properties of guar galactomannan. *Carbohydrate Research*, 107, 17–32.
- Shibayama, M. (2006). Universality and specificity of polymer gels viewed by scattering methods. *Bulletin of the Chemical Society of Japan*, 79(12), 1799–1819.
- Shibayama, M., & Norisuye, T. (2002). Gel formation analyses by dynamic light scattering. *Bulletin of the Chemical Society of Japan*, 75(4), 641–659.
- Sikorski, P., Mo, F., Skjåk-Braek, G., & Stokke, B. T. (2007). Evidence for egg-box-compatible interactions in calcium-alginate gels from fiber X-ray diffraction. *Biomacromolecules*, 8(7), 2098–2103.
- Sletmoen, M., Draget, K. I., & Stokke, B. T. (2010). Alginate oligoguluronates as a tool for tailoring properties of Ca-alginate gels. *Macromolecular symposia*, 291–292(1), 345–353. Weinheim: WILEY – VCH Verlag, GmbH & Co, KGaA.
- Smidsrød, O. (1974). Molecular basis for some physical properties of alginates in the gel state. *Faraday Discussions of the Chemical Society*, 57(0), 263–274.
- Smidsrød, O., Glover, R. M., & Whittington, S. G. (1973). The relative extension of alginates having different chemical composition. *Carbohydrate Research*, 27, 107–118.
- Stepto, R. F. T. (1998). *Polymer networks: Principles of their formation, structure and properties*. London: Blackie Academic & Professional.
- Stokke, B. T., Draget, K. I., Smidsrød, O., Yuguchi, Y., Urakawa, H., & Kajiwara, K. (2000). Small-angle X-ray scattering and rheological characterization of alginate gels. 1. Ca-alginate gels. *Macromolecules*, 33(5), 1853–1863.
- Stokke, B. T., Smidsrød, O., Zanetti, F., Strand, W., & Skjåk-Braek, G. (1993). Distribution of uronate residues in alginate chains in relation to alginate gelling properties. 2. Enrichment of β -D-mannuronic acid and depletion of α -L-guluronic acid in sol fraction. *Carbohydrate Polymers*, 21, 39–46.
- Sun, J. Y., Zhao, X. H., Illeperuma, W. R. K., Chaudhuri, O., Oh, K. H., Mooney, D. J., et al. (2012). Highly stretchable and tough hydrogels. *Nature*, 489(7414), 133–136.
- Svanem, B. I. G., Skjåk-Braek, G., Ertesvåg, H., & Valla, S. (1999). Cloning and expression of three new *Azotobacter vinelandii* genes closely related to a previously described gene family encoding mannuronan c-5-epimerases. *Journal of Bacteriology*, 181, 68–77.
- te Nijenhuis, K. (1997). Thermoreversible networks. Viscoelastic properties and structure of gels. *Advances in Polymer Science*, 130, 1–252.
- Vold, I. M. N., Kristiansen, K. A., & Christensen, B. E. (2006). A study of the chain stiffness and extension of alginates, in vitro epimerized alginates, and periodate-oxidized alginates using size-exclusion chromatography combined with light scattering and viscosity detectors. *Biomacromolecules*, 7, 2136–2146.

Paper II

Effects of added oligoguluronate on mechanical properties of Ca-alginate-oligoguluronate hydrogels depend on chain length of the alginate.

A.M.Padoł, K.I.Draget, B.T.Stokke
Submitted to Carbohydrate Polymers

Is not included due to copyright

Paper III

Local structure of Ca induced hydrogels of alginate –oligoguluronate blends

Y.Yuguchi, A.Hasegawa, A.M.Padoł, K.I.Draget, B.T.Stokke
In preparation

Is not included due to copyright

